Changes in Chromatin Conformation During Replicative Senescence of Normal Human Diploid Fibroblasts

Edward J. Peckham

B.S., University of Maryland College Park, 2004

A Dissertation submitted in partial fulfillment of the requirements for the degree of Doctor of Philosophy in the Division of Biology and Medicine at Brown University Providence, Rhode Island May 2012

Signature Page

This dissertation by Edward J. Peckham is accepted in its present form by the Division of Biology and Medicine as satisfying the dissertation requirement for the degree of Doctor of Philosophy

Date_____ _____

John M. Sedivy, Ph.D., Advisor

Recommended to the Graduate Council

Date_____ _____

Stephen Helfand, M.D., Reader

Date_____ _____

Alexander Brodsky, Ph.D., Reader

Date_____ _____

Mark Zervas, Ph.D., Reader

Date_____ _____

Bradley Johnson, M.D., Ph.D., Reader

Approved by the Graduate Council

Date_____ _____

Peter Weber, Ph.D.,

Dean of the Graduate School

Edward J Peckham
Curriculum Vitae

Education

Brown University

Ph.D. candidate in the Department of Molecular Biology, Cell Biology, and Biochemistry, Division of Biology and Medicine. Expected graduation spring 2012.

University of Maryland College Park

B.S. In Cell Biology, Molecular Biology and Genetics, May 2004. GPA: 3.17

Mount St. Mary's College

Received College credit in Molecular Biology, Summer 1998. GPA: 4.00

Experience

Graduate Thesis Research: Cellular Senescence, 2007-present

Studied the changes in chromatin organization in senescent cells. Developed the FAIRE assay to be used to evaluate two cellular conditions; replicating and senescent. Generated a novel trandgenic mouse line to study the expression and localization of murine p16.

Teaching Assistant, 2007

Bio 470 Genetics, Brown University. Lead laboratory exercises. Graded exams and assignments.

Research Assistant, 2004-2006

Investigated the activity of transposable elements in the mosquito species *Aedes aegypti*.

Undergraduate Research Assistant, 2002-2004

Investigated the activity of transposable elements in the mosquito species *Aedes aegypti*

Awards and Honors

Dean's list, University of Maryland College Park 1999

NIH Pre-Doctoral Fellowship Trainee, Brown University, 2006 to present. NIH funded departmental training grant

Publications

O'Brochta, D. A., Subramanian, R. A., Orsetti, J., Peckham, E., Nolan, N., Arensburger, P., Atkinson, P. W., and Charlwood, D. J. (2006). hAT element population genetics in Anopheles gambiae s.l. in Mozambique. Genetica *127*, 185-198.

Wilson, R., Orsetti, J., Klocko, A. D., Aluvihare, C., Peckham, E., Atkinson, P. W., Lehane, M. J., and O'Brochta, D. A. (2003). Post-integration behavior of a Mos1 mariner gene vector in Aedes aegypti. Insect Biochem Mol Biol *33*, 853-863.

Acknowledgements

I would like to start by thanking my advisor, John Sedivy, for his guidance and patience. I perhaps came into this program behind many of my peers, but I have learned a tremendous amount under your tutelage and plan to take these lesions with me into my future endeavors, wherever they may take me.

I would like to thank my committee members for Mark Zervas, Stephan Helfand, and Alex Brodsky for your advice and help. Thank your time and advice at my committee meetings, and defense it was great help and very much appreciated. I would also like to thank my outside reader Brad Johnson for taking the time to come to Brown and participate in my examination.

I would like to thank Nicola Neretti and Sara Hellenmyer in the 'Superfly Bioinformatics Center.' Without your help and bioinformatics expertise I would have nothing to show for after all these years. I would also like to thank Christoph Shorl in the Center for Genomics and Protiomics core facility. You provided essential support and technical assistance that is greatly appreciated.

I would like to thank the members of the Sedivy lab for your support and help. Abby, you have been a tremendous help in my time here; you showed me the ropes and have always been there if I needed help with my protocols. Jessie and Jill, you were great resources and I could always talk to you if I had any research related questions. Meena, you have always been there keeping things going; I really appreciate all the ordering and dealing with my initial cluelessness of that system. Marco, you have been a great friend, and have helped me think through some of my most difficult situations. To the current members Ursula, Jeff, Xiaoai, Sherida, Tak and past members, Zach, Beth, Mimi and Chui Sun; it has been a privilege to work with you all, you are all fantastic lab-mates.

I would like to thank all the friends that I have made along the way you have helped me maintain my sanity these long years. I would especially like to thank my roommates Courtney and Selena, you have been the best roommates and friends I could have hoped for, and you have helped me get by when times were tough, and shared in the laughter when times were good. I would also like to thank my parents for their love and support; I know I will always have you on my side when I need you.

Table of Contents

Signature Page ii

Curriculum Vitae iii

Acknowledgements iv

Table of Contents v

List of Figures ix

List of Tables xi

Chapter 1: Introduction 1

1-1) Aging 2

1-2) Cellular Senescence 3

1-3) Causes of Senescence 4

1-3A) Replicative Cellular Senescence: Telomere Attrition 4

1-3B) Premature Cellular Senescence 6

1-3C) p53 and RB 6

1-4) Biomarkers of Senescent Cell 8

1-5) Senescence and Aging 12

1-6) Chromatin Organization 18

1-7) Epigenetic Modifications 22

1-7A) CpG Methylation 22

1-7B) Histone modifications 23

1-8) Chromatin Modifications Associated with Aging and Senescence 24

1-9) Methods for Globally Evaluating Chromatin State 30

1-10) FAIRE 31

1-11) Repetitive Sequences 33

Chapter 2: Materials and Methods 38

2-1) Methods for Chapter 3: FAIRE and Expression Microarray Analysis 39

2-1A) Cell Culture 39

2-1B) Formaldehyde Assisted Isolation of Regulatory Elements (FAIRE) 39

2-1C) Affymetrix Tiling Microarrays 41

2-1D) qPCR Peak Validation 42

2-1E) Gene- Expression Microarrays 43

2-1F) Comparison of Expression and Tiling Microarray Data 44

2-1G) FAIRE Signal to Gene Density Correlation 44

2-2) Methods for Chapter 4: Analysis of Repetitive DNA Enrichment and Expression 45

2-2A) DNA isolation 45

2-2B) Dot-blot Probe Design 45

2-2C) Dot Bloting and Hybridization 46

2-2D) Normalization of Dot Blots 48

2-2E) Calculation of Signal Intensity and Enrichment 49

2-2F) Multiplex Real-Time PCR 49

2-2G) Transposable Element Expression Analysis 50

Chapter 3: FAIRE Analysis of Genome-Wide Changes in Chromatin Accessibility During Cellular Senescence 58

3-1) Goals of the Study 59

3-2) Overview of Experimental Design 59

3-3) Implementation of the FAIRE-chip method 60

3-4) qPCR validation of FAIRE-chip data 61

3-5) FAIRE enrichment in regulatory elements 62

3-5A) Transcription Start Sites 62

3-5B) Enhancers 63

3-5C) Replication Domains and Origins of Replication 63

3-6) Clustering analysis of TSS FAIRE enrichment 64

3-7) Correlation of FAIRE enrichment atTSS with gene expression data 65

3-8) Global patterns of FAIRE enrichment 67

3-8A) Chromatin painting 67

3-8B) Comparison of total genomic enrichment with enrichment in regulatory regions 68

3-8C) Correlation between FAIRE enrichment signal and gene density 69

3-9) Summary 70

Chapter 4: Changes in Chromatin Accessibility of the Repetitive Human Genome During Cellular Senescence 101

4-1) Goals of the Study 102

4-2) Overview of Experimental Design 102

4-3) Dot Blot Analysis of LINE and SINE Sequences in FAIRE Fractions 103

4-4) Analysis of L1 Retrotransposition Events 107

4-5) Analysis of Alu and L1 Transcription 108

4-6) Summary 108

Chapter 5: Discussion 124

5-1) FAIRE is a Promising Method to Study Genome Wide Chromatin Changes 125

5-2) FAIRE Enrichment of Regulatory Elements 125

5-3) Genome-wide Patterns of FAIRE Enrichment 129

5-4) FAIRE Enrichment of LINE and SINE Repetitive Elements 132

5-5) Relationship Between FAIRE Enrichment and Transcription 134

5-6)Conclusions 137

5-7) Future Directions 139

Supplemental Tables 141

Literature Cited 148

List of Figures

Figure 1-1 Morphologies of senescent human diploid fibroblasts..... 34

Figure 1-2 The p53 and RB pathways regulate senescence by arresting cells in G1 phase. 36

Figure 2-1 Measurement of the DNA concentrations of dot blot samples using qPCR ... 52

Figure 2-2 Signal intensities from dot blots plotted against the amount of DNA present in each spot..... 56

Figure 3-1. Comparison of FAIRE-chip output from our study with the original study published by Lieb's group. 73

Figure 3-2. Real time qPCR Validates FAIRE enrichment. 75

Figure 3-3 qPCR validates FAIRE enrichment at the TSS of the PPM1B gene. 77

Figure 3-4 Distribution of FAIRE enrichment across the PPM1B gene. 79

Figure 3-5 FAIRE enrichment distribution and qPCR validation of the C19orf62 gene. 81

Figure 3-6 Averaged FAIRE enrichment at TSS is decreased in senescent cells..... 83

Figure 3-7 FAIRE enrichment at enhancers decreases in senescent cells 85

Figure 3-8 FAIRE Enrichment at origins of replication is reduced in senescent cells 87

Figure 3-9 FAIRE enrichment at TSS segregate into 2 clusters: Open and Closed 89

Figure 3-10 Open cluster genes are more highly expressed than closed cluster genes 91

Figure 3-11 Change in FAIRE signal correlates with a change in expression in senescent cells 93

Figure 3-12 Global FAIRE enrichment becomes homogeneous in senescent cells 95

Figure 3-13 Normalization and distribution of genomic FAIRE signal 97

Figure 3-14 Correlation of TSS clustering to positive FAIRE signal in early passage cells 99

Figure 4-1 Alu and L1 dot blot probe templates..... 110

Figure 4-2 Dot blots hybridized with L1 probe. 112

Figure 4-3 Dot blots hybridized with Alu probe..... 114

Figure 4-4 Normalized blot signal for 5 ng of DNA show increased TE enrichment in senescent cells..... 116

Figure 4-5 normalized FAIRE enrichment values show increased TE enrichment in senescent cells..... 118

Figure 4-6 No increase of L1 copy number in the genome of senescent cells. 120

Figure 4-7 RNA expression of L1 and Alu elements increases in senescent cells..... 122

List of Tables

Table 2-1 Calculation of the DNA concentrations of dot blot samples based on qPCR measurements 54

Table S-1 Primers from Jason Lieb's group 142

Table S-2 Peak Validation Primers 144

Table S-3 Primers used for generating a standard curve for dot blot sample calculations 146

Chapter 1: Introduction

1-1) Aging

Aging is a complex and profound biological process that while universally recognized, remains poorly understood on a mechanistic level (Jeyapalan and Sedivy, 2008; Kirkwood, 2005; Sinclair and Oberdoerffer, 2009). The causes of aging fall into a broad spectrum of genetic factors, environmental stimuli, and epigenetic modifications (Antosh et al., 2011; Lorenzini et al., 2009; Thompson et al., 2010). Despite the litany of internal and external stimuli that may contribute to the process of aging, there are certain aspects that remain consistent in many species. The aging phenomenon presents as a progressive degeneration of biological function at the cellular, organ and organismal level, eventually leading to organismal death (Flatt and Schmidt, 2009; Hughes and Reynolds, 2005; Kong et al., 2011). A fascinating aspect of the aging process is that because most organisms have already exited the reproductive phase of their life cycles at the onset of aging-related decline, natural selection has little chance to directly affect late life factors that contribute to the aging phenotype. Never-the-less age related changes appear to be regulated by conserved molecular pathways under the influence of evolutionary selection (Flatt and Schmidt, 2009; Garinis et al., 2008; Kirkwood et al., 2000).

One major contributing force behind aging has been proposed to be accumulated DNA damage (d'Adda di Fagagna et al., 2004; Ding and Shen, 2008; Herbig et al., 2006; Hinkal and Donehower, 2008; Lorenzini et al., 2009). The affronts to the delicate genome are many, ranging from external threats to internal chemical byproducts and mechanical failures (Burhans and Weinberger, 2007; Di Micco et al., 2006; Salmon et al., 2010). External dangers include environmental ionizing, solar UV radiation and free radicals, while internal ones include reactive oxygen species produced by natural cellular

metabolic processes, such as super oxides, hydrogen peroxide and hydroxyl radicals. All of these species have the potential to cause damage to necessary bio-molecules within the organism, including DNA (Barja and Herrero, 2000; Bohr, 2002; De Bont and van Larebeke, 2004; Ku et al., 1993).

Yet mechanisms are in place to reduce the accumulation of damage to the genome. The DNA damage responses are a set of conserved processes that have evolved to repair both single and double strand DNA breaks, inter and intra strand cross-links, base alterations, DNA adducts, insertions, deletions, and base pair mismatches (Li et al., 2008a; Lombard et al., 2005; Maynard et al., 2009; Shumaker et al., 2006). These repair mechanisms, though generally effective, are not without error and, given time, DNA damage and mutations accumulate, eventually reaching a critical point at which the cell undergoes one of three possible permanent changes: transformation, apoptosis, or cellular senescence (Campisi, 2005; Lindahl, 1993; Vijg, 2004).

1-2) Cellular Senescence

Cellular senescence, as first discovered in 1961 by Hayflick and Moorehead, has been used to describe the phenomenon in which cells undergo a physiological change rendering them incapable of further replication. In the initial experiment normal human fibroblasts were cultured and serially passaged, allowing for continual population doublings (Hayflick and Moorhead, 1961). After a seemingly preset number of doublings the cells irreversibly lost their ability to replicate. Despite the inability of such cells to replicate, it is important to establish that these cells continue to live, and are, in fact, metabolically active and genetically stable, as well as resistant to apoptosis (Hampel et

al., 2005; Marcotte et al., 2004; Matsumura et al., 1979; Pignolo et al., 1994; Wang, 1995). In addition to the loss of replication capability, a number of additional phenotypic changes occur in cells that have entered the senescent state, including modified cell morphology, gene expression patterns, chromatin organization and secretory profiles (Bayreuther et al., 1988; Coppe et al., 2006; Dimri et al., 1995; Narita et al., 2003; Zhang et al., 2003). Though the underlying molecular biology involved in senescence was not known at the time of its discovery, it was proposed to be a potential mechanism of aging, as the limited number of cellular divisions seemed to indicate a finite level of regeneration over time within the organism, eventually leading to a biological decline (Hayflick, 1965). Many of the causes for cellular senescence have since been elucidated and although they vary, they all lead to the activation of similar signaling pathways that inhibit the cell cycle (Collado et al., 2007; Herbig and Sedivy, 2006; Jeyapalan and Sedivy, 2008).

1-3) Causes of Senescence

1-3A) Replicative Cellular Senescence: Telomere Attrition

Cellular senescence induced by continual proliferation, as it was first discovered, is caused by the shortening of the telomeres (Bodnar et al., 1998; Harley et al., 1990; Hayflick and Moorhead, 1961). In vertebrates the repetitive nucleotide sequence associated with telomeres consists of TTAGGG and, in human cells, occupies approximately 5,000-15,000 bp on either end of each chromosome (de Lange, 2005; Herbig and Sedivy, 2006). The primary function of telomeres is to prevent chromosome ends from being recognized as double strand breaks by the cellular DNA damage repair

machinery, and to overcome the incomplete end replication problem inherent with linear chromosomes (Chan et al., 2001; Olovnikov, 1973; Sfeir et al., 2005). Formation of new DNA during replication proceeds only in the 5’ to 3’ direction, as DNA polymerase enzymes are only able to add bases to the free hydroxyl at the 3’ end of a DNA strand, which allows for the full replication to the end of the leading strand of the replication fork by Pol ε. The lagging strand however must be replicated through a series of Okazaki fragments, small DNA fragments primed by short RNA polynucleotides which are later excised and replaced by Pol δ (Bermudez et al., 2011). When the replication fork reaches the end of the chromosome a final RNA primer is used to generate a DNA fragment, however once the primer is excised, polymerase is unable to replicate the sequence covered by the primer resulting in a shorter 5’ end of the replicated lagging strand (Harley et al., 1990; Olovnikov, 1973). Telomerase is a ribonucleoprotein containing an integral RNA template (TERC) and a reverse-transcriptase enzymatic sub-unit (TERT) that allows for the extension of the 3’ end of the chromosome (Greider and Blackburn, 1985; Harley et al., 1990; Mitchell et al., 2010). Human telomerase maintains and elongates the telomeres in germ-line, embryonic tissues, and cancers, but is inactive in most healthy adult somatic tissue (Hiyama et al., 1995; Shay and Bacchetti, 1997; Ulaner et al., 2001; Wright et al., 1996). As cells continue to replicate, the length of the telomeres grow increasingly shorter, effectively establishing a molecular clock that continually counts down until the telomeres reach the critical length at which they can no longer maintain proper structure (d'Adda di Fagagna et al., 2003; Harley et al., 1990; Stewart et al., 2003). When this minimum telomere length is reached the DNA damage response becomes activated, triggering a cascade of molecular signals that result in the activation of the p53

tumor suppressor, a powerful cell cycle regulator, and entry into the senescent state (Ben-Porath and Weinberg, 2005; Campisi, 2005; Collado et al., 2007; d'Adda di Fagagna et al., 2003; Herbig et al., 2004; Takai et al., 2003).

1-3B) Premature Cellular Senescence

In addition to telomere attrition, cellular senescence can be induced prior to telomere dysfunction by a number of other factors (Jeyapalan and Sedivy, 2008; Kong et al., 2011; Kuilman et al., 2010). Stress induced senescence can occur *in vitro* when cells are grown in improper culture conditions (Parrinello et al., 2003; Ramirez et al., 2001; Sherr and DePinho, 2000). Senescence can also be induced, both *in vitro* and *in vivo*, by the activation of certain oncogenes in otherwise normal cells (Lin et al., 1998; Serrano et al., 1997; Zhu et al., 1998). Additionally, mutations that cause a loss of function in tumor suppressor genes, such as PTEN, NF1 and VHL, can also lead to a senescent state (Chen et al., 2005; Courtois-Cox et al., 2006; Young et al., 2008). In all of these conditions, there is an activation of either or both of two prominent tumor suppressors, the p53 and retinoblastoma (RB) proteins (Campisi and d'Adda di Fagagna, 2007; Hara et al., 1991; Shay et al., 1991; Wei et al., 2003).

1-3C) p53 and RB

As mentioned previously, in most instances of cellular senescence, regardless of stimuli, there is a common activation of either of the p53 or RB tumor suppressor pathways, or both (Atadja et al., 1995; Ben-Porath and Weinberg, 2005; Campisi, 2005; Stein et al., 1990). Though the results of p53 and RB activity are similar, the upstream activating mechanisms of these signal transduction cascades are different for each (Kong et al., 2011).

p53 primarily mediates senescence caused by telomere dysfunction, DNA damage signals, and oncogene activation. The Ataxia Telangiectasia Mutated (ATM) protein kinase phosphorylates and activates p53 in response to double strand breaks, while the Ataxia Telangiectasia and Rad3 Related (ATR) kinase activates p53 when single-stranded DNA persists within the cell, a hallmark of stalled replication forks(d'Adda di Fagagna et al., 2003; Herbig et al., 2004). Activated p53 then promotes the expression of the CDK inhibitor p21, which in turn binds to and inhibits the activity of CDK2 and CDK4 complexes (Sherr and Roberts, 1999; Stein et al., 1999). The complex of CDK2 with Cyclin E and its activity is necessary for the progression of the cell cycle through the G1 phase, and so through p21, p53 activity acts as a brake for cell cycle progression (Koff et al., 1992).

The CDK inhibitor p16 inactivates CDK4 and CDK6, preventing them from forming complexes with Cyclin D. The CDK4/CDK6-Cyclin D complex phosphorylates RB, causing it to no longer bind and inhibit the E2F-DP transcription factor complex that promotes progression of the cell cycle from the G1 phase to the S phase(Fahraeus et al., 1996; Serrano et al., 1993; Siegert et al., 2000). The presence of p16 maintains RB in its active deposphorylated, E2F-DP binding state, thus causing the cell cycle to stall at G1 (Fahraeus et al., 1996; Serrano et al., 1993). The p16 pathway responds to many non-genotoxic stimuli, though the mechanisms leading to its up-regulation are not as well knows as those for the p53 pathway (Jeyapalan and Sedivy, 2008). Interestingly E2F-DP also promotes the transcription of p16.

There appears to be some cross talk between these two pathways, as p21 and p16 both inhibit CDK4/6, maintaining RB activation. In addition, the gene that encodes p16,

CDKN2A, also encodes an alternate reading frame (ARF) protein, p14ARF, that inhibits Mdm2, a negative regulator of p53 (Clark et al., 2002; Gil and Peters, 2006; Kim and Sharpless, 2006; Ofir-Rosenfeld et al., 2008). In some instances the p53-21 and p16-RB pathways are induced by the same oncogenic activity, such as RAS, albeit through different mechanisms, while in other instances, the two pathways are independently activated (Di Micco et al., 2006; Mallette et al., 2007; Ohtani et al., 2001)

1-4) Biomarkers of Senescent Cell

The most prominent of the physiological changes that occurs in cells entering the senescent state is the loss of their ability to replicate (Hayflick and Moorhead, 1961; Jeyapalan and Sedivy, 2008). This inability to replicate should be distinguished from cellular terminal differentiation, observed in many somatic tissues, which also results in cessation of division. However, differentiated cells typically do not express the tumor suppressor pathways that are active in most senescent cells, and their exit from the cell cycle is the result of a controlled biological program, rather than a response to a critical failure in DNA maintenance (Campisi and d'Adda di Fagagna, 2007). While senescence has typically been described as an irreversible loss of the ability to replicate, some studies have shown that under certain conditions senescent cells can return to the cell cycle (Beausejour et al., 2003; Choi et al., 2011; Coppe et al., 2008; Dirac and Bernards, 2003; Kuilman et al., 2010). The loss or inactivation of some key components of both the p53 and RB pathways are required for such reentry, and as such are likely to represent events leading to tumorgenesis if they occur *in vivo*.

Cells that undergo senescence also display a range of changes to their usual morphology (Jeyapalan and Sedivy, 2008; Kuilman et al., 2010). Depending on the cell type and the triggering stimuli, these morphological changes can differ greatly. In human lung fibroblast cells, the usual fibroblastic morphology alters into a large and flattened change. This condition has also been observed in other cell types in stress induced and DNA damage induced senescence (Chen et al., 2001; Denoyelle et al., 2006; Parrinello et al., 2003; Serrano et al., 1997). Some senescence phenotypes caused by oncogene activation or tumor suppressor loss display a more varied array of morphologies (Chan et al., 2005; Denoyelle et al., 2006; Michaloglou et al., 2005).

Senescence-associated beta galactosidase (SA-ß-GAL) activity has been shown to increase in senescent cells, and has been widely used as a biomarker of cellular senescence (Debacq-Chainiaux et al., 2009; Dimri et al., 1995; Itahana et al., 2007; Kuilman et al., 2010; Satyanarayana et al., 2003). The elevated SA-ß-GAL activity in senescent cells is thought to result from an increase in the size of the cellular lysosomal compartment, the organelle to which the enzyme is localized (Kurz et al., 2000; Lee et al., 2006). The human genome encodes a single lysosomal beta-galactosidase (GLB1) whose pH optimum is 4.5 to match that of the organelle in which it resides however, due to the increased abundance of the enzyme in senescent cells, activity can be detected at the greatly sub-optimal pH of 6. The activity detectable at pH 6.0 has been designated as SA-ß-GAL, and provides a convenient mark of delineation between senescent and non-senescent cells (Lee et al., 2006; Yang and Hu, 2005).

Telomere dysfunction-induced foci (TIFs) are another important marker of senescence. These foci are identified by immunoflourescent labeling of a phosphorylated form of the

histone 2A variant H2AX, designated as γ-H2AX. γ-H2AX is found in nuclear foci which localize to sites of double strand breaks (d'Adda di Fagagna et al., 2003; Rogakou et al., 1998; Sedelnikova et al., 2004). Given that double strand breaks are a hallmark of telomere dysfunction, visualization of γ-H2AX foci by immunoflourescence can be used to identify sites of double strand breaks in intact nuclei (d'Adda di Fagagna et al., 2004; Herbig and Sedivy, 2006; von Zglinicki and Martin-Ruiz, 2005). Used in conjunction with the visualization of telomeres using fluorescence in situ hybridization (FISH) techniques, or immunoflourescent detection of telomere binding proteins such as TRF1, the TIFF assay can be used to identify colocalization of double strand breaks with telomeres (d'Adda di Fagagna et al., 2003; Herbig et al., 2004; Takai et al., 2003). The TIF assay has been used to identify senescent cells in either cell culture or tissue samples (d'Adda di Fagagna et al., 2003; Garcia-Cao et al., 2006; Herbig et al., 2006).

Another potential marker of senescenct cells are senescence-associated heterochromatin foci (SAHF), which have been identified in a subset of senescent cells (Kosar et al., 2011; Narita et al., 2003). These regions of highly condensed chromatin were first identified as bright punctate foci in DAPI-stained nuclei of senescent cells. These foci possess many, but not all common markers associated with heterochromatin found in replicating cells (Funayama et al., 2006; Narita et al., 2006; Zhang and Adams, 2007). SAHF are also noted for excluding constitutively heterochromatic regions such as telomeres and centromeres (Sedivy et al., 2008; Ye et al., 2007; Zhang and Adams, 2007; Zhang et al., 2007). Of the factors associated with SAHF, the histone 2A variant macro H2A (mH2A), which also associates with facultative heterochromatin in inactivated X-chromosomes,

has recently been shown to significantly increase with age in mouse, human, and baboon tissues (Kreiling et al., 2011; Zhang et al., 2005).

Senescent cells, regardless of the causal stimuli, exhibit a significant change in their transcriptome compared to replicating cells of the same cell type. In some cases these changes in transcription result in a greatly increased production and secretion of some extracellular proteins, such as cytokines, chemokines, extracellular matrix components, and matrix remodeling enzymes (Campisi, 2005; Krtolica et al., 2001). The secretion of a multitude of factors into the surrounding environment has been termed the senescence-associated secretory phenotype (SASP) (Coppe et al., 2008; Kuilman et al., 2010; Rodier et al., 2009). This change in the secretory behavior of senescent cells resembles in some aspects the behavior of cells undergoing an inflammatory response that accompanies wound healing (Campisi, 2005; Grinnell, 2003). Some, but not all of the factors associated with SASP are only present in senescent cells with persistent DNA damage and thus not all SASP factors are necessarily markers for all senescent cells (Kuilman et al., 2010; Rodier et al., 2009).

The reasons for the described changes in secretion are not well understood, however there are some interesting observations in regards to how the secreted factors affect neighboring cells. In some instances senescent cells co-cultured with pre-cancerous cells can cause an increase in their tumorgenic potential (Dilley et al., 2003; Krtolica et al., 2001; Parrinello et al., 2005; Yang et al., 2006). In other instances, secretion of the interleukin-6 cytokine and interleukin-8 chemokine, which are released during the inflammatory response, are required for cells to enter the senescent state under certain stimuli (Acosta et al., 2008; Kuilman et al., 2010; Kuilman et al., 2008). The modified

secretome of senescent cells appears to act in a contradictory manner, providing some pre-cancerous cells stimulation towards transformation, while suppressing others. It is possible that the complex secretions also activate the innate immune response, which then might act to clear pre-cancerous and/or senescent cells (Xue et al., 2007).

1-5) Senescence and Aging

Due to the relationships between senescence and aging, there are strong implications of a causal connection between the two, though it has been difficult to link them directly. Much work has shown that in aging organisms there is a reduced capacity for cellular replication compared to tissues of younger individuals. Tough not universally observed, there are data that indicate the *in vitro* capacity of cells, obtained from human subjects, as well as mice and non human primates, to replicate is inversely correlated to the age of the donor (Baerlocher et al., 2006; Bierman, 1978; Bruce et al., 1986; Cawthon et al., 2003; Cristofalo et al., 1998; Kimura et al., 2007; Martin et al., 1970; Schneider and Mitsui, 1976; Sugimoto et al., 2006). This would indicate that with progressing age, a larger proportion of replicating cells within the organism have undergone increased rounds of replication, thus bringing them closer to the end of their replicative lifespan. In addition, samples obtained from patients suffering from severe progeroid conditions, such as Werner's syndrome, dyskeratosis congenita and aplastic anemia, show a similar reduction in proliferative capacity when compared to cells obtained from similarly aged healthy individuals (Blasco, 2005; Chang et al., 2004; Crabbe et al., 2007; Goldstein et al., 1989; Huang et al., 2008; Lebel and Leder, 1998; Mason and Bessler, 2004; Multani and Chang, 2007). Studies on multiple different human tissues in culture have shown that

cells loose 33-120 base pairs of telomeric DNA per round of replication (Cawthon et al., 2003; Olovnikov, 1973; Sfeir et al., 2005). Tissue comparisons from subjects covering the range of the human lifespan have indicated that this rate of telomere attrition seen *in vitro* corresponds to an *in vivo* loss of telomere length as well.

However, whether or not replicative senescence plays a role in aging has been debated, as there is no direct evidence that sufficient numbers of cells reach telomere crisis (or other forms of senescence) to have a physiological impact on the organism within its natural lifespan. Some evidence has been obtained from patients with the premature aging (progeroid) diseases dyskeratosis congenita and aplastic anemia. In the case of diskeratosis congenita, a mutation in the gene coding for the RNA sub-unit of human telomerase (hTERC) (Vulliamy et al., 2001), or for Dyskerin, a pseudouridine synthase that plays a role in both ribosomal RNA (rRNA) processing and telomerase formation (Heiss et al., 1998), leading to impaired telomerase activity and dysfunctional bone marrow (Marciniak et al., 2000; Vulliamy et al., 2001; Vulliamy et al., 2004). Aplastic anemia is a similar condition arising from mutations in the gene coding for the TERT reverse transcriptase component of telomerase, also resulting in reduced telomerase activity and loss of hematopoietic tissue in the bone marrow (Ball et al., 1998; Yamaguchi et al., 2005). Additionally mouse studies have provided evidence that telomere shortening could be a contributing factor to the aging phenotype. Normal mouse (*Mus musculus*) cells do not undergo replicative senescence for two reasons: first, they have very long telomeres that do not sufficiently degrade within the 2-3 year lifespan of this species, and second, the telomerase gene in mice is active, allowing for the regeneration of shortened telomeres (Kipling and Cooke, 1990; Prowse and Greider,

1995). Telomerease deficient mice, however, after several generations eventually do suffer from telomere crisis in a significant fraction of their cells, and exhibit a number of premature aging phenotypes (Blasco et al., 1997; Lee et al., 1998; Rudolph et al., 1999). Further, there are data that show overexpression of telomerase in mice leads to extension of median lifespan (Tomas-Loba et al., 2008).

In addition to evidence concerning the role that telomere attrition can play in triggering cellular senescence and contributing to a variety of aging phenotypes, there is considerable evidence of senescenct cells being found in increasing numbers in aged individuals. This has been obtained using several markers, and includes both replicative senescence and stress-induced premature senescence. First, a number of studies have documented an increased frequency of SA-β-GAL positive cells in biopsies of tissues obtained from aged or unhealthy human subjects when compared to young, healthy counterparts (Castro et al., 2003; Kurz et al., 2000; Matthews et al., 2006; Paradis et al., 2001; Price et al., 2002). As discussed previously, increased SA-β-GAL staining has been associated with increased lysosomal size that is a hallmark of many senescent cells (Kurz et al., 2000; Lee et al., 2006; Yang and Hu, 2005). The double strand break marker γ-H2AX is typically observed in senescent cells, and both TIF and non-TIF γ-H2AX foci appear with increased frequency in cells of old tissues (Herbig et al., 2004; Jeyapalan et al., 2007; Sedelnikova et al., 2004). It should be kept in mind that non-TIF γ-H2AX foci are simply a marker of double strand breaks, which may result from DNA damage or genotoxic stress not associated with cellular senescence. The components of the p53 and RB signal transduction pathways are also useful markers for the identification of senescent cells (Atadja et al., 1995; Bunz et al., 1998; Lin et al., 1998; Serrano et al.,

1997; Stein et al., 1990; Vaziri et al., 1997; Wei et al., 2001). p16 has been shown to be up-regulated in most if not all senescent cells due to a variety of stimuli. Several tissues of humans, mice and non-human primates have been documented to express increased p16 with age (Campisi, 2005; Michaloglou et al., 2005; Ressler et al., 2006; Serrano et al., 1997; Zindy et al., 1997). Evidence is also accumulating, using some of the markers discussed above, that senescent cells may increase in frequency at sites of several pathological conditions including osteoarthritis, atherosclerosis, dementia, cirrhosis and respiratory disease (Flanary et al., 2007; Kong et al., 2011; Matthews et al., 2006; Minamino and Komuro, 2007; Muller et al., 2006; Price et al., 2002; Tsuji et al., 2006; Vasile et al., 2001; Wiemann et al., 2002).

There are two ways in which it has been hypothesized that senescent cells might directly contribute to the aging phenotype (Collado et al., 2007). The first is by the simple accumulation of senescent cells as the organism ages (Campisi, 2005; Collado et al., 2007; Sharpless and DePinho, 2004). As time progresses, an increasing fraction of cells would be expected to enter into a senescent state, and as they are believed to be resistant to apoptosis, they would persist. The altered physiology of the senescent cells is not likely to be compatible with their pre-senescent function in the tissue, and as such could lead to tissue or organ failure if enough were to accumulate. Additionally, the senescent secretome has the potential of inducing inflammation in the surrounding environment, leading to higher levels of stress in tissues that accumulate senescent cells. Evidence of this effect can be seen in the amelioration of the aging phenotype in mouse BubR1 hypomorphs when p16 positive senescent cells are conditionally cleared from their systems (Baker et al., 2011).

The second way in which senescence could contribute to aging is by the depletion of the regenerative capacity of tissues, by diluting or exhausting the pools of adult stem cells. Most cells in the adult human are post-mitotic and fully differentiated and have a finite chronological lifespan. Accordingly, humans rely on a small population of undifferentiated stem-cells to replenish and repair damaged tissue (Chambers et al., 2007; Krishnamurthy and Sharpless, 2007; Pollina and Brunet, 2011; Sharpless and DePinho, 2007). Stem-cells have been identified in almost all tissue types including epithelial, muscle and neuronal, and play important roles in the replenishment of high-turnover tissues, as well as damage repair and wound healing in low turnover tissues (Beltrami et al., 2003; Lois and Alvarez-Buylla, 1993; Morrison and Weissman, 1994). Stem cells have been shown to acquire very similar senescent phenotypes as the more widely studied fibroblasts with increased passage and age *in vivo* (Chambers et al., 2007; Morrison et al., 1996). In addition, the replicative capacity of stem cells has been shown to decrease with age, a strong indicator that these cells are undergoing senescence, and thus limiting the ability of tissues to regenerate and heal, potentially leading to decline in health and to age related pathology (Krishnamurthy and Sharpless, 2007; Pollina and Brunet, 2011).

Although the link between aging and senescence is not yet directly established the role of senescence as a cancer-suppression mechanism has been well documented (Campisi, 2005; Sager, 1991; Sharpless and DePinho, 2004; Wright and Shay, 2001). The removal from the cell cycle of a cell that has acquired aberrant growth control is one of the most powerful methods of preventing its development into cancer (Kong et al., 2011; Kuilman et al., 2010). In fact, an anti-cancer role was first proposed by Hayflick soon after the

discovery of the existence of senescence (Hayflick, 1965; Hayflick, 1976). The observation that one common trait of almost all metastatic cancers is the activation of the normally repressed telomerase gene, or acquisition of alternative methods to maintain telomere length, is further evidence of this connection(Bryan et al., 1995; Kim et al., 1994; Muntoni and Reddel, 2005; Shay and Bacchetti, 1997). Additionally, the pivotal roles that the two canonical tumor suppressors p53 and RB play in the promotion and maintenance of the senescent state contribute to the idea that senescence is an anti cancer mechanism (Campisi, 2005; Hanahan and Weinberg, 2000; Kim and Sharpless, 2006; Lowe et al., 2004).

The apparent contradiction between the presumed deleterious effect of cellular senescence during aging, and the beneficial one as a cancer-suppression mechanism, has been reconciled by invoking a principal of antagonistic plieotropy. According to this hypothesis, senescence would contribute to the fitness of the organism by activating inhibiting (or removing) potentially harmful pre-cancerous cells. In young organisms, due to the stochastic nature of oncogenic mutations, these occurrences would be rare and the senescence response to damage and aberrant replication would be minimal. As organisms age however, they accumulate DNA damage and other stressors that can lead to dysfunction in normal cellular physiology. Additionally, continued replication of cells for natural regenerative processes leads to the erosion of the telomeres. Under these conditions, the senescence response becomes more frequent with time, and the accumulation of senescent cells could then provide further stressors, leading or contributing to the aged phenotype. This potential feedback situation can be inferred from studies of the altered secretory behavior of senescent cells. Such cells begin to secrete

matrix metalloproteases and cytokines, which lead to a local inflammation response, likely causing increased stress to surrounding cells, and even potentially promoting their senescence. Given that the deleterious and pro-aging manifestations of senescence are likely to occur at a post-reproductive age, they would be largely removed from the effects of natural selection. Through such antagonistically pleiotropic connections between senescence, cancer and aging, the seemingly contradictory notion that aging, which should not be under the influence of natural selection, can be regulated by highly conserved mechanisms, can be somewhat resolved.

1-6) Chromatin Organization

Maintaining the integrity of the genetic information contained within the DNA of each cell is of crucial importance to the survival of any organism. To that end, the relatively delicate DNA molecule in each chromosome is packaged and secured into a complex nucleoprotein structure, which is critical for the regulation of gene transcription, as well as DNA replication and repair (Berger, 2007; Groth et al., 2007; Guenther et al., 2007; Li et al., 2007; Munoz-Najar and Sedivy, 2011; Zhang and Reinberg, 2001). The basic unit of chromatin, called the nucleosome, is composed of an octomer of histone proteins, two each of the core histones H2A, H2B, H3 and H4 that form a compact structure around which 147 base pairs of DNA is wrapped (Kouzarides, 2007; Luger et al., 1997). The histone proteins are primarily globular, but possess unstructured tails at their N-terminals that protrude from the core nucleosome structure, and contain sites for a multitude of posttranslational modifications (Jenuwein and Allis, 2001; Khorasanizadeh, 2004; Kouzarides, 2007; Margueron et al., 2005). Modifications to the histone tails, as well as

direct methylation of DNA on cytosine residues, can promote conformational changes in the organization of the basic structure of chromatin (Bird, 2002; Gonzalo, 2010; Kouzarides, 2002; Kouzarides, 2007; Munoz-Najar and Sedivy, 2011; Sedivy et al., 2008).

The modifications of chromatin can also lead to changes in the higher order structure of chromosomes. Two basic primary states of chromatin on a genome-wide scale have been described: euchromatin and heterochromatin (Grewal and Jia, 2007). Euchromatin has a structure that is more accessible to, and associated with transcriptional machinery and active transcription. The distribution of euchromatin can differ from cell to cell and change with time due to regulation by epigenetic factors. Heterochromatin is characterized by being highly compacted with closely and regularly spaced nucleosomse, leading to a highly ordered structure. This level of chromatin compaction makes access to the DNA by enzymes and non-histone proteins difficult, and these regions are typically associated with a high degree of gene silencing, DNase resistance and genomic stability (Li et al., 2007; Weaver et al., 2007). Heterochromatin can be further categorized as either constituative or facultative (Munoz-Najar and Sedivy, 2011; Trojer and Reinberg, 2007). Facultative heterochromatin is dynamic: while it is associated with gene silencing, the regions in which it is found, and the genes affected by this silencing, can change depending on the tissue, specific cell type, location or even over time within the same cell, much like euchromatin (Grewal and Jia, 2007; Heard, 2005). Constitutive heterochromatin tends to inhabit the same chromosomal regions in all cells regardless of tissue type, is stable throughout the life of the organism, and is rarely if ever in a euchromatic state. These regions of the genome are usually associated with particular

structural functions, such as telomeres, centromeres and highly repetitive transposable elements (Munoz-Najar and Sedivy, 2011).

Repetitive DNA accounts for approximately half of the total human genome (Lander et al., 2001; Smit, 1996). Some of these sequences are very small and highly conserved, forming functional components of the higher chromosomal structure. These include minisatellite tandem repeats which are associated primarily with the telomeres and sub-telomeric regions, alpha satellite DNA that forms a component of the centromere and centrosomes, and gamma satellite DNA that is found in the pericentromeric DNA, acting as a boundary to prevent the spread of constitutive centromeric heterochromatin to the rest of the chromosome (Kim et al., 2009; Yunis and Yasmineh, 1971). The great majority of repetitive sequences in the genome are comprised of a variety of transposable elements. These are sequences of DNA that can autonomously replicate and relocate around the genome when the proper enzymes are available. There are two classes of transposable elements, class 1 and class 2. Class 2 are DNA transposons: they utilize a transposase enzyme to excise their DNA sequence from one site in the genome, and reinsert it in another. The relative abundance of the class 2 transposable elements in the human genome is quite small, and there are believed to be no currently active elements within this class. The class 1 transposable elements are referred to as retrotranspososns. They transpose through an RNA intermediate that is transcribed from the donor site, converted back into DNA using reverse transcriptase, and the resulting DNA fragment inserted elsewhere in the genome. The class 1 transposable elements are further subdivided into endogenous retroviruses, long terminal repeat (LTR)-RNA transposons (derived from retrovirus sequences), long interspersed elements (LINEs), and short

interspersed elements (SINEs). Of these, only LINEs and SINEs are believed to be currently active in the human genome, and have proliferated to a large degree in the preceding tens of millions of years. There are approximately 800,000 copies of the LINE L1, and 1,000,000 copies of the SINE Alu (Lander et al., 2001). Together these two retrotransposon elements make up roughly one third of the human genome, with L1 being 17% and Alu 11% of the total (Richard et al., 2008). A fraction of retrotransposable elements have been shown to be transcriptionally active at detectable levels human somatic cells (Belancio et al., 2010; Faulkner et al., 2009; Rangwala et al., 2009), and have been shown to increase in activity under certain conditions: L1 elements transcripts are highly up-regulated in cancer (Skowronski et al., 1988; Skowronski and Singer, 1985), while Alu elements were shown to be induced by genotoxic stresses (Hagan et al., 2003; Li and Schmid, 2001; Liu et al., 1995; Rudin and Thompson, 2001). It is important to note though, that while the transcriptional activity of these retrotransposable elements is detectable, the activity is quite small when normalized to actual element number in the genome, indicating that the majority of these retrotransposable elements are inactive. Since heterochromatinization is thought to be the primary mechanism for the inactivation of retrotransposable elements it is important to see if redistribution of heterochromain in senescent cells has an effect on the regulation of retrotransposable elements (Conley et al., 2008; Liu et al., 1994; Phokaew et al., 2008; Yang and Kazazian, 2006). Also, considerable evidence implicates senescence as a mechanism to respond to DNA damage and prevent oncogenic transformation, examining the chromatin status of these elements in senescent cells should provide further insight into how replicative senescence may play a role in aging.

1-7) Epigenetic Modifications

Epigenetics is a term used to describe chromosomal modifications that do not involve the alteration of the genomic DNA sequence, yet do result in observable and heritable cellular phenotypes (Berger et al., 2009; Goldberg et al., 2007). Epigenetic modification and regulation contributes to the differential expression patterns of genes, both spatially and temporally. The remodeling of chromatin by epigenetic modifications has been found to be an important regulatory mechanism of gene activity (Li et al., 2007). While loss of telomeric sequences and the accumulation of mutations and DNA damage are all genetic alterations that lead to the senescent state, the sweeping changes that occur in response to these stimuli to induce senescence, and which must be maintained in order to sustain this altered cell state, are believed to be under epigenetic regulation (Adams, 2007a; Denoyelle et al., 2006; Herbig et al., 2006; Narita, 2007). The primary mechanisms through which chromatin modifications are mediated are histone modifications and DNA methylation (Gonzalo, 2010; Kouzarides, 2007).

1-7A) CpG Methylation

Of the modifications attributed to epigenetic regulation and chromatin organization, DNA methylation is the only one that occurs as a modification of the DNA molecule itself. Cytosine residues present as CpG dinucleotides can be methylated, and these dinucleotide pairs are found in abundance proximal to the promoters of genes where they are referred to as CpG islands (Bird, 2002; Klose and Bird, 2006). CpG islands tend to be found in an unmethylated state in genes that are actively transcribed, and methylation of these sites has been shown to be a strong indicator of transcriptional repression (Goll and Bestor,

2005). DNA methylation is also associated with condensed heterochromatin in silenced regions (Ballestar and Esteller, 2005; Bernstein et al., 2007; Eden et al., 1998; Klose and Bird, 2006). DNA methylation is catalyzed by the DNA methyltransferases (DNMTs), which methylate the C-5 of the cytosine nucleotide (Okano et al., 1999; Okano et al., 1998). DNMT3a and DNMT3b methylate cytosines in a *de novo* fashion, while DNMT1 methylates newly replicated DNA to maintain the previously established methylation pattern (Chen et al., 2004; Okano et al., 1999; Okano et al., 1998).

1-7B) Histone modifications

Histone modifications encompass a wide array of post-translational additions to the N-terminal domains that protrude from the central nucleosome core structure (Gonzalo, 2010; Kouzarides, 2007; Li et al., 2007). These domains are subject to acetylation, methylation, phosphorylation, ubiqutination, ADP-ribosylation, and sumolation. Of these, histone methylation and acetylation have been characterized the most extensively and their role in regulating gene activity and chromatin structure has been, at least in part, elucidated (Nowak and Corces, 2004; Shilatifard, 2006; Sterner and Berger, 2000). These modifications can function to alter the structure of chromatin either by altering the association of nucleosomes and DNA, or by acting as a binding platform for the recruitment of additional, non-histone proteins (Kouzarides, 2007).

Acetylation of histones occurs on lysine residues, and the acetylation state has an effect on the transcription of associated promoters. Histone acetylation is generally associated with transcriptional activation, and can act as a platform for the binding of additional chromatin modification complexes (Dhalluin et al., 1999; Grunstein, 1997; Hassan et al., 2002; Jacobson et al., 2000; Kuo and Allis, 1998). Conversely, loss of acetylation has

been associated with the repression of transcription, and a transition to a more closed chromatin state (Pena et al., 2006; Pruitt et al., 2006; Shi et al., 2006; Sterner and Berger, 2000; Vaquero et al., 2004).

Histone methylation has a variable effect on the transcriptional state of the genes in the vicinity of the modified nucleosomes, depending both on the specific residue that has been methylated, and the degree to which it has been methylated(Gonzalo, 2010; Kouzarides, 2007). The lysine and arginine residues on histones 3 and 4 are the most studied targets of methylation. Lysine residues H3K4, H3K9, H3K27, H3K36, H3K79 and H4K20 are some of the targets of these modifications (Feser and Tyler, 2011; Gonzalo, 2010). Of these, H3K4, H3K36, and H3K79 are associated with active transcription, while H3K9, H3K27 and H4K20 are associated with heterochromatin formation and gene repression (Kouzarides, 2002; Li et al., 2007; Mikkelsen et al., 2007).

1-8) Chromatin Modifications Associated with Aging and Senescence

The changes in transcription profile in aging and senescent cells have been well documented, along with a reorganization of distribution of nucleosomes (Gruber et al., 2010; Hardy et al., 2005; Ishimi et al., 1987; Macieira-Coelho and Puvion-Dutilleul, 1989; Shelton et al., 1999). There are a significant number of factors that are likely to play important roles in the remodeling of chromatin and changes in epigenetic control that are increasingly being associated with cellular senescence and aging (Adams, 2007a; Feser and Tyler, 2011; Gonzalo, 2010; Jeyapalan and Sedivy, 2008; Kuilman et al., 2010; Sedivy et al., 2008). The DNA in senescent cells has been shown to be hypomethylated on a global scale, indicating a possible decrease in the extent of heterochromatinization,

and consequent effects on gene regulation (Bjornsson et al., 2008; Fuke et al., 2004; Romanov and Vanyushin, 1981; Singhal et al., 1987; Wilson and Jones, 1983; Wilson et al., 1987). There are certain loci, however, primarily associated with CpG islands, where marked increases in methylation have been observed (Ahuja et al., 1998; Fraga and Esteller, 2007; Issa et al., 1994; Issa et al., 1996; Kim et al., 2005; So et al., 2011; So et al., 2006; Waki et al., 2003; Yatabe et al., 2001). The modifications in DNA methylation patterns could be attributed, at least in part, to changes in the expression and/or activity of DNMT1 and DMT3b. DNMT1 is responsible for maintaining DNA methylation patterns in heterochromatic regions during DNA replication, and has been shown to have decreased expression in aging cells resulting in reduced enzyme activity, whereas DNMT3b methylates *de novo* sites, and is upregulated with age and has increased activity (Casillas et al., 2003; Fraga and Esteller, 2007; Gonzalo, 2010). These changes in DNMT activity could explain why DNA methylation in heterochromatic regions decreases, while certain CpG islands, associated with euchromatin, increase in methylation levels.

The family of lysine deacetylases known as sirtuins (named after the Silent Information Regulator (SIR) proteins initially discovered in yeast), have been found to impact aging in diverse species, including *Caenorhabditis elegans*, and *Drosophila melanogaster* (Kaeberlein et al., 1999; Lin et al., 2000; Rogina and Helfand, 2004; Sinclair and Guarente, 1997; Tissenbaum and Guarente, 2001; Wang and Tissenbaum, 2006). Mammalian genomes encode seven members of the sirtuin family, SIRT1-SIRT7. SIRT1, 3, 6 and 7 are located in the nucleus and may play a role in the chromatin modifications associated with the senescence response and aging(Mao et al., 2011; Nemoto et al., 2005; Scher et al., 2007; Tsai et al., 2012). SIRT3, 4 and 5 are located in the mitochondria

where they play a role in cellular metabolism and insulin secretion (Haigis and Guarente, 2006; Haigis et al., 2006; Scher et al., 2007). SIRT2 is the only sirtuin to be found predominantly in the cytoplasm, where it is thought to play a role in cell cycle regulation through the deacetylation of tubulin (Dryden et al., 2003; Haigis and Guarente, 2006). Sirtuins are unique among all other deacetylaces in that their enzymatic activity is nicotinamide adenine dinucleotide (NAD) dependent. Sirtuins deacetylate not only histones but also a wide variety of other proteins, some of which are important regulators, such as p53 (Luo et al., 2001; Vaziri et al., 2001) ERRα (Wilson et al., 2010), PGC1 (Rodgers et al., 2005), AMPK (Canto et al., 2009), NFkB(Yeung et al., 2004). SIRT1 expression has been noted to decrease with age in mouse tissues that have high mitotic activity, and is also reduced in both mouse and human cells where mitotic activity ceases due to replicative senescence (Sasaki et al., 2006). The deacetylation of p53 by SIRT1 reduces its activity (Vaziri et al., 2001), and hence a reduction of SIRT1 activity would correlate with the up-regulation of p53 activity seen in many senescent cells. Up regulation of SIRT1 expression by the chemical resveratrol in mouse models has failed to reproduce the same lifespan extending phenotypes seen in yeast, worms and flies, however, these animals do show reduced signs of age related disease and have an extended health-span, indicating the role of SIRT1 in maintaining or prolonging healthy metabolic processes (Pearson et al., 2008). SIRT6 is an ADP-ribosyl-transferase, and plays a role in DNA damage repair (Liszt et al., 2005; Mostoslavsky et al., 2006). Down regulation of SIRT6, which is necessary for DNA base excision repair, can lead to a premature aging phenotype, likely through constitutive activation of the DNA damage response (Mostoslavsky et al., 2006). SIRT7 plays a role in the transcription of ribosomal

RNA (rRNA), implicating it as a moderator of cellular metabolism (Ford et al., 2006). SIRT7 expression is high in proliferating tissues, but low in non proliferating ones (Ford et al., 2006). SIRT2 deacetylates tubulin and plays a role in mitotic cycle progress, development and differentiation. The role this Sirtuin plays in senescent cells is currently not established, but studies have revealed accumulation of the SIRT2 protein in mouse neuronal tissue with age and it is thought to be a contributor to age related neurodegeneration (Maxwell et al., 2011; Pfister et al., 2008; Suzuki and Koike, 2007). SIRT3, 4 and 5 are located in the mitochondria where they play a role in cell metabolism (Finkel et al., 2009; Guarente, 2011; Haigis and Sinclair, 2010; Verdin et al., 2010). SIRT3 has been shown to mediate oxidative stress by activating antioxidant enzymes (Qiu et al., 2010; Tao et al., 2010). The roles, if any, SIRT3, 4 and 5 play in either senescence or aging have not been established.

Several changes in histone modification have been documented to occur during aging and cellular senescence. Histone acetylation at lysine residues act as binding platforms for transcription factors and chromatin-remodeling complexes (Dhalluin et al., 1999; Hassan et al., 2002; Jacobson et al., 2000). Lysine acetylation is generally associated with transcriptional activity and DNA repair, while loss of acetylation indicates a closed and inactive chromatin state (Grunstein, 1997; Jacobson et al., 2000). The Sir2 protein and mammalian homolog SIRT1, described previously, are histone deacetylases, and SIRT1 deacetylates H4K16 and H3K9 (Pruitt et al., 2006; Vaquero et al., 2004). As discussed previously, SIRT1 expression decreases in senescent cells, and interestingly, is upregulated in a large number of human cancers that also have a loss of H4K16 acetylation (Fraga et al., 2005).

In addition to changes in acetylation, the methylation state of a number of histone residues is also an important factor in the regulation of heterochromatin structure (Lachner et al., 2003; Martin and Zhang, 2005; Shilatifard, 2006). Methylation of H3K9, H3K27, and H4K20 is associated with transcriptional repression while H3K4, H3K36 and H3K79 methylation is associated with transcriptional activation (Kouzarides, 2002) H3K4me3 associates with genes that are transcriptionally active, while H3K27me3 associates with transcriptionally repressed genes (Mikkelsen et al., 2007). H3K36me3 indicate sites of non-coding RNA (ncRNA), while H3K9me3 and H4K20mes associate with structural heterochromatin domains such as pericentric and telomeric heterochromatin (Mikkelsen et al., 2007). Methylated H3K9 acts as a binding site for heterochromatin protein 1 (HP1) and methylated H3K27 is a binding site for polycomb group (pgc) proteins (Zhang and Reinberg, 2001). Changes in the methylation patterns of these histone residues have been observed in aging tissues as well as senescent cells. Early studies showed a decline in overall H3 and H4 methylation in rats with age (Thakur and Kanungo, 1981). More specific studies have shown an increase in H4K20me3 in aged rat liver and kidneys (Sarg et al., 2002). Experiments using senescence-accelerated prone mouse 8 (SAMP8) have shown a number of changes in histone methylation associated with age in this model system. H4k20me and H3K36me3 decreased in the brain while while H3K27me3, H3K79me and H3K79me2 increased (Wang et al., 2010). Specific genomic loci have also been reported to undergo changes in histone modification during senescence. As mentioned previously, H3K27me3 acts as a binding site for PcG proteins which are important repressors of the ink4a/ARF locus (Agherbi et al., 2009). The PcG proteins make up two distinct complexes; Polycomb complex 2 (PRC2),

composed of EZH2, EED and Suz12 which acts as the initiation complex, and Polycomb complex 1 (PRC1), containing RNF2, HPC and BMI1 which acts as a maintenance complex (Cao and Zhang, 2004; Kuzmichev et al., 2004). In young mouse embryonic fibroblasts (MEFs) the PcG complexes bind to and repress the Ink4a/ARF locus which contains H3K27me3, allowing for progression through the cell cycle (Core et al., 2004; Gil and Peters, 2006). When these cells senesce, there is a loss of H3K27me3, and as such the PcG complexes disassociate with the Ink4a/ARF locus which becomes active and halts cell cycle progression (Agherbi et al., 2009).

In addition to histone post-translational modifications (PTM), there are changes in the abundance of total histone proteins, as well as histone variants which contain alternative amino acid sequences from the canonical histones. A decrease in H3 variants 1 and 2 (H3.1, H3.2), and H2A varient1 (H2A.1), and an increase in the H3 variant 3 (H3.3) and H2A variant 2 (H2A.2) have been reported in aged rat brain neurons and serially cultured human diploid fibroblasts (HDF) approaching senescence(Pina and Suau, 1987; Rogakou and Sekeri-Pataryas, 1999). Increased expression of the histone chaperone HIRA, responsible for the incorporation of H3.3 into nucleosomes was also noted (Adams, 2007b; Adams, 2009; DeRan et al., 2008; Jeyapalan et al., 2007). H3.3 unlike H3.1 and H3.2, is more easily removed from nucleosomes, and its increased abundance in senescent cells and aged tissue may result in changes to chromatin organization (DeRan et al., 2008; Feser and Tyler, 2011; Jin et al., 2009).

The Asf1A/B and CAF-1 chaperones which play a role in the disassembly and reassembly of chromatin during DNA replication, damage repair and transcription have been shown to have reduced abundance with passage in HDF (Eitoku et al., 2008; Feser

et al., 2010; O'Sullivan et al., 2010). Loss of these chaperones could lead to a disruption in the normal chromatin organization in senescent cells. Interestingly, an increase in the levels of the H2A variant macro-H2A (mH2A), and heterochromatin protein 1 beta (HP1ß) has been observed in senescent fibroblasts in culture, as well as in some mouse and primate tissues (Kreiling et al., 2011).

Currently the leading hypothesis is that there is an increase in heterochromatin in senescent cells (Adams, 2007a; Dang et al., 2009; Greer et al., 2011; Kreiling et al., 2011). This hypothesis is mostly supported by the presence in senescent cells of highly condensed chromatin, in the form of SAHF (Narita et al., 2003), as well as an overall increase in the abundance of heterochromatin constituents (Kreiling et al., 2011). HP1ß and mH2A are constituents of SAHF, and their formation is dependent on HIRA, all 3 of which are more abundant in senescent cells (Narita et al., 2003; Zhang et al., 2005).

1-9) Methods for Globally Evaluating Chromatin State

A number of assays can be used to evaluate on a genome-wide scale the abundance and localization of chromatin modifications, as well as the conformational stability and acessability of chromatin. These include assays to examine DNA methylation such as methyl-sensitive restriction PCR assays (Singer-Sam et al., 1990), sodium bisulfate assays (Frommer et al., 1992), and MethyLight (Eads et al., 2000); DNase sensitivity such as nucleosome phasing (Henikoff et al., 2011; Lohr et al., 1977), DNase-chip(Crawford et al., 2006), and DNase-seq(Song and Crawford, 2010); and chromatin conformation assays such as chromosome conformation capture (Hagege et al., 2007), circularized chromosome conformation capture (Zhao et al., 2006), and chromosome

conformation capture carbon-copy (Dostie et al., 2006); Chromatin Immunoprecipitation assays, XChIP (Breiling and Orlando, 2001), NChIP (O'Neill and Turner, 2003), and ChIP-loop (Simonis et al., 2007). Of these, cross-linked chromatin immunoprecipitation (XChIP) has been a popular method, which allows the targeting of individual proteins, or their post-translational modification, by using antibodies specific for these targets. The method also exploits cross-linking with formaldehyde to covalently stabilize short-range interactions between DNA and associated chromatin proteins (Bulyk, 2004; Luger et al., 1997; Solomon and Varshavsky, 1985). Following the shearing of cross-linked chromatin and immuneprecipitation, the DNA fragments that are pulled down can be isolated and analyzed by a variety of methods. This technique is particularly powerful for identifying the genomic binding regions and distribution of specific proteins, including histone modifications.

1-10) FAIRE

An interesting alternative technique, called formaldehyde-assisted isolation of regulatory elements (FAIRE), has been used to enrich DNA regions associated with open chromatin, as judged by correlation with other methods, including multiple histone marks, DNase sensitivity, and RNA polymerase occupancy.

FAIRE was pioneered in 2003 by the group of Jason Lieb, using *S. cerevisiae* as the model system, and shown to enrich regions of the genome just upstream of active genes (Nagy et al., 2003). Subsequent studies demonstrated that similar results could be obtained using human cells, whose genomic complexity is orders of magnitude higher than that of yeast (Giresi et al., 2007; Giresi and Lieb, 2009). The basis for this method

lies in the ability of phenol-chloroform extraction to segregate nucleic acids and proteins into the aqueous and organic phases. DNA normally partitions into the aqueous phase, however, upon formaldehyde crosslinking of chromatin, DNA is pulled into the organic phase by virtue of being covalently bound with histones. Genomic regions that are relatively free of nucleosomes or other proteins are thus enriched in the aqueous phase. This technique has been shown to enrich DNA associated with transcriptional start sites (TSS), active promoters, and DNase hypersensitive sites, and shows a negative correlation with nucleosome occupancy. Additionally, the frequency with which fragments were associated with the TSS of specific genes was correlated positively with the activity of that gene.

In any of the methods for isolating regulatory elements mentioned above, genome-wide profiling of the enriched fragments is done using one of two platforms; tiling microarrays or high-throughput sequencing. Microarrays typically employ oligonucliotide probes that represent all the unique regions of the genome fixed to a chip. The enriched DNA fragments are labeled, hybridized to the chips, and detected using fluorescence. The resolution is dependent on probe length and the size of the gap between probes. High-throughput sequencing relies on generating a library from the enriched DNA samples that contain primer sequences affixed to the fragment ends. These primer sequences are complementary to probes that are immobilized on a flowcell. The fragments anneal to the primer sequences and are sequenced as the complementary strand is elongated. Sequencing can be performed by collecting single end reads, or paired-end reads (Kircher and Kelso, 2010).

1-11) Repetitive Sequences

One major caveat for both these methods is the lack of information provided on repetitive regions of the genome. Microarrays omit these regions entirely, as the probes to detect these sequences are not present on the chip. In contrast, high-throughput sequencing returns data on all the fragments resent in the enriched DNA sample. However, mapping and quantifying reads derived from the repetitive portions of the genome is computationally challenging. Algorithms are currently being developed for these tasks. These efforts are aided by the continuing improvements of sequencing technologies, making the acquisition of long paired-end reads, which greatly aid the mapping, increasingly accessible. The repetitive regions of the genome are substantial (some 50% of total in humans), but understanding their chromatin structure will be important for obtaining a comprehensive picture of chromatin regulation during senescence.

Figure 1-1

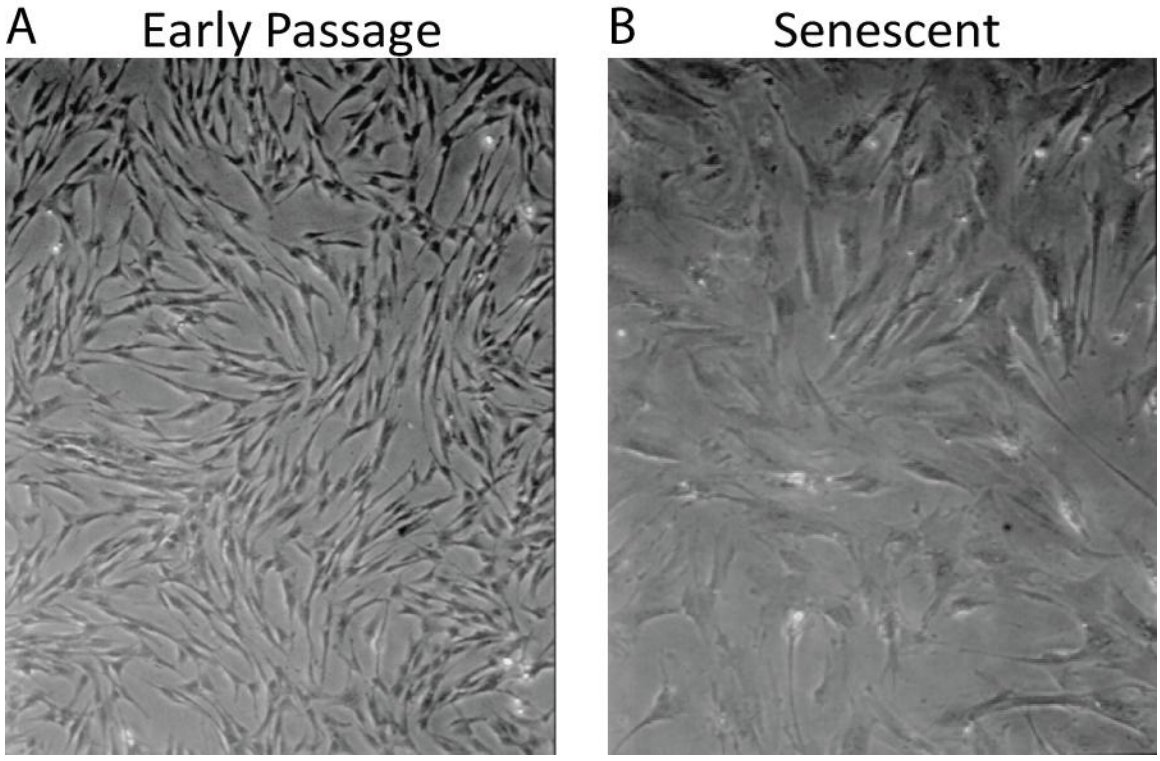

Figure 1-1 Morphologies of senescent human diploid fibroblasts.

Both images were obtained using the embryonic lung HDF strain designated LF1, under standard culture conditions (give reference). (A) A culture at low passage, in exponential growth phase. (B) A culture of the same strain passaged into senescence.

Figure 1-2

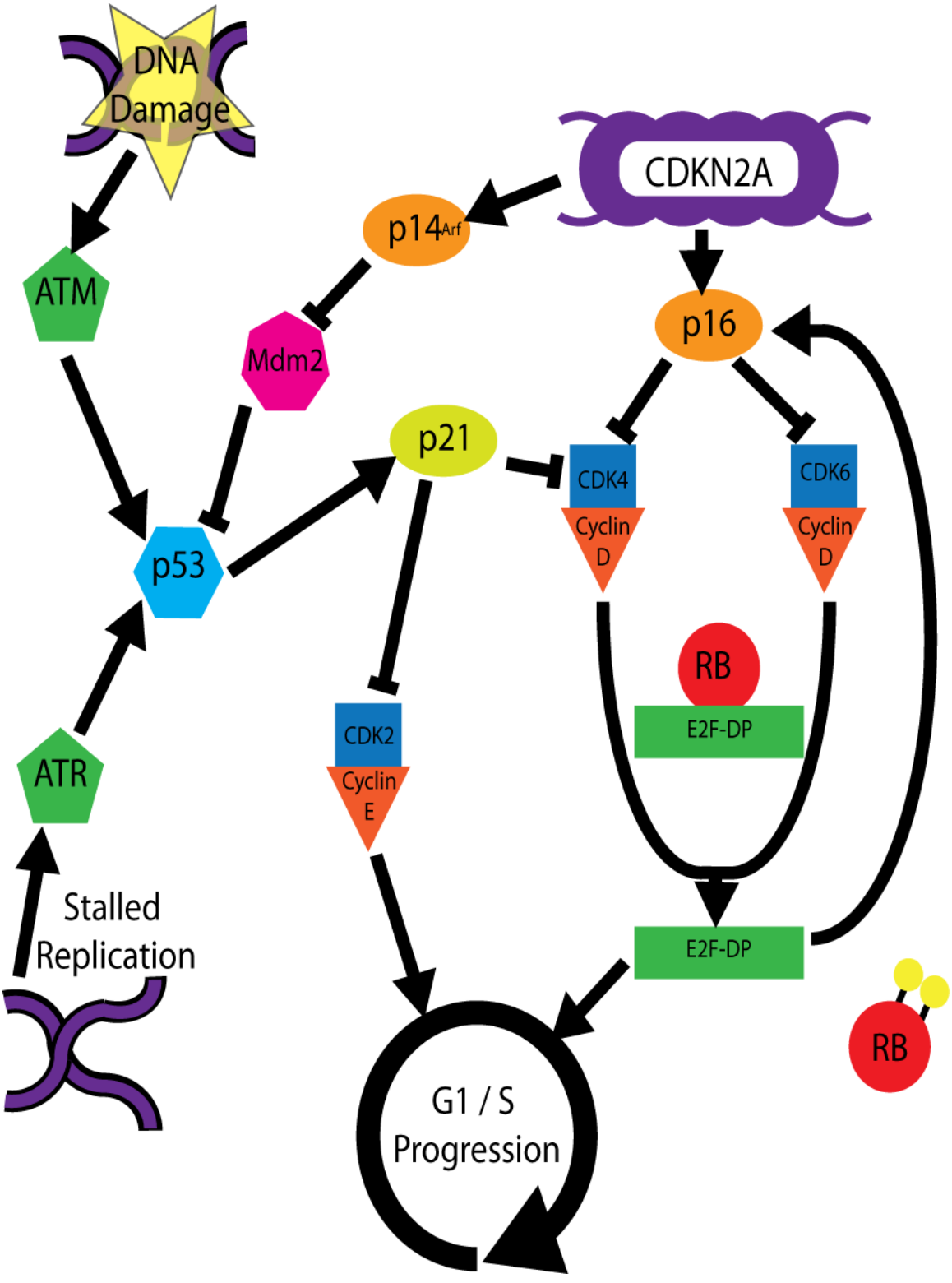
DNA Damage
CDKN2A
p14Arf
ATM
p16
Mdm2
p21
CDK4
CDK6
Cyclin D
Cyclin D
p53
RB
E2F-DP
CDK2
Cyclin E
ATR
Stalled Replication
E2F-DP
RB
G1 / S Progression

Figure 1-2 The p53 and RB pathways regulate senescence by arresting cells in G1 phase.

The CDKN2A gene expresses both $p16^{Ink4a}$ and p^{14Arf}. $p16^{Ink4a}$ inhibits CDK4 and CDK6 by preventing them from interacting with Cyclin D. $p14^{Arf}$ inhibits MDM2, an E3 ligase that targets p53 for degradation. p53 protein is activated by DNA damage signaling: double strand breaks and telomere dysfunction act through ATM, and DNA replication stalling acts through ATR. Activated p53 promotes the transcription of p21, which inhibits both CDK2 and CDK4/6 by binding to pre-formed CDK-cyclin complexes and inhibiting their kinase activity. CDK2 and CDK4/6 phosphorylate and inactivate RB. Inhibition of CDK2 and/or CDK4/6 thus maintains RB in its active form, which remains bound to the E2F-DP transcription factors and inhibits their activity. Since E2F-DP is required for the activation of genes necessary for progression into S phase, cells remain arrested in G1 phase.

Chapter 2: Materials and Methods

2-1) Methods for Chapter 3: FAIRE and Expression Microarray Analysis

2-1A) Cell Culture

Human diploid fibroblast cells (HDF) strain derived from embryonic fetal lung, designated LF1(Brown et al. 1997) was grown at 37^{o}C in an atmosphere of 5% CO_2 and 2.5% O_2 in F-10 nutrient medium (Thermo Scientific) supplemented with 10% fetal bovine serum, penicillin, streptomycin and L-glutamine (Brown et al., 1997; Herbig et al., 2004). Cells were serially passaged at 1:4 dilutions when reaching 80-90% confluence. For the preparation of FAIRE DNA cells were grown in 15 cm culture dishes and were collected at 80-90% confluence. To obtain senescent cells, cultures were propagated to replicative exhaustion (passage 50-52, approximately 100-104 population doublings). Cultures were monitored by microscopic observation every 2-3 days to assess cell division. When replication ceased, the cultures were incubated further for at least 4 weeks prior to harvesting.

2-1B) Formaldehyde Assisted Isolation of Regulatory Elements (FAIRE)

DNA was isolated from early passage cells (passage 12) and from senescent cells (passage 52) as described by the group of Jason Lieb (Giresi et al., 2007); (Giresi and Lieb, 2009). Cells were crosslinked by adding 37% formaldehyde directly to the culture media to a final concentration of 1% and incubating at room temperature for 4 minutes on a rotating platform. Formaldehyde was quenched by adding glycine to a final concentration of 125 mM and incubation was continued for an additional 10 minutes at

room temperature. The dishes were washed twice with 5 ml chilled phosphate buffered saline (PBS) (Sambrook and Russell, 2001). 1.5 ml PBS containing 1%PMSF was then added to each plate on ice, and the cells were dislodged using a cell scraper and transferred to a 15 ml tube. Non-crosslinked early passage and senescent cells were also processed in parallel as reference chromatin controls and are henceforth referred to as "input DNA". Early passage crosslinked cell samples were pooled from four 15cm dishes and, senescent crosslinked samples were pooled from five 15 cm dishes. Early passage control samples (input) consisted of one 15 cm dish, and senescent control samples (input) consisted of two 15 cm dishes. The cells were pelleted for 4 minutes at 2,000 rpm and 4^{o}C (Forma 3L GP 4500R centrifuge), The supernatant was aspirated, and the cell pellets were resuspended in 1 ml of FAIRE lysis buffer (2% Triton X-100, 1% SDS, 100mM NaCl, 10mM Tris-HCl pH 8.0, 1mM EDTA), transferred to 2 ml microcentrifuge tubes and further homogenized by brief vortexing. Cell suspensions were sonicated in an ice water bath using a Fischer Scientific Sonic Dismembrator model 500. Each sample received 5 sessions, 2 minutes in length with one second on and one second off at 25% intensity, followed by 2 minutes of rest incubation on ice. The samples were spun at maximum speed for 5 minutes at 4^{o}C in a table top microfuge to remove cellular debris, and the supernatants were collected in fresh 1.5 ml microfuge tubes for phenol extraction. The supernatants from each sample were divided evenly such that each microfuge tube had a maximum of 500 µl of supernatant. An equal volume of phenol:chloroform:isoamyl-alchohol 25:24:1 (Sigma) was added to each sample. Samples were mixed by vortexing at high speed for 30 seconds, and then centrifuged for 1 minute at 12,000 rpm in a table top microfuge at 4^{o}C. The top aqueous layer was

removed to a new tube and extracted again with an equal volume of phenol:chloroform:isoamyl-alchohol, while 500 µl of 10mM Tris-HCl pH 7.5, 1 mM EDTA (TE) was added to the remaining organic phase. Samples were again vortexed and centrifuged, aqueous phases were combined, and extracted a final time with an equal volume of phenol:chloroform:isoamyl-alcohol. DNA was precipitated by addition of 2 volumes of 95% ethanol, 0.1 volumes of 3 M sodium acetate, and glycogen to a final concentration of 20µg/ml. Pellets were resuspended in 50 µl 10 mM Tris-HCl pH 7.5 (without EDTA) and incubated at 37^{o}C for 2 hours with an RNase cocktail at a final concentration of 0.2mg/ml RNase A and 50U/ml RNase T1 (Fermentas). Proteinase K (Invitrogen) was then added to a concentration of 0.2mg/ml and the samples were incubated overnight at 65^{o}C. The DNAs derived from the same samples were pooled and all samples were adjusted to a volume of 500 µl with 10 mM Tris-HCl pH 7.5. A phenol extraction was performed as previously described, followed by an ethanol precipitation and resuspension in 100µl of 10mM TE.

2-1C) Affymetrix Tiling Microarrays

Affymetrix human tiling 2.0 arrays require 50µg of DNA for each full set. In order to prepare enough DNA for processing, FAIRE and input DNA were linearly amplified with Klenow (3’ exo-) enzyme using a random oligonucleotide priming protocol (NEB). In addition to template DNA, the reactions contained labeling buffer (NEB) supplemented with all dNTPs at 100 µM final concentration. 1µg of each sample was amplified for 2 hours at 37^{o}C in 50µl reactions and the reactions from each biological replicate were pooled, phenol extracted and ethanol precipitated. Klenow-amplified DNA samples were

sent to the Brown Center for Genomics and Proteomics for processing, where they were hybridized to Affymetrix Human Tiling 2.0 Arrays (Affymetrix).

The data from all tiling arrays were quantile normalized together (FAIRE / input DNA / early passage / senescent) to compare the signal level of different arrays, then a non-parametric test was applied to the comparison of the FAIRE and input DNA samples. The Wilcoxon rank sum test was used on all signals within a sliding window centered on each probe to compute a p value for signal enrichment, and to compute the fold-change between FAIRE and input probes for the early passage and senescent samples using the Hodges-Lehmann estimator.

K-means clustering with 2 clusters was performed on the linearly interpolated FAIRE signal from the +/-1500 bp window around the transcription start site to determine FAIRE enriched versus non-enriched TSS. Early passage and senescent signals were stacked for clustering, and then plotted separately.

FAIRE enrichment data was expressed as a heat map across the human chromosomes where the higher the enrichment signal, the brighter the image. The signal represents an averaged FAIRE signal of all probes within a sliding window with a range of 1Mb sliding every 100,000 base pairs.

2-1D) qPCR Peak Validation

Validation of array peaks was performed by qPCR on the FAIRE and input DNA samples, following Klenow amplification as described previously, in 25µl reactions using SYBR green Master Mix (Applied Biosystems) at default cycling conditions with a dissociation curve step. First, a set of 15 primers associated with orphan peaks across an

8,000 bp region of chromosome 21, as published by Jason Lieb's group, were used and are listed in Table S-1 (Giresi et al., 2007). Assays were run in triplicate for each biological replicate and standardized so that primer set 1 was set to background and FAIRE samples were then normalized to input DNA.

Following the analysis of our data we identified a number of peaks in our samples which were used for further verification. First a significant peak present in both senescent and early passage samples in the PPM1B house-keeping gene was seen in Integrated Genome Browser (IGB) (Nicol et al., 2009). PCR primers were designed to amplify 60-80 nucleotide fragments from genomic coordinates determined to be associated with the apex of the PPM1B enrichment peak, as well as flanking regions successively farther from the central peak. Quantitative PCR was performed as above (Table S-2A). Peak enrichment was determined for each primer set by calculating the ddCT between the peak and flanking primers using primer set PPM1B-1 as background and normalizing FAIRE to input DNA. Subsequently an additional 24 peaks were examined by qPCR for validity in this manner (Table S-2B).

2-1E) Gene- Expression Microarrays

Whole cell total RNA was harvested in biological triplicates from early passage and senescent cells using Trizol reagent (Invitrogen) according to the manufacturers instruction. RNA samples were sent to the Brown Center for Genomics and Proteomics, where they were processed and hybridized to Affymetrix Human Genome U133 Plus 2.0 Arrays. The data from all expression arrays were quantile normalized and processed using the full model gcRMA with mismatch probes (Smyth, 2005). The probesets were

annotated using all of the mappings in hgu133plus2 REFSEQ from Bioconductor. Data were collapsed to account for multiple probe sets mapping to a single gene. For each unique gene, the median expression of all probesets that mapped to the gene was used. Fold changes and p values were calculated using Limma (Smyth, 2005).

2-1F) Comparison of Expression and Tiling Microarray Data

18,549 out of 19,524 REFSEQ transcripts mapped to unique TSS identified in the clustering analysis of the FAIRE data, and 18,264 of these had unambiguous transcription start sites. Probe-sets, using this method, can be counted more than once, if they are annotated for more than one gene. In this case, there were 18,142 unique values for early passage cell expression, and 18,100 unique values for senescent cell expression, indicating that most of the probe-sets were only counted once. To examine correlations between a change in chromatin accessibility and fold-change in gene expression two lists of genes were generated: those that move from cluster 1 to cluster 2 between early passage and senescent cells (FAIRE-gain) and those that move from cluster 2 to cluster 1 (FAIRE-loss). A t-test analysis was run to compare fold change-gain to fold change-all and fold change-loss to fold change-all.

2-1G) FAIRE Signal to Gene Density Correlation

The mean positive FAIRE signal was calculated in non-overlapping windows of 100,000 bp across each chromosome. Additionally, for each window, the total number of unique TSS was counted. These data were then plotted against each other to generate a scatter

plot of FAIRE signal versus TSS content for each 100,000 bp window. The Spearman's rank coefficient was calculated for each plot, with the samples from replicating cells having a rho of 0.235 and the samples from senescent cells having a rho of 0.069.

2-2) Methods for Chapter 4: Analysis of Repetitive DNA Enrichment and Expression

2-2A) DNA isolation

For the dot-blot experiments DNA was isolated using the FAIRE procedure from early passage and senescent cells in biological triplicates as described in the previous section with the following alterations.

Non-crossinked cells were not used for control input DNA, instead, 0.1 volumes of the sonicated FAIRE lysate from each biological replicate was removed and decrosslinked in an overnight 65^{o}C incubation with 0.2mg/ml proteinase K prior to phenol extraction. Samples were then processed under the same conditions as described previously.

2-2B) Dot-blot Probe Design

The Alu probe was designed as a PCR amplified fragment of 285 bp in length based on the consensus sequence of the Alu element (Batzer et al., 1996; Weisenberger et al., 2005) . The primers used to amplify the probe were; forward (AluF) CTCACGCCTGTAATCCCAGC; reverse (AluR) TTGAGACGGAGTCTCGCTC (Figure 2-1A). The L1 probe was designed as a PCR amplified fragment approximately

383 bp in length based on sequences archived in L1 Base (Zemojtel and Penzkofer). The primers used to amplify the probe were; forward (L1F) TCGCCAAGTCAATCCTAAGC; reverse (L1R) AATGCCTAGGTTTTCTTCTAGGG (Figure 2-1B). The 3' ORF2 was chosen as the majority of L1 elements in the genome are 5' truncated (Coufal et al., 2009). The sequence of this template probe is subject to the natural variability of the L1 sequence, but showed >95% sequence homology with all full length L1 intact elements and full length L1 with ORF1 disrupted elements annotated in L1 Base. DNA fragments to be used for the preparation of radioactive probes were generated by performing PCR with the above-indicated primers on human genomic DNA, and purifying the resultant fragments on an agarose gel.

2-2C) Dot Bloting and Hybridization

DNA from the 3 biological replicates for each condition (early passage input, early passage FAIRE, senescent input, and senescent FAIRE) were deposited in serial 2-fold dilution (from 40ng to 2.5ng per spot) onto a positively-charged nylon membrane (BioRad) under alkaline conditions using a 96 well vacuum manifold. DNA was fixed by heat incubation at 80^{o}C for 2 hours. Membranes were washed in 0.5 X saline sodium citrate (SSC) buffer (Sambrook and Russell, 2001), 0.5% SDS for one hour at 65^{o}C in a rocking water bath within a sealed Tupperware container. Membranes were transferred to glass hybridization tubes and 15ml of 65^{o}C prehybridization solution (6 X SSPE (SSC additionally buffered with phosphate and containing EDTA,) (Sambrook and Russell, 2001), 5 X Denhardt's solution, 0.5% SDS, 100 µg/ml denatured herring sperm carrier

DNA) was added to each tube and incubated with rotation in a hybridization oven at 65^{o}C for 2 hours.

To prepare labeled 100 ng of Alu or L1 PCR amplified and gel purified fragments in a volume of 0.5 X TE were boiled in a 1.5ml microfuge tube for 2 minutes. The tubes were immediately placed in an ice water bath and 2µl of octadeoyribonucleotide 10 X labeling buffer (NEB) were added. dATP, dGTP and dTTP were added to a final concentration of 25 µM followed by 1 µl of Klenow (3' exo-) enzyme (NEB), and 2.5 µl of dCTP [α-32P] 6,000 Ci/mmol (Perkin Elmer). The reaction, pipetted to mix, and incubated at 37^{o}C for 1-2 hours. Labeling reactions were stopped by adding 1 µl of 0.5 M EDTA, and brought to a volume of 100 µl with TNE (Sambrook and Russell, 2001) (100mM Tris-HCl pH 7.4, 2.0 M NaCl, 10 mM EDTA). Unincorporated nucleotides were removed using Illustra microspin G-25 gel filtration columns (GE Biomedical) and the labeled probe was collected. 1 µl of the probe was tested for incorporation in a scintillation counter.

Hybridization buffer (5% dextran sulfate (Fisher Scientific), 6 X SSPE, 0.5% SDS) was in 50 ml conical tubes in a hot water bath to 65^{o}C. 100µl of labeled probe was added to 1 ml of 1.5 mg/ml carrier DNA, boiled for 2 minutes, and then added to the hybridization buffer. Prehybridization buffer was drained from the hybridization tubes containing the membranes, and replaced with the hybridization buffer. Membranes were hybridized for 24 hours. Washing was done twice for 10 minutes in 2 X SSC and 1% SDS at 65^{o}C, followed by a stringent wash at 60^{o}C in 0.1 X SSC and 0.1 % SDS for 30 minutes. The latter was repeated until the average background signal on the membrane fell below 200 cpm using a handheld Geiger counter. The membranes were exposed to storage phosphor screens over night and imaged on a Typhoon 9410. Alu blot 1 and L1 blot one indicate

the membrane that was originally hybridized with the respective probe. After the first hybridization, the membranes were stripped by a 30 minute wash in 0.4 M NaOH at room temperature, followed by a 10 minute wash in 1 M Tris pH 8 at room temperature and finally two 15 minute washes in 0.1% SDS/10 mM Tris pH 8 at room temperature. These washes were sufficient to remove any detectable probe signal using the Geiger counter, however to ensure no contamination from the previous probes affected the second hybridization the membranes were stored in 0.1% SDS/10 mM Tris pH 8 for two months and imaged on the Typhoon to determine that there was no residual signal. The membrane designated Alu blot 1 was used to hybridize the L1 probe and was re-designated L1 Blot 2, while the membrane designated L1 Blot 1 was hybridized with Alu probe and re-designated Alu Blot 2.

2-2D) Normalization of Dot Blots

The concentrations of the DNA samples used to prepare the dot blots initially determined using the Nano-Drop instrument (Thermo Scientific), and equivalent amounts of each sample were deposited in a dilution gradient on the membrane. To improve the accuracy fo the quantitative hybridization, careful qPCR measurements on the DNA samples used to prepare the membranes were performed. First, 5 primer sets (TNF1, ETF3, Z281, CCD1, C191), which were previously determined to be in FAIRE non-enriched regions of the genome for both early passage and senescent cells, were used to perform qPCR on highly purified human genomic DNA of known concentration to generate a standard curve (Figure 2-1A). The slope of the best fit line generated from this dilution series was then used to quantify the yield of qPCR reactions run on the FAIRE and input DNA

samples that were used to prepare the dot blots (Figure 2-1B, Table 2-1A). These effective DNA concentrations were then used to correct the amounts of DNA blotted on the membrane (Table 2-1B & C).

2-2E) Calculation of Signal Intensity and Enrichment

The signal intensity of each spot on the dot blot membranes was measured as the average pixel intensity within a circle with an area of 0.204 centimeters centered on the spot. Background and standard error were calculated by measuring 20 evenly spaced circles of equal size around the periphery of the membrane. The probe signal relative to total DNA was calculated by plotting the background-subtracted signal (Table 2-1D) intensity of each spot against the qPCR corrected DNA concentrations in that spot. A best-fit line was generated for each sample, and the signal was calculated from the equation of that line corresponding to a DNA content of 5 ng (Figure 2-2). 5 ng was chosen as each sample had at least one spot that was determined to be close to that value after the DNA concentrations were corrected. Biological replicates were then averaged, and FAIRE samples were normalized relative to their inputs. Finally, the data from the two separate blots, Alu-1/Alu-2 and L1-1/L1-2, were then averaged. Senescent FAIRE signals were normalized to early passage FAIRE signals to visualize the increase in FAIRE enrichment in senescent cells. Standard error was calculated at each step presented above and converted into % error. The % errors were carried through and combined at each successive calculation, and the final error bars reflect this combined error calculation.

2-2F) Multiplex Real-Time PCR

This assay was adapted from the quantitative PCR experiments described in Coufal et al., (2009). Total genomic DNA was isolated from 3 biological replicates of senescent and early passage cells. Mutiplex qPCR experiments were performed on ABI 7900 Fast Sequence Detection Instruments using Taqman Gene Expression Mastermix (Applied Biosystems). The primer and probe sets used in the assays were as follows: L1 ORF2: Probe: 5'-AGGTGGGAATTGAAC-VIC, Forward: 5'-CAAACACCGCATATTCTCACTCA, Reverse: 5'-CTTCCTGTGTCCATGTGATCTCA; L1 5' UTR: Probe: 5'-TCCCAGCACGCAGC-6FAM, Forward: 5'ACAGCTTTGAAGAGAGCAGTGGTT, Reverse: 5'-AGTCTGCCCGTTCTCAGATCT; 5S rDNA: Probe: 5'-AGGGTCGGGCCTGG-6FAM, Forward: 5'-CTCGTCTGATCTCGGAAGCTAAG, Reverse: 5'-GCGGTCTCCCATCCAAGTAC. The reactions were optimized by limiting reaction components until duplex reaction efficiencies were equal to individual reactions. The ORF2 probe was conjugated with the VIC flourophore while the 5' UTR and 5S rDNA control probes were conjugated with 6FAM. The relative copy number of ORF2 was calculated as the ratio of ORF2 to control probe and normalized relative to the lowest early passage cell value.

2-2G) Transposable Element Expression Analysis

The expression activity of LINE-1 and Alu elements was determined using quantitative PCR methods. Total RNA was prepared from biological triplicates of early passage and senescent cells using Trizol reagent (Invitrogen). 1 µg of total RNA was transcribed into cDNA in 50µl reactions using the Taqman Kit (Applied Biosystems) supplemented with

poly-T primers, according to the manufacturer's protocol. 1 µl of this reaction was used for each sample in subsequent qPCR reactions. qPCR analysis was performed using SYBR Green Master Mix (Applied Biosystems) as described previously. Reactions for L1 expression used the L1 ORF2 forward and reverse primers described in the Multiplex analysis. Alu transcription primers were based on the expressed Alu repeat (EAR) as described by Marullo et al., (2010). The EAR primers were: forward: 5'-GAGGCTGAGGCAGGAGAATCG, and reverse: 5'-TGTCGCCCAGGCTGGAGTG. In each experiment GAPDH was used as the normalization control, and relative expression was further normalized to the lowest early passage sample.

Figure 2-1

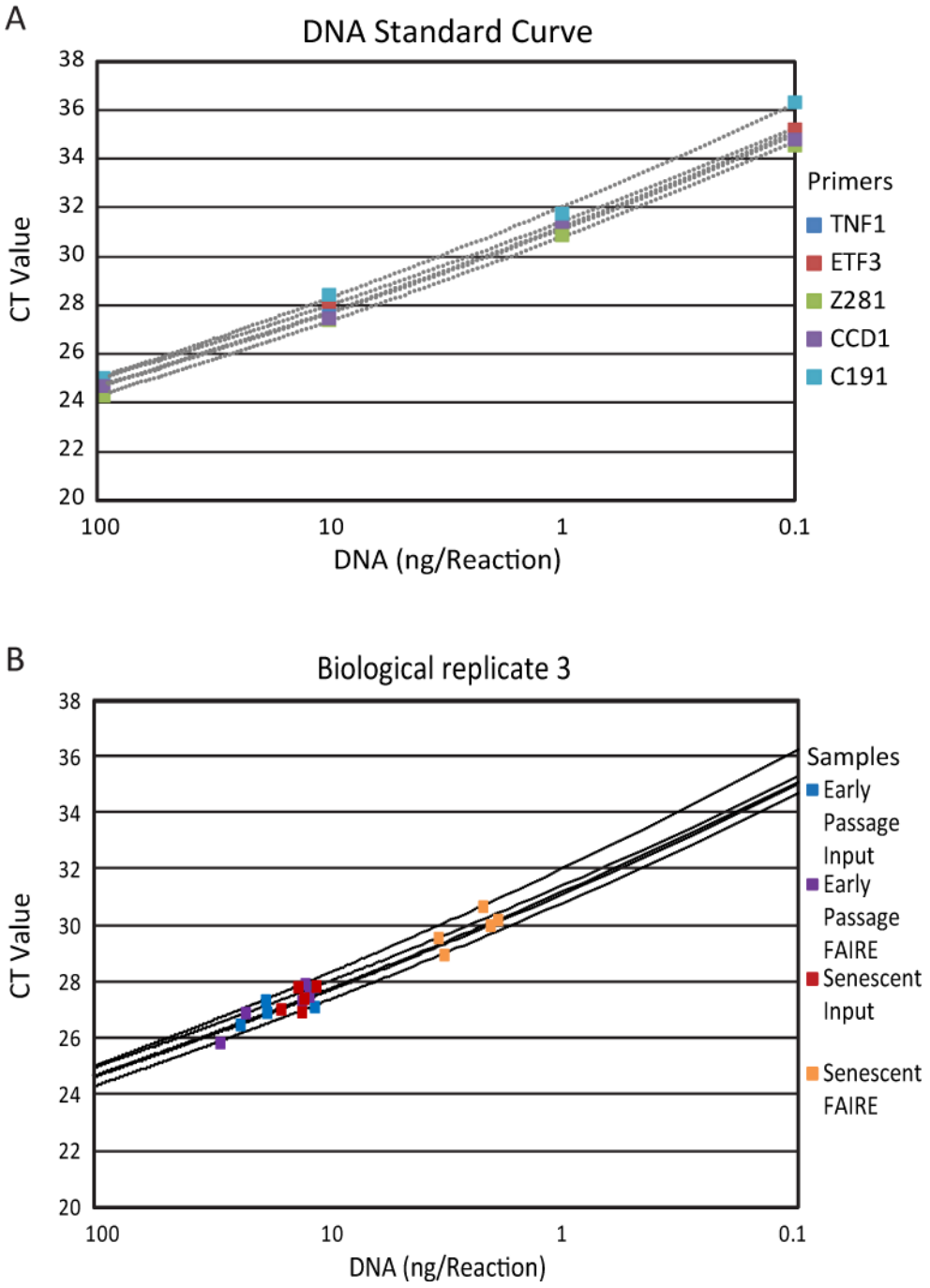
A
DNA Standard Curve
CT Value
38
36
34
32
30
28
26
24
22
20
100
10
1
0.1
DNA (ng/Reaction)
Primers
TNF1
ETF3
Z281
CCD1
C191
B
Biological replicate 3
CT Value
38
36
34
32
30
28
26
24
22
20
100
10
1
0.1
DNA (ng/Reaction)
Samples
Early Passage Input
Early Passage FAIRE
Senescent Input
Senescent FAIRE

Figure 2-1 Measurement of the DNA concentrations of dot blot samples using qPCR

(A) Standard curve generated from qPCR amplification of purified genomic human DNA using 5 background primer sets: TNF1, ETF3, Z281, CCD1, C191. Y-axis: Ct values. X-Axis: amount of DNA (ng) per reaction. A best fit line for each primer set is depicted by a dashed line. DNA concentrations for the experimental samples were calculated using the equations of the best fit lines generated in A. (B) qPCR results obtained with the samples used in the dot blots. Replicate 3 for each condition is shown here. Y-axis: Ct values. X-axis: amount of DNA (ng) per reaction

Table 2-1

A DNA concentration for biological replicate 3 samples

Primers →	TNF1	ETF3	Z281	CCD1	C191	average = sample ng/ul
EPI 3	55.43	34.91	34.77	71.99	56.17	50.65
EPF 3	36.58	68.33	88.05	39.31	38.09	54.07
SI 3	19.24	17.11	19.72	24.13	20.43	20.12
SF 3	1.15	2.06	1.95	1.23	1.33	1.54

B Calculated DNA (ng) deposited on blot for all samples for the highest concentration spot

	EPI 1	EPI 2	EPI 3	EPF 1	EPF 2	EPF 3	SI 1	SI 2	SI 3	SF 1	SF 2	SF 3
DNA (ng)	45.13	68.80	40.52	27.38	24.11	36.77	54.68	48.73	49.91	9.06	9.92	10.06
% error	23.16	13.83	18.10	20.47	27.55	24.68	6.37	4.51	7.34	19.15	15.29	15.97

C Dilution series DNA calculated for each spot deposited on blot for all samples

	EPI 1	EPI 2	EPI 3	EPF 1	EPF 2	EPF 3	SI 1	SI 2	SI 3	SF 1	SF 2	SF 3
1x	45.13	68.80	40.52	27.38	24.11	36.77	54.68	48.73	49.91	9.06	9.92	10.06
0.5x	22.56	34.40	20.26	13.69	12.06	18.38	27.34	24.36	24.95	4.53	4.96	5.03
0.25x	11.28	17.20	10.13	6.84	6.03	9.19	13.67	12.18	12.48	2.27	2.48	2.52
0.125x	5.64	8.60	5.07	3.42	3.01	4.60	6.84	6.09	6.24	1.13	1.24	1.26
0.0625x	2.82	4.30	2.53	1.71	1.51	2.30	3.42	3.05	3.12	0.57	0.62	0.63

D Pixel intensity calculated for each spot using ImageJ

	EPI 1	EPI 2	EPI 3	EPF 1	EPF 2	EPF 3	SI 1	SI 2	SI 3	SF 1	SF 2	SF 3
16x	4056.9	3237.3	3712.0	1312.8	1222.0	1174.3	2400.9	2053.8	2019.6	643.3	658.1	593.2
8x	2133.4	1720.8	1995.3	653.3	515.0	481.5	1361.6	1267.7	1100.0	278.9	305.9	330.0
4x	1500.0	1041.0	1219.9	420.5	238.2	234.5	905.4	732.3	641.8	101.1	149.0	213.4
2x	1025.2	612.4	645.4	211.0	221.4	126.8	573.0	426.6	306.9	68.7	77.9	120.3
1x	501.3	344.8	700.4	46.6	11.4	82.2	446.3	211.2	167.0	-5.9	21.6	22.0

Table 2-1 Calculation of the DNA concentrations of dot blot samples based on qPCR measurements

Using the plots from Figure 2-1, the amount of DNA in each spot on the nylon membranes was determined. (A) The concentrations derived from 4-4 B averaged across the 5 primer sets for biological replicate 3. (B) the amount of DNA blotted in the topmost spot on each of the blots for all three biological replicates based on the calculated concentration in A and the volume of sample used in the blotting process. The calculated error is shown as % error. (C) The entire dilution series for the DNA blotted onto the nylon membranes based on the calculated concentrations for L1 blot 1. (D) Background subtracted signal intensity calculations for each spot on L1 blot 1. The signal intensity for each spot was calculated by averaging the pixel intensity in ImageJ within a circle with an area of 0.204 centimeters centered on each spot. Background was calculated from 20 equally sized spots measured around the periphery of each blot.

Abbreviations: EPI, early passage input; EPF, early passage FAIRE; SI, senescent input; SF, senescent FAIRE. The number following each abbreviations designates the replicate (1,2,3).

Figure 2-2

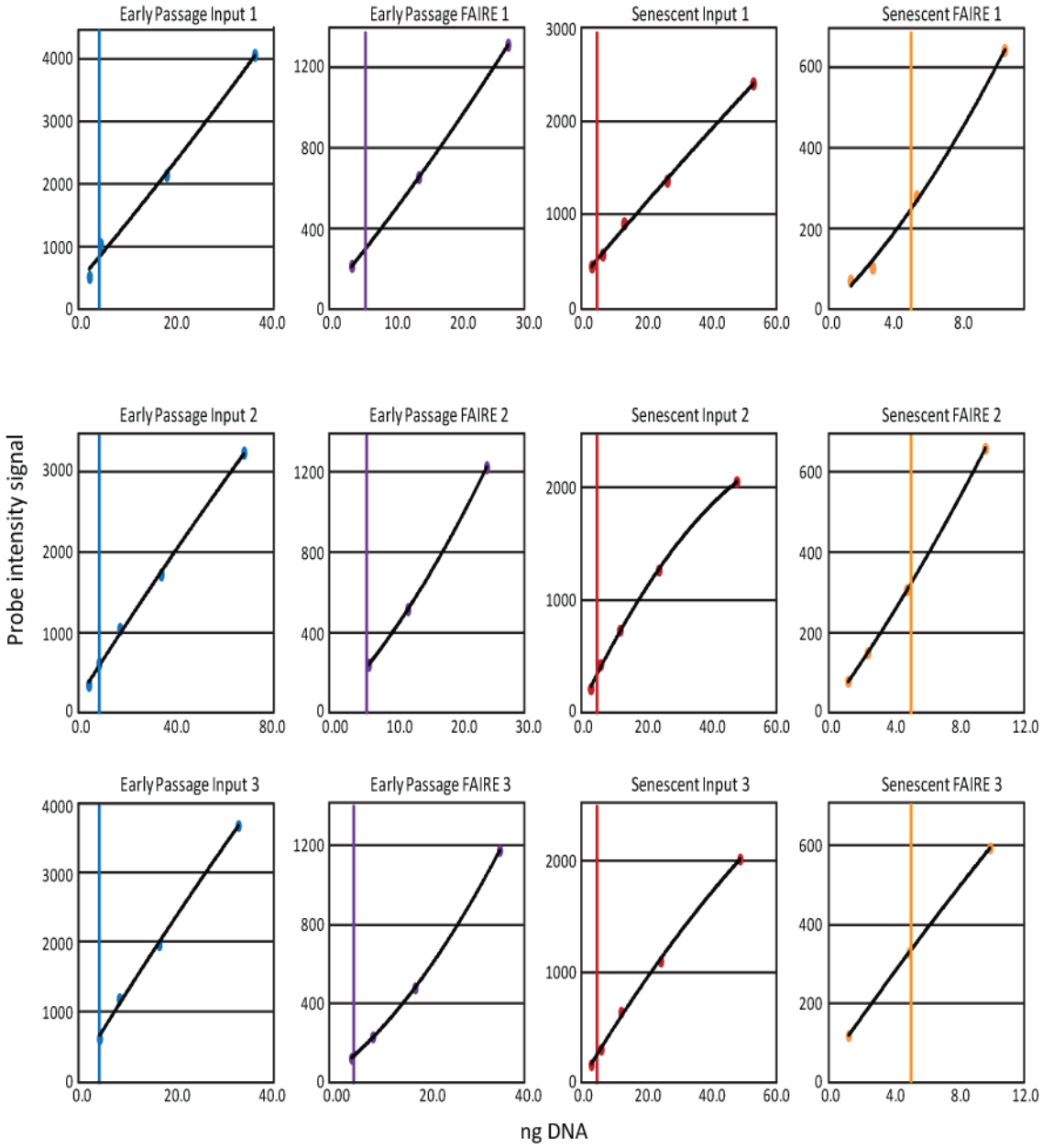
Early Passage Input 1
Early Passage FAIRE 1
Senescent Input 1
Senescent FAIRE 1
Early Passage Input 2
Early Passage FAIRE 2
Senescent Input 2
Senescent FAIRE 2
Early Passage Input 3
Early Passage FAIRE 3
Senescent Input 3
Senescent FAIRE 3
Probe intensity signal
ng DNA

Figure 2-2 Signal intensities from dot blots plotted against the amount of DNA present in each spot

Best fit lines were generated for each sample. The DNA normalized signal for each sample was calculated from the equation of the regression based on an intersection at position of 5 ng DNA (vertical line). Y-axis: probe intensity signal. X-axis: DNA content.

Chapter 3: FAIRE Analysis of Genome-Wide Changes in Chromatin Accessibility During Cellular Senescence

3-1) Goals of the Study

The objective of this set of experiments was to investigate global patterns of chromatin reorganization that occur as cell senesce. For this purpose we chose the FAIRE methodology (Giresi et al., 2007) to map open chromatin regions from replicating and senescent HDF. After preparing DNA from replicating and senescent cells the FAIRE enriched samples were analyzed using microarray technologies (chip) on Affymetrix whole genome tiling arrays. Using this FAIRE approach, we found a detectable global change in chromatin organization that indicates a larger proportion of TSS become resistant to isolation in senescent cells. In addition we performed gene expression profiling and found that the genes that showed the greatest reduction in FAIRE isolation also had the greatest reduction in expression.

3-2) Overview of Experimental Design

DNA was isolated from replicating and senescent human LF1 cells using the FAIRE method described previously. 2 biological replicates were collected for 4 experimental conditions: passage 12 replicating cells that were formaldehyde crosslinked, passage 12 replicating cells that were not crosslinked, passage 53 senescent cells that were crosslinked, and passage 53 senescent cells that were not crosslinked. The experimental conditions will hereafter be respectively referred to as early passage FAIRE, early passage input, senescent FAIRE and senescent input.

FAIRE and input DNA were linearly amplified and hybridized to Affymetrix Human Tiling 2.0 Arrays. The data from all tiling arrays were used to compute the fold-change between FAIRE and input probes for the early passage and senescent samples and used to

separate TSS into two clusters, open and closed. FAIRE enrichment data was expressed as a heat map across the human chromosomes representing an averaged FAIRE signal within a sliding window. We identified a number of peaks in our samples which were validated by qPCR on the FAIRE and input DNA. Whole cell total RNA was harvested in biological triplicates from early passage and senescent cells and hybridized to Affymetrix Human Genome U133 Plus 2.0 Arrays. REFSEQ transcripts were mapped to unique TSS identified in the clustering analysis. The correlations between a change in chromatin accessibility and fold-change in gene expression were examined as well as the correlation between mean FAIRE signal and gene density.

3-3) Implementation of the FAIRE-chip method

In order to validate our implementation of the FAIRE methodology for further experimentation, replicate 1 of the early passage FAIRE and early passage input samples were analyzed to investigate the reproducibility of the results reported by the Lieb group (Giresi et al., 2007). The Lieb group detected a set of FAIRE peaks in an 8,000 bp intergenic region of chromosome 21, and also reported a qPCR validation of these peaks. The peaks were not associated with any promoters and so were dubbed 'orphan' peaks. FAIRE and input samples that we prepared from early passage cells were hybridized to array C of the Affymetrix human tiling array 2.0 set, which contains chromosome 21 probes. The array data were examined using the Integrated Genome Browser (IGB) software (GenoViz.org (Nicol et al., 2009)). In the region of interest we found a very similar pattern of FAIRE enrichment (Figure 3-1). This was encouraging because we employed a different HDF cell line (LF1 versus CRL 2091 used by the Lieb group) as

well as a different array platform (Affymetrix versus Nimblegen used by the Lieb group). The enrichment observed on the array was further validated using qPCR, employing the same primers as described by Giresi *et al.*, (2007). The resulting qPCR data (Figure 3-2) showed good agreement with both the Affymetrix tilling array profile, and with the previously published data from the Lieb group (Giresi et al., 2007). Having obtained these data, which we considered to be an adequate validation of the FAIRE methodology in our hands, we proceeded to process the remainder of our samples. The full data set that was subsequently analyzed for genome-wide FAIRE enrichment was obtained from biological duplicates of early passage FAIRE, early passage input, senescent FAIRE and senescent input that were hybridized to full sets of the Affymetrix human tiling 2.0 arrays.

3-4) qPCR validation of FAIRE-chip data

Peaks were identified in the microarray data using Affymetrix TAS software, as detailed in Chapter 2. A selection of these peaks were evaluated using qPCR, on the same DNA prepared for the microarray analyses, to further validate the quality of the array data. The housekeeping gene PPM1B was chosen as an example of a gene having a pronounced FAIRE enrichment peak in both senescent and early passage samples. Primer pairs were designed to amplify sequences located at the apex of the peak detected in the microarray data, as well as in flanking regions (Figure 3-3). The qPCR enrichment for each probe set was calculated using the comparative Ct method, normalizing FAIRE samples to input and using one of the flanking amplicons as a reference control. The qPCR enrichment correlated very well with the observed FAIRE enrichment detected by microarray both in

early passage and senescent samples. It is worth noting that although the magnitude of the enrichment detected by microarray was similar in early passage and senescent cells, the enrichment detected by qPCR (which is likely to be more accurate assessment) was lower in senescent cells. An expanded view of the PM1B gene, covering some 70 kbp (Figure 3-4) shown by expanding the X-axis, showed that the FAIRE enrichment in this entire region is primarily located at the promoter, with little enrichment across the gene. We also analyzed in a similar manner a situation where a prominent peak appeared in one biological condition but not the other. The gene C19orf62 displayed strong enrichment at its TSS in early passage but not senescent cells (Figure 3-5), and in both cases the correspondence between the microarray and qPCR data was very good.

3-5) FAIRE enrichment in regulatory elements

3-5A) Transcription Start Sites

The first analysis conducted on the whole genome array data examined the enrichment of FAIRE samples for regulatory elements associated with genic regions. Previously FAIRE peaks had been shown to identify nucleosome-free regions associated with transcription start sites (TSS) in both yeast and human cell lines (Giresi et al., 2007; Hogan et al., 2006; Nagy et al., 2003; Yuan et al., 2005). We selected 19,524 of the 26,083 refseq genes annotated in the NCBI36/hg18 build of the human genome for analysis as they contained unique, or non overlapping TSS. FAIRE enrichment at each TSS was calculated as the log2 fold change of FAIRE versus input signals for each probe within a 10,000 bp window centered on the TSS. Background signal was calculated for early passage and senescent samples separately, each by interpolating signal over 530,000

random 10,000 bp regions across the genome. The averaged interpolated signal, minus the background, for all 19,524 refseq genes that we thus analyzed is shown in Figure 3-6. A distinct peak centered on the TSS can be seen in both early passage and senescent cells, and notably the magnitude of the peak is considerably higher in the early passage samples Thus, on average, TSS in early passage cells display a more open chromatin signature when examined using FAIRE.

3-5B) Enhancers

Enhancers are cis-acting DNA elements that regulate transcription, and can act over long distances and on multiple promoters. Promoters themselves may be acted upon by multiple different enhancers (Maston et al., 2006). 36,589 enhancers were identified by Heintzman *et al*. (2009). We examined this set of elements for FAIRE enrichment. As for TSS the FAIRE signal was calculated for each enhancer within a 10,000 bp window centered on the enhancer site (Figure 3-7). We found that there was an average enrichment of enhancer regions in early passage cells as well as senescent cells, but as we saw in the TSS analysis, the enrichment in senescent cells was significantly lower than in early passage cells.

3-5C) Replication Domains and Origins of Replication

Replication domains, also referred to as N-Domains, are regions of genomic organization which are flanked at their borders by origins of replication (Huvet et al., 2007). It has been observed that in the human genome, the density of genes decreases in the replication domain as the distance from a flanking origin increases (Huvet et al., 2007). The 679 replication domains identified by Huvert *et al*. (2007) were analyzed for FAIRE

enrichment as described above. The transition regions associated with origins and the central regions associated with low gene density were assessed. FAIRE enrichment signal was calculated in a 10,000 bp window centered at either the origin containing transition sites (Figure 3-8BA, or the central regions of the replication domains (Figure 3-8B). We found a distinguishable peak in early passage cells at the origins of replication in the replication domain transition sites. This peak was absent in senescent cells. The central regions of the replication domains show no detectable FAIRE enrichment over background in either early passage or senescent cells.

3-6) Clustering analysis of TSS FAIRE enrichment

We next sought to examine how FAIRE enrichment changes from early passage to senescent cells. We therefore performed k-means clustering on the interpolated FAIRE signal using the 19,524 TSS selected in our dataset (See Section 3-5A), initially varying the number of clusters over a range from 2 to 10 and the window of analysis from 2,000 to 10,000 bp. No features that were considered significant were detected using the larger windows or higher numbers of clusters, however, the analysis reliably detected high and low magnitude peaks centered on the TSS. The analysis was therefore performed using 2 clusters and a window of 3,000 bp centered on the TSS. We further designated the cluster with higher enrichment as “signal present” or “open”, and the cluster with the lower enrichment as “signal absent” or “closed”. Using this analysis, we found that 7,963 genes lacked signal in early passage cells, compared to 10,337 genes in senescent cells. Conversely 11,561 genes had signal in early passage cells, as compared to 9,187 genes in senescent cells (Figure 3-9A). More TSS were open in early passage cells (approximately

60% of all TSS measured), while less than 50% were in this category in senescent cells. These data are in agreement with the observation of higher average TSS signal in the early passage cells than the senescent cells (Figure 3-6). Of the TSS in the open FAIRE cluster, 6,698 genes were common to both early passage and senescent cells (Figure 3-9B). 4,863 genes that had an open FAIRE TSS in early passage cells moved to the closed cluster in senescent cells. 2,489 genes had an open TSS uniquely in senescent cells. This indicates that of the genes that undergo chromatin reorganization during senescence, the majority (66%) lose FAIRE enrichment, while a smaller proportion gains FAIRE enrichment.

3-7) Correlation of FAIRE enrichment atTSS with gene expression data

We next evaluated whether FAIRE enrichment at TSS correlated with gene expression data, and hence, whether changes in FAIRE enrichment could have an impact on transcriptional control. To do this we obtained gene expression data from early passage and senescent cells, and intersected this data set with the FAIRE clustering analysis described above (Section 3-6). RNA expression was obtained using the Affymetrix microarray platform (U133 Plus 2.0 arrays; see Materials and Methods in Chapter 2). An expression value for each gene was calculated by averaging the expression score of all probe-sets that mapped to the gene. Of the 19,524 genes used in the clustering analysis, 18,549 mapped to corresponding transcripts in the gene expression data set, and 18,264 had unambiguous TSS. The results for these 18,264 genes (Figure 3-10A.B) show a positive correlation between FAIRE status and gene expression. In other words, genes associated with an open TSS FAIRE signal have higher average gene expression, both in

early passage and senescent cells. Of the genes in cluster 1 (open) in early passage cells, 80% have an average log2 expression value greater than the median expression value of genes in cluster 2 (closed). In senescent cells a similar trend was seen, with 75% of cluster 1 genes having an average expression value greater than the cluster 2 median. Also of interest is the observation that cluster 1 genes have a higher overall median expression value in early passage cells.

To further examine changes in chromatin accessibility and gene expression we focused on the two sets of genes that change their FAIRE TSS status between early passage and senescent cells. Genes that move from cluster 1 (open) in early passage cells to cluster 2 (closed) in senescent cells were designated as "FAIRE-loss" genes, and conversely, genes that move in the opposite direction (become open in senescent cells) were designated as "FAIRE-gain" genes. For all genes that showed a change in expression value between early passage and senescent cells, the percent that increased in expression was calculated using a series of log2 fold change expression cutoffs. The same calculations were performed for the FAIRE-loss and FAIRE-gain groups as well. The results of these computations are shown in Figure 3-11. At a log2 fold change of 0, where there is no selection, the total population of genes segregates randomly, with 51% counted as having increased expression and 49% showing decreased expression, and a similar segregation is seen in the FAIRE-gain and FAIRE-loss groups. As the cutoff threshold is increased, the pool of total genes observed decreases, and interesting shifts in the behavior of the 3 gene groups emerge. The genes in the total population show a decrease in the percentage of genes that have increased expression in senescent cells, indicating that of the genes that undergo a change in expression during senescence, a larger (and increasing) proportion

experience a decrease in expression. The FAIRE-gain and FAIRE-loss populations show distinct behaviors from that of the total gene population. The FAIRE-loss population shows a much smaller proportion of associated genes increasing expression as the fold cutoff increases. This indicates that genes that lose FAIRE enrichment, and thus likely have more compact chromatin, lose expression at a higher rate than the general population of genes. Conversely, the FAIRE-gain population shows a larger proportion of associated genes increasing expression as the fold change cutoff increases, indicating that when genes become enriched in FAIRE signal in senescent cells, they tend to also acquire increased expression.

3-8) Global patterns of FAIRE enrichment

3-8A) Chromatin painting

In order to assess changes in chromatin conformation on a global scale, the average FAIRE enrichment was calculated in 1 mega bp sliding windows that were shifted at 100,000 bp intervals across the entire genome (Figure 3-12). These data were then used to "paint" the chromosomes using a heat map associated with average FAIRE signal intensities. The chromosomes were grouped together based on their localization on the tiling arrays (for example, chromosomes 1 and 6 were grouped together as they both are represented on array A). The average FAIRE signal for early passage cells is shown as the top track for each chromosome, and the senescent FAIRE signal is displayed across the bottom. The degree of FAIRE enrichment is visualized as a heat map, where lighter colors represents a higher degree of FAIRE enrichment. Using this analysis we found that a higher overall FAIRE enrichment signal was evident across all chromosomes in the

senescent cells. It also appeared that the chromatin painting had more “texture” in early passage cells, evident as lighter and darker regions of banding, while the senescent cells presented a more homogeneous pattern.

3-8B) Comparison of total genomic enrichment with enrichment in regulatory regions

As an alternative method to assess patterns of global FAIRE enrichment across the genome, the signal intensities of the entire set arrays were quantile normalized and the result of this normalization is shown in Figure 3-13A. It can be seen that the distribution of raw array signals for each sample after the normalization was very uniform. Enrichment signal was calculated as the log2 fold-change between corresponding FAIRE and input samples. Finally FAIRE enrichment signals for early passage and senescent cells were calculated for three categories of probes: total genome, probes within a 3,000 bp window centered on regulatory regions (TSS, enhancers and replication origins), and for probes in non-regulatory regions. The histograms for these three measurements are shown in Figure 3-13B-D. In this representation, the greatest number of probes (the peaks in the histograms) for all conditions show minimal changes and are thus clustered close to log2 = 0. However, the means show small deviations from these trends that are characteristic of the individual conditions. Thus, the log2 mean for all probes in early passage cells is 0.0195 while in senescent cells it is 0.0381. While absolute magnitude of these shifts from zero (no enrichment) is small, the fold change between early passage and senescent cells means is 2-fold. It is this difference that was picked up in a visual representation in the chromatin painting representation (Figure 3-12). Conversely, when the analysis is shifted to probes in regulatory regions, an inverse relationship is seen,

namely, the mean of the early passage cells is some >2-fold higher than the mean for senescent cells. These data are also consistent with earlier analyses (Figures 3-6, 3-7, 3-8) which showed greater enrichment in early passage cells. Finally, data for non-regulatory and intergenic regions show a similar trend as that for total probes. In summary, the analysis demonstrates quantitatively that there is a higher overall FAIRE enrichment across the genome in senescent cells, but in early passage cells regulatory regions are enriched by FAIRE to a higher degree.

3-8C) Correlation between FAIRE enrichment signal and gene density

To determine if the areas of high relative FAIRE signal in the chromatin painting analysis corresponded to the higher FAIRE signal observed in the TSS of early passage cells, both the mean FAIRE signal and number of TSS present were calculated in a series of non-overlapping tiled windows with a size of 100 kb that covered the genomic regions represented on the arrays. For both the early passage and senescent cells the FAIRE signal was plotted against the number of unique TSS for each window (Figure 3-14). We found that there is indeed a small correlation between the strength of the FAIRE signal and the number of TSS, with a positive Sprearman's coefficient of 0.235 in a given window for early passage cells. Correlation between FAIRE signal strength and the number of TSS was more than 3 times weaker in senescent cells, with Spearman's coefficient of 0.069. These data indicate that while senescent cells have higher mean FAIRE signals in this non-overlapping tiled window analysis, these means remain constant regardless of the number of gene TSS present in any given genomic region. On the other hand, early passage cells have a lower mean FAIRE signal, especially notable in

the regions containing no TSS, but the mean signal increases as the number of TSS per window increases.

3-9) Summary

Using whole genome tiling array analysis of FAIRE DNA, we were able to demonstrate a significant difference in the magnitude of the TSS signal between early passage and senescent cells. Senescent cells showed a decrease in the FAIRE enrichment at TSS, suggesting a loss of open chromatin at these loci. We found that this enrichment occured in both early passage and senescent cells, but when the averaged signals were compared between the two we saw a distinct decrease in the magnitude of the TSS enrichment in senescent cells. To further examine the potential loss of open chromatin in important regulatory regions of senescent cells, we compared the enrichment of enhancers between early passage and senescent cells. As with the TSS regions, we were able to identify FAIRE enrichment peaks in both early passage and senescent cells and we found a decrease in the enrichment of the enhancer regions in senescent cells relative to early passage cells. In addition to TSS and enhancers we evaluated the FAIRE enrichment patterns associated with replication domains and found a pattern of enrichment across regions proximal to origins in early passage cells that was not seen in the replication domain centers. Enrichment was not detectable in senescent cells either in the transitional (origin) or central regions.

A clustering analysis was generated 4 groups based on TSS enrichment: early passage FAIRE enriched, senescent FAIRE enriched, early passage non-enriched and senescent non-enriched. From this analysis it emerged that senescent cells had a reduced number of

genes enriched by FAIRE, and those that were enriched had lower average enrichment signals. In addition to the reduced number of TSS that were enriched in senescent cells, we also noted an overall reduction in the magnitude of the FAIRE enrichment peak. These observations further indicate an overall loss of open chromatin at the TSS of senescent cells. However, the presence of TSS that lack enrichment in early passage cells but gain enrichment in senescent cells is indicative of gene regulation patterns occurring in both directions during senescence, which has been amply demonstrated by gene expression studies.

We examined the total FAIRE signal across the genome in both early passage and senescent cells and found that the total mean FAIRE enrichment signal was slightly higher in senescent cells when compared to early passage cells. This was also the case for probes in non-regulatory regions (which were defined as the total probes minus the probes in the regulatory regions), where senescent cells had a slightly higher mean signal compared to early passage cells. It should be pointed out that the mean signal in total (as well as non-regulatory) probes was very close to zero (0.0195 and 0.0139 for early passage total and non-regulatory, respectively), and that the changes in senescent cells were very small (0.0381 and 0.0378 for senescent total and non-regulatory, respectively). It is unlikely that the very small differences in the mean signals (FAIRE-input log2 fold change) between early passage versus senescent cells have a significant meaning.

We also observed noticeable variations in the patterns of FAIRE signal distribution between early passage and senescent cells. Whereas in senescent cells the signal was more evenly distributed, in early passage cells the distribution showed more distinct regions of high and low FAIRE enrichment.

To explore this connection between FAIRE enrichment and gene expression we first compared the FAIRE TSS data obtained from the genome tiling arrays to gene expression data obtained from mRNA expression arrays. We focused on genes that showed changes in TSS FAIRE enrichment between early passage and senescent cells, and compared the direction of the TSS enrichment with the mRNA expression level. We indeed observed a positive relationship between the change in TSS FAIRE enrichment and transcriptional activity. If a TSS showed an increased enrichment in senescent cells, the associated gene tended to be more active in senescent cells, and the same was also observed in the other direction. First, mean expression scores were calculated for all the genes whose TSS were analyzed in the FAIRE data..

Figure 3-1

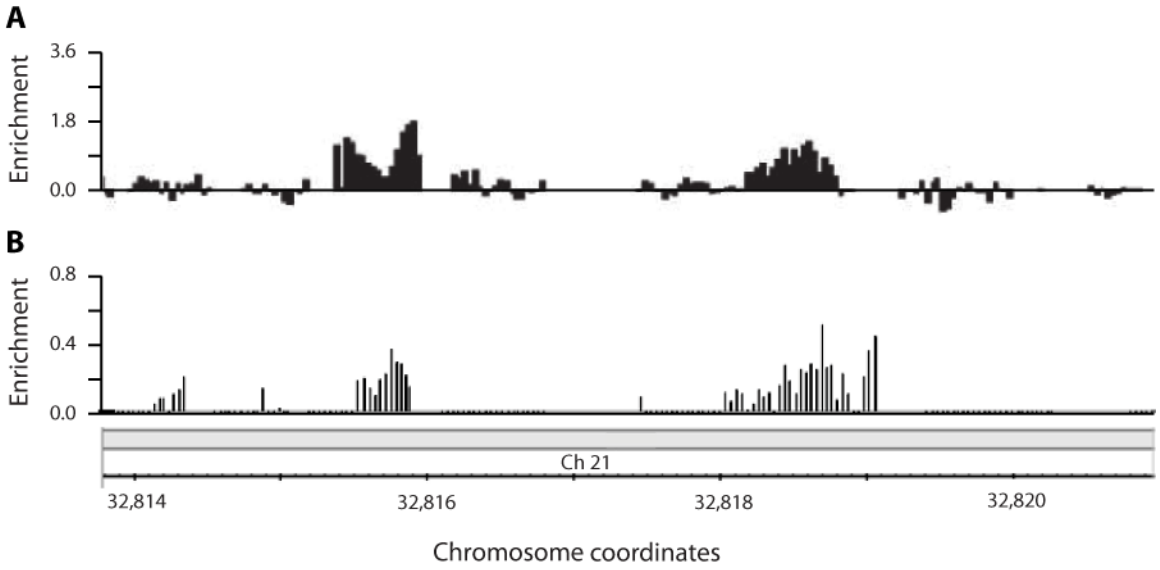
A
Enrichment
3.6
1.8
0.0
B
Enrichment
0.8
0.4
0.0
Ch 21
32,814
32,816
32,818
32,820
Chromosome coordinates

Figure 3-1 Comparison of FAIRE-chip output from our study with the original study published by Lieb's group (Giresi et al., 2007)**.**

Giresi *et al.* (2007) used the foreskin HDF strain CRL 2091 (ATCC) and NimbleGen ENCODE tiling arrays, while we used the lung HDF strain LF1 (Brown et al., 1997), and Affymetrix Human 2.0 tiling arrays. (A) Portion of Fig. 3D reproduced from Giresi *et al.* (2007); (B) The corresponding 8 kbp region of chromosome 21 from our data. Y-axis: FAIRE enrichment is shown as the log2 ratio relative to input signal at each position. X-axis: chromosomal position in kbp.

Figure 3-2

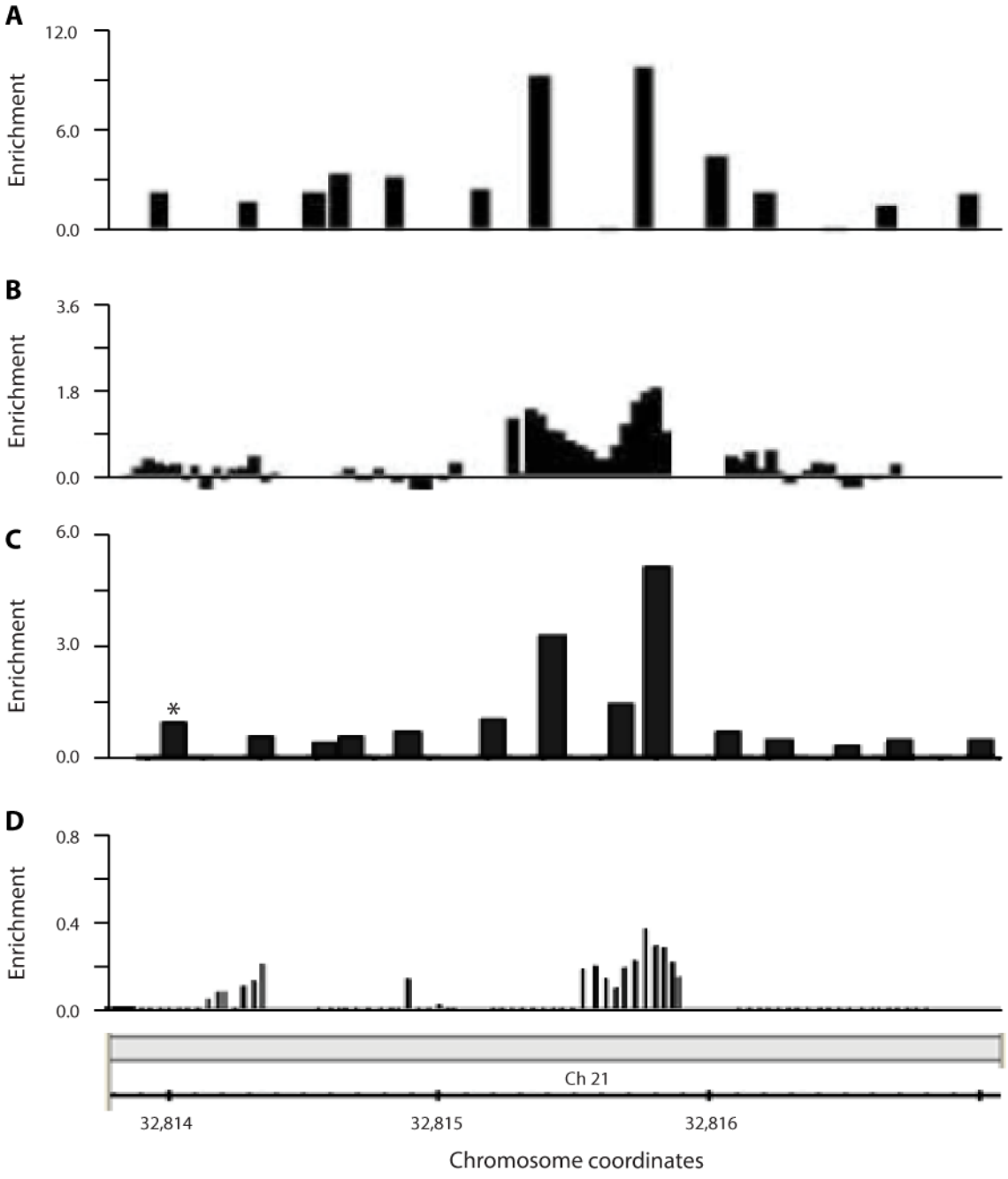
A
12.0
6.0
0.0
Enrichment
B
3.6
1.8
0.0
Enrichment
C
6.0
3.0
0.0
Enrichment
*
D
0.8
0.4
0.0
Enrichment
Ch 21
32,814
32,815
32,816
Chromosome coordinates

Figure 3-2 real time qPCR Validates FAIRE enrichment.

A subregion (approximately 3 kbp) of the 8 kbp region shown in Figure 3-1 was used in this analysis. The relevant regions of Fig. 3D from Giresi *et al.* (2007) have been reproduced in panels A and B. (A)qPCR enrichment; (B) FAIRE enrichment. Our data are shown in panels C and D, and utilized the same primers as those used by Giresi *et al.* (2007). (C) qPCR enrichment; (D) FAIRE enrichment. Y-axis: FAIRE enrichment (B,D) is shown as in Figure 3-1. qPCR enrichment (A,C) was calculated using the comparative Ct method (Livak and Schmittgen, 2001), normalized to input and is shown as the ratio relative to one reference amplicon (asterisk). qPCR signal bars are shown in positions corresponding to their genomic coordinates. X-axis: chromosomal position in kbp.

Figure 3-3

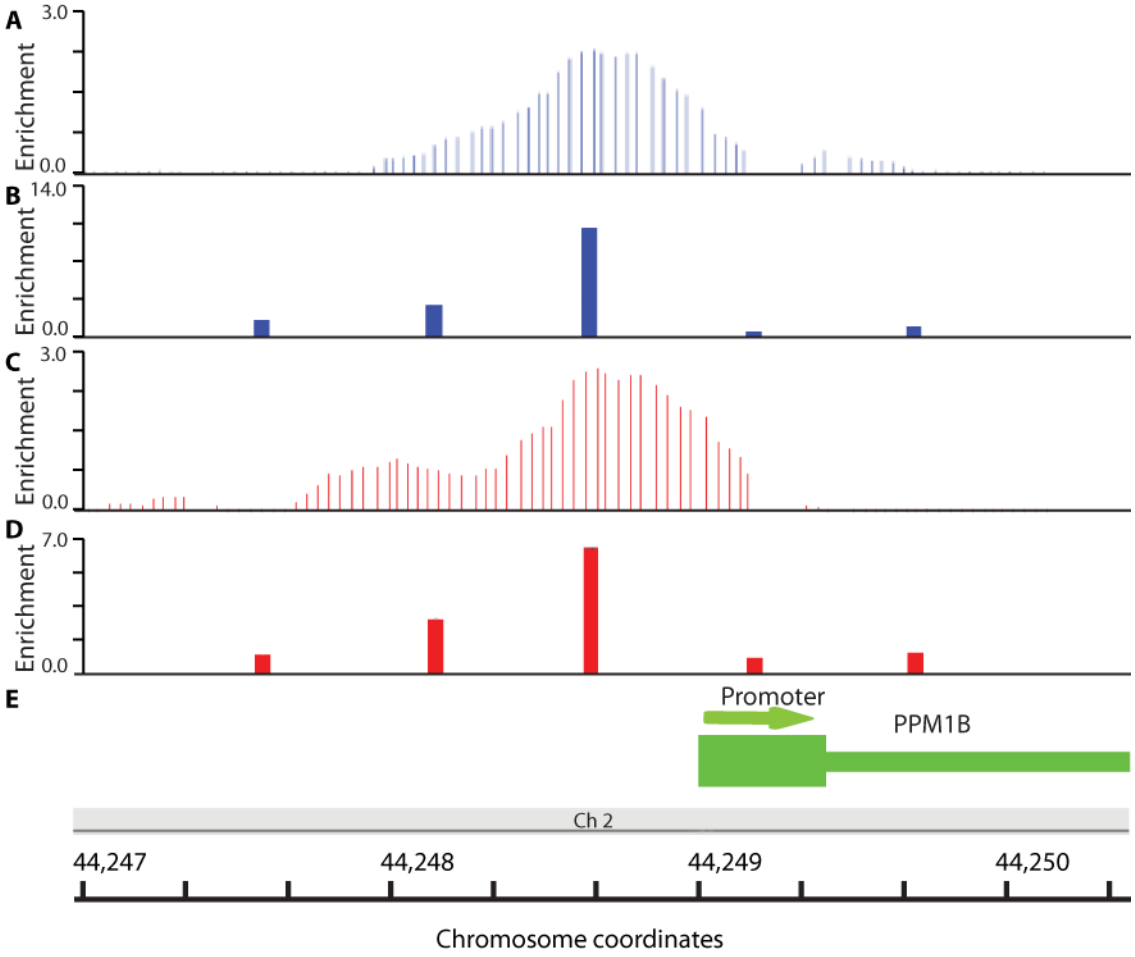
A
3.0
Enrichment
0.0
B
14.0
Enrichment
0.0
C
3.0
Enrichment
0.0
D
7.0
Enrichment
0.0
E
Promoter
PPM1B
Ch 2
44,247
44,248
44,249
44,250
Chromosome coordinates

Figure 3-3 qPCR validates FAIRE enrichment at the TSS of the PPM1B gene.

A 3 kbp region centered at the PPM1B promoter was used in this analysis. Data from early passage cells are shown in panels A and B, and from senescent cells in panels C and D. (A, C) FAIRE enrichment; (B, D) qPCR enrichment. (E) Schematic of the PPM1B gene with the promoter region indicated. Y-axis: FAIRE enrichment (A,C) is shown as the log2 ratio relative to input signal for each probe. qPCR enrichment (B, D) was calculated using the comparative Ct method as in figure 3-2. X-axis: chromosomal position in kbp.

Figure 3-4

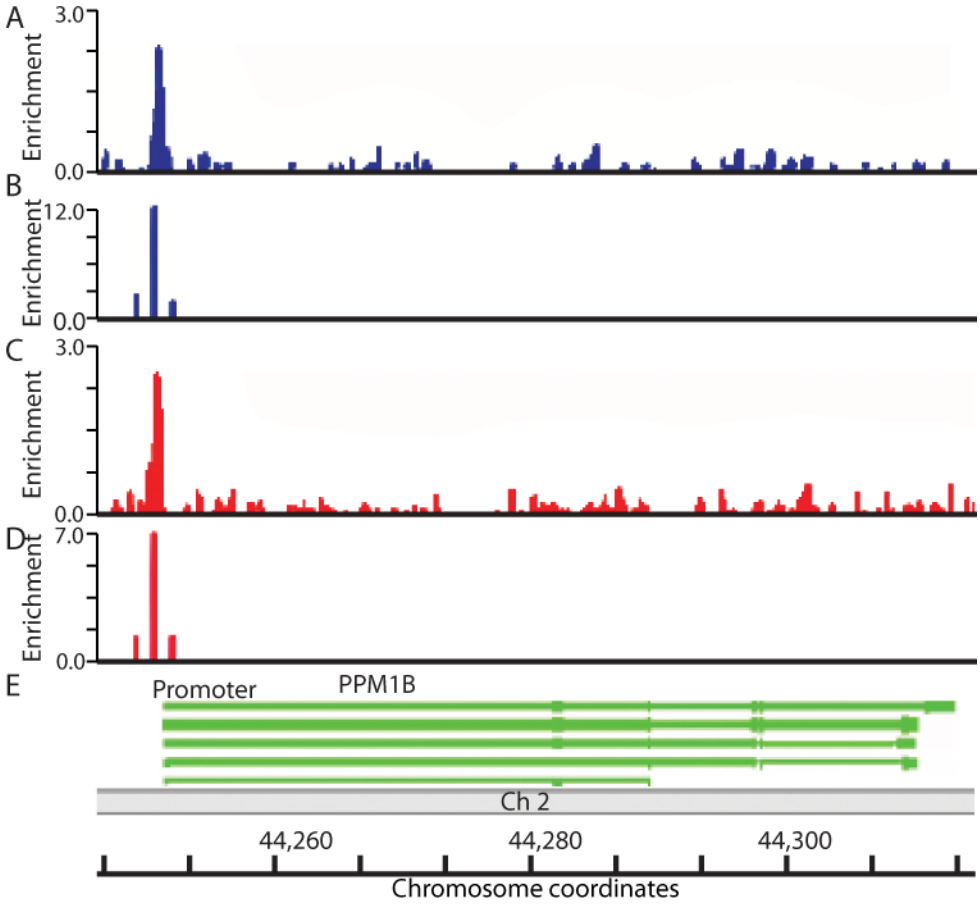
A
3.0
Enrichment
0.0
B
12.0
Enrichment
0.0
C
3.0
Enrichment
0.0
D
7.0
Enrichment
0.0
E
Promoter
PPM1B
Ch 2
44,260
44,280
44,300
Chromosome coordinates

Figure 3-4 Distribution of FAIRE enrichment across the PPM1B gene.

The coverage of Figure 3-3 has been expanded to approximately 70 kbp to include the entire PPM1B gene. Data from early passage cells are shown in panels A and B, and from senescent cells in panels C and D. (A,C) FAIRE enrichment; (B,D) qPCR enrichment. (E) schematic of the PPM1B gene. Y-axis: FAIRE enrichment (A,C) is shown as the log2 ratio relative to input signal for each probe. qPCR enrichment (B,D) was calculated using the comparative Ct method as in Figure 3-2. X-axis: Chromosomal position in kbp.

Figure 3-5

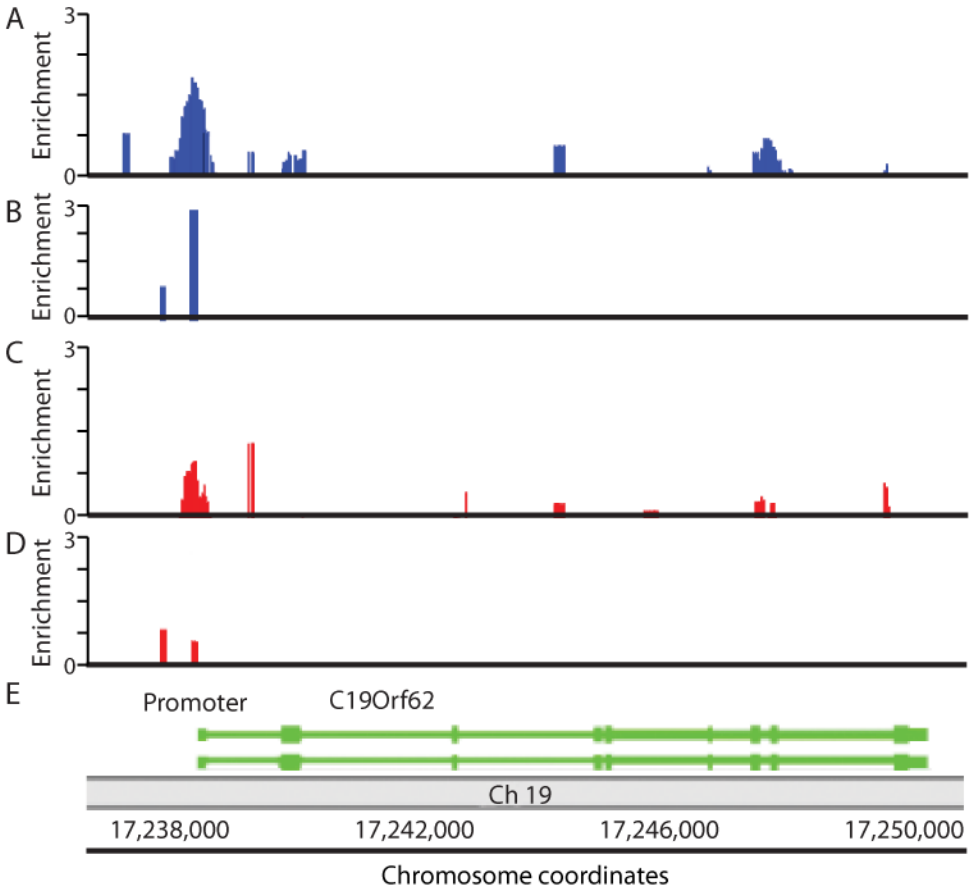
A
Enrichment
3
0
B
Enrichment
3
0
C
Enrichment
3
0
D
Enrichment
3
0
E
Promoter
C19Orf62
Ch 19
17,238,000
17,242,000
17,246,000
17,250,000
Chromosome coordinates

Figure 3-5 FAIRE enrichment distribution and qPCR validation of the C19orf62 gene.

The gene C19orf62 was identified as having a prominent difference in FAIRE enrichment between replicating and senescent cells and qPCR was used to verify this difference. A 15 kbp region containing the entire C19orf62 gene is shown. Data from early passage cells are shown in panels A and B, and from senescent cells in panels C and D. (A,C) FAIRE enrichment; (B,D) qPCR enrichment. (E) schematic of the C19oef62 gene with the promoter indicated. Y-axis: FAIRE enrichment (A,C) is shown as the log2 ratio relative to input signal for each probe. qPCR enrichment (B, D) was calculated using the comparative Ct method as in previous figures. X-axis: chromosomal position in kbp.

Figure 3-6

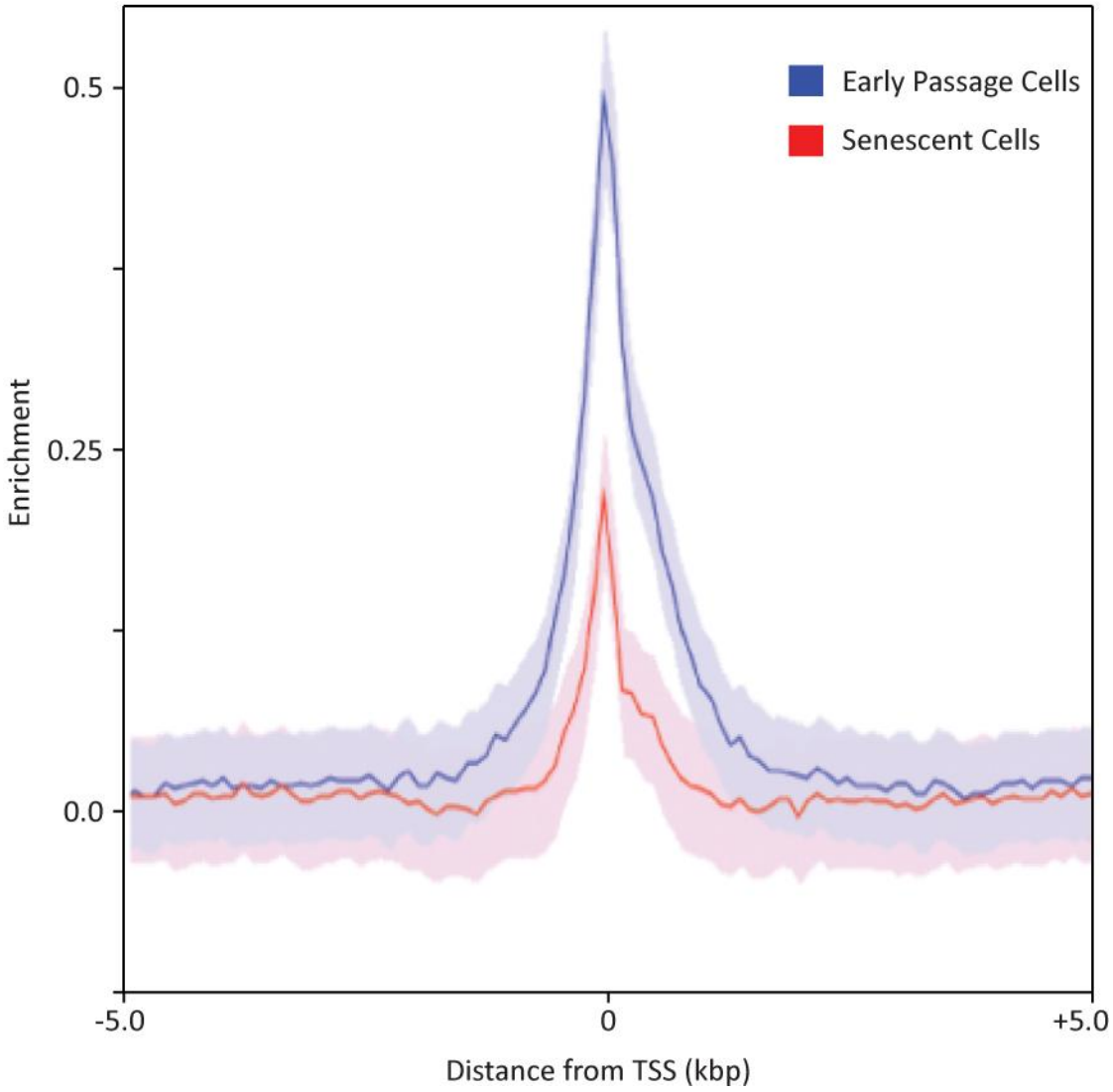
Early Passage Cells
Senescent Cells
0.5
0.25
0.0
Enrichment
-5.0
0
+5.0
Distance from TSS (kbp)

Figure 3-6 Averaged FAIRE enrichment at TSS is decreased in senescent cells

Enrichment was calculated as the averaged log2 ratio of FAIRE relative to input signals for each probe within a 10,000 bp window centered on the TSS. The interpolated data is shown as a solid line (blue: early passage; red: senescent) and the shaded region represents the standard deviation envelope above and below the mean. Data shown is corrected for background, which was calculated by interpolating over 530,000 random 10,000 bp regions signals from across the genome. Y-axis: FAIRE enrichment is shown as the log2 ratio relative to input signal. X-axis: distance from the TSS in kbp. Figure adapted from an image generated by Sara Hellenmyer.

Figure 3-7

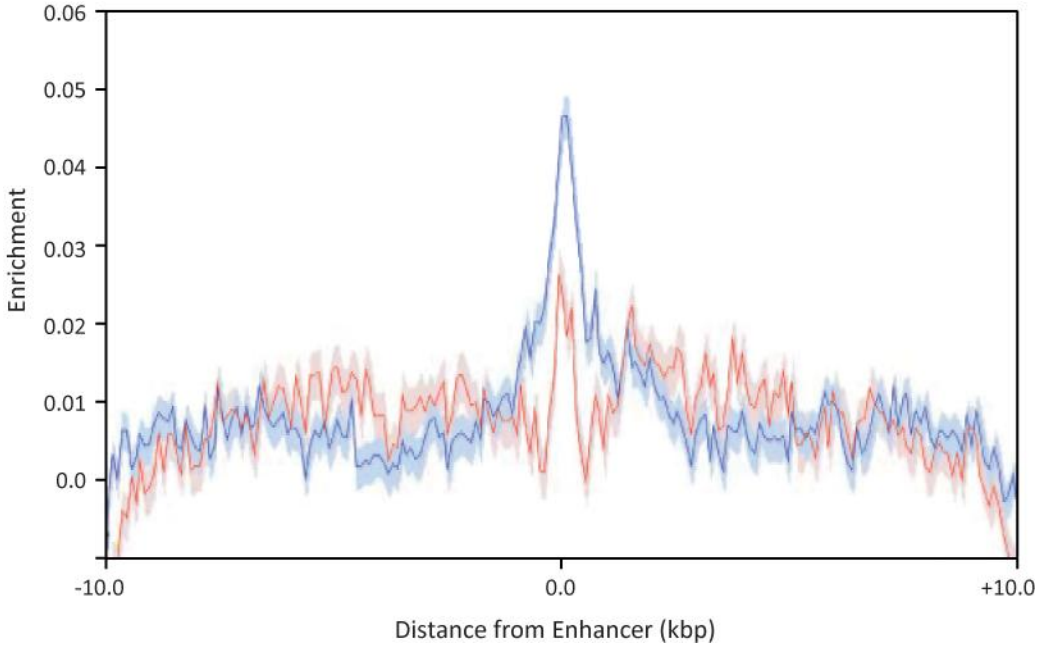
0.06
0.05
0.04
0.03
0.02
0.01
0.0
Enrichment
-10.0
0.0
+10.0
Distance from Enhancer (kbp)

Figure 3-7 FAIRE enrichment at enhancers decreases in senescent cells

Average interpolated FAIRE enrichment at 36,589 enhancer regions. Enrichment was calculated as the averaged log2 ratio of FAIRE relative to input signals for each probe within a 10,000 bp window centered on the enhance. The interpolated data is shown as a solid line (blue: early passage; red: senescent) and the shaded region represents the standard deviation envelope above and below the mean. Background was calculated by interpolating over 530,000 random 10,000 bp regions signals from across the genome. Y-axis: FAIRE enrichment is shown as the log2 ratio relative to input signal. X-axis: distance from the center of an enhancer in kbp. Figure adapted from an image generated by Sara Hellenmyer.

Figure 3-8

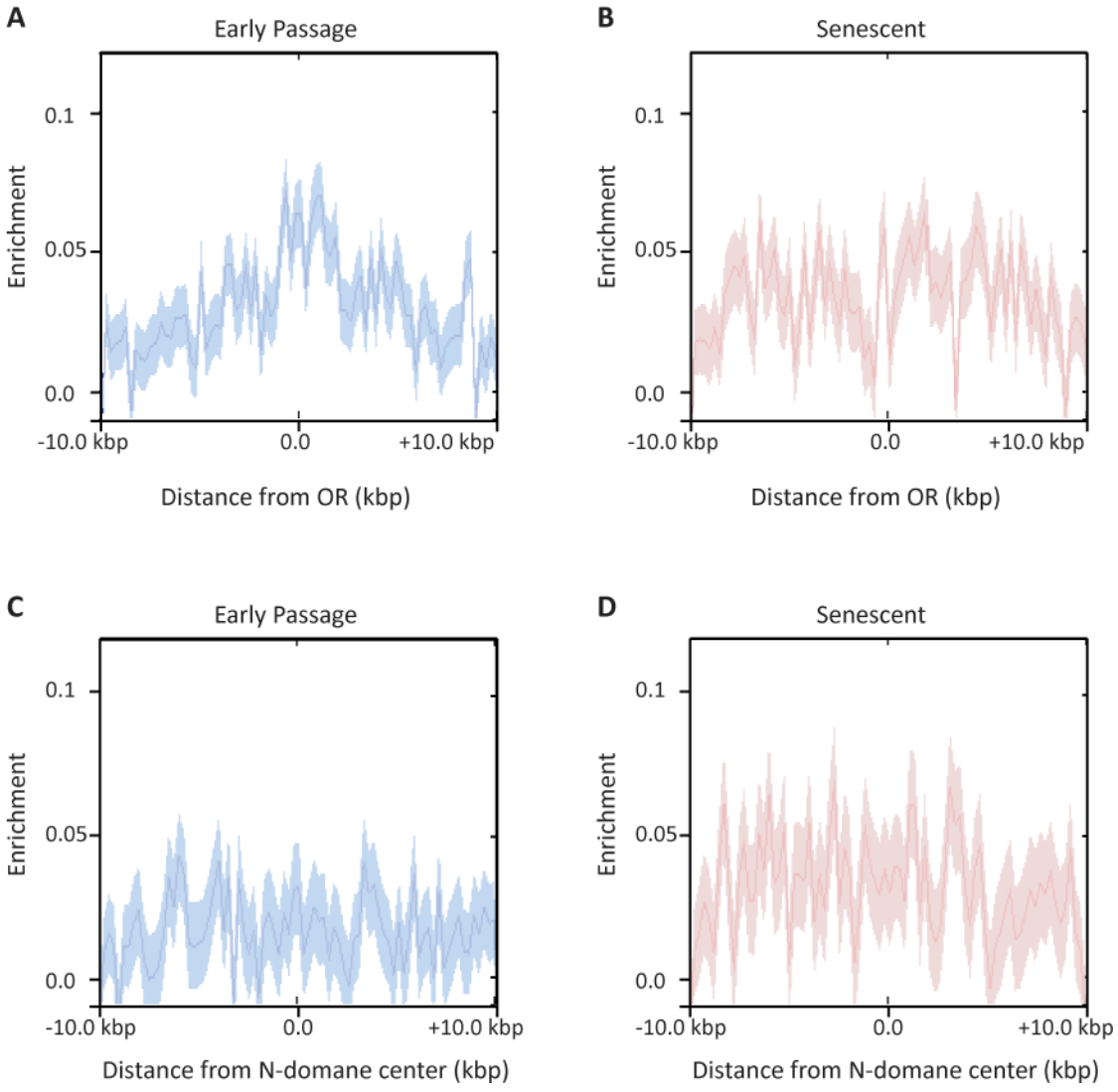
A
Early Passage
Enrichment
0.1
0.05
0.0
-10.0 kbp
0.0
+10.0 kbp
Distance from OR (kbp)
B
Senescent
Enrichment
0.1
0.05
0.0
-10.0 kbp
0.0
+10.0 kbp
Distance from OR (kbp)
C
Early Passage
Enrichment
0.1
0.05
0.0
-10.0 kbp
0.0
+10.0 kbp
Distance from N-domane center (kbp)
D
Senescent
Enrichment
0.1
0.05
0.0
-10.0 kbp
0.0
+10.0 kbp
Distance from N-domane center (kbp)

Figure 3-8 FAIRE Enrichment at origins of replication is reduced in senescent cells

(A, B) Average interpolated FAIRE enrichment at 679 replication domain transition zones (origins) for early passage (A) and senescent (B) cells. (C, D) Average interpolated FAIRE enrichment at the same 679 replication domains with the window positioned in the center of each domain for early passage (C) and senescent (D) cells. Enrichment was calculated as the averaged log2 ratio of FAIRE relative to input signals for each probe within a 10,000 bp window centered on the enhance. The interpolated data is shown as a solid line (blue: early passage; red: senescent) and the shaded region represents the standard deviation envelope above and below the mean. Background was calculated by interpolating over 530,000 random 10,000 bp regions signals from across the genome. Y-axis: FAIRE enrichment is shown as the log2 ratio relative to input signal. X-axis: distance from the center of an OR (A, B), or non regulatory region (C, D) in kbp. Figure adapted from an image generated by Sara Hellenmyer.

Figure 3-9

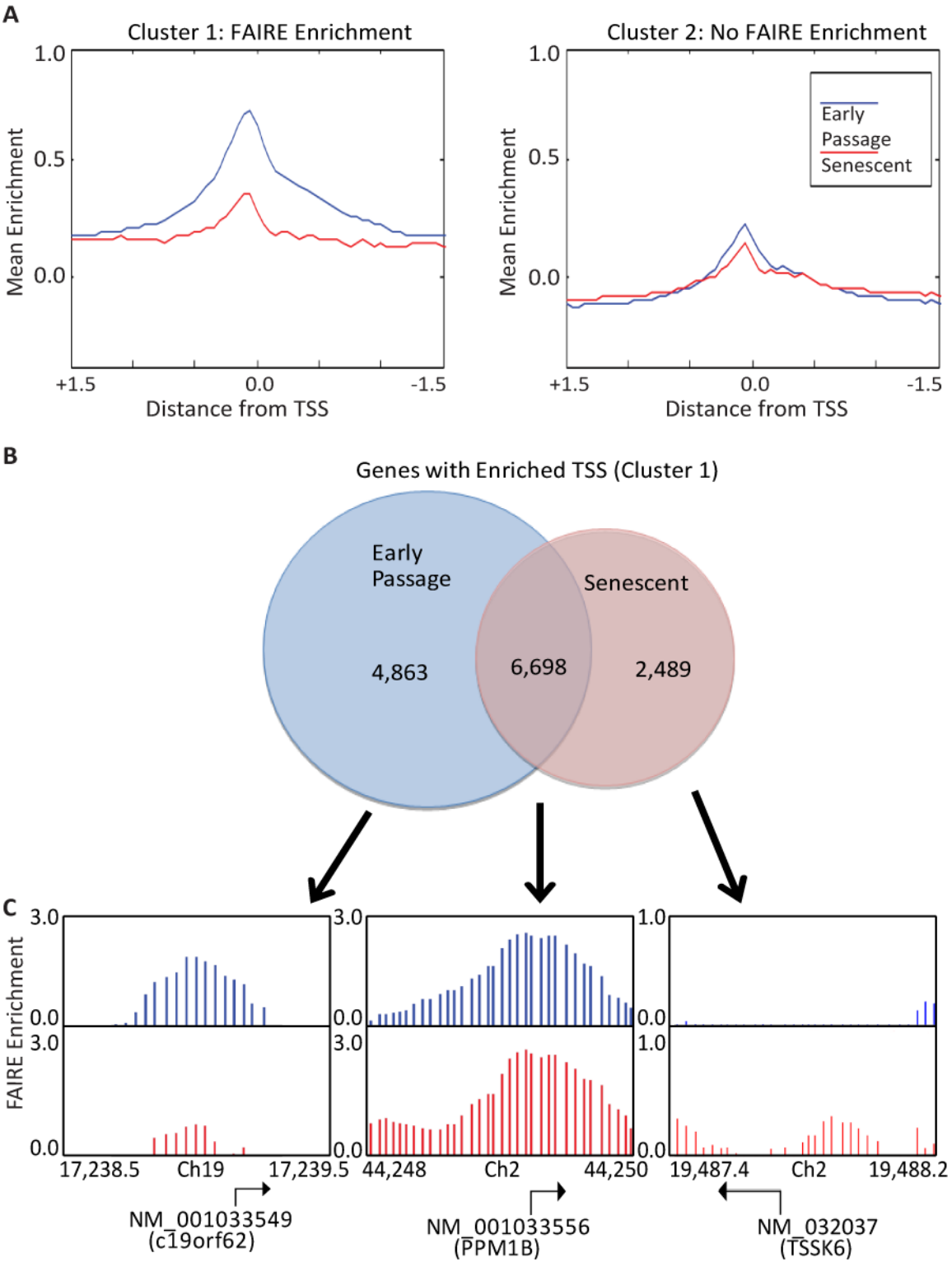
A
Cluster 1: FAIRE Enrichment
Cluster 2: No FAIRE Enrichment
Mean Enrichment
1.0
0.5
0.0
+1.5
0.0
-1.5
Distance from TSS
Early Passage
Senescent
B
Genes with Enriched TSS (Cluster 1)
Early Passage
Senescent
4,863
6,698
2,489
C
FAIRE Enrichment
3.0
0.0
1.0
17,238.5
Ch19
17,239.5
44,248
Ch2
44,250
19,487.4
Ch2
19,488.2
NM_001033549
(c19orf62)
NM_001033556
(PPM1B)
NM_032037
(TSSK6)

Figure 3-9 FAIRE enrichment at TSS segregate into 2 clusters: Open and Closed

(A) K-means clustering was performed on the average interpolated FAIRE enrichment signal of the 19,524 selected Refseq genes (Section 3-5A) in a 3.0 kbp region centered on the TSS to yield 2 clusters. Cluster 1 (left panel) contains genes with greater FAIRE enrichment at the TSS while cluster 2 (right panel) contains genes with lesser FAIRE enrichment at the TSS. Y-axis: FAIRE enrichment is shown as the log2 ratio relative to input signal. X-axis: distance from the TSS in kbp. (B) The distribution of cluster 1 genes between early passage and senescent cells. 6,698 are enriched in both early passage and senescent cells; 4,863 are uniquely enriched in early passage cells and 2,489 are uniquely enriched in senescent cells. (C) Actual enrichment profiles for TSS of representative genes in the three categories o panel B. Left panels: genes open in early passage cells that become closed in senescent cells. Middle panels: genes open in both early passage and senescent cells. Right panels: genes closed in early passage cells that become open in senescent cells. Y-axis: FAIRE enrichment is shown as the log2 ratio relative to input signal. X-axis: chromosomal position in kbp. Figure adapted from an image generated by Sara Hellenmyer.

Figure 3-10

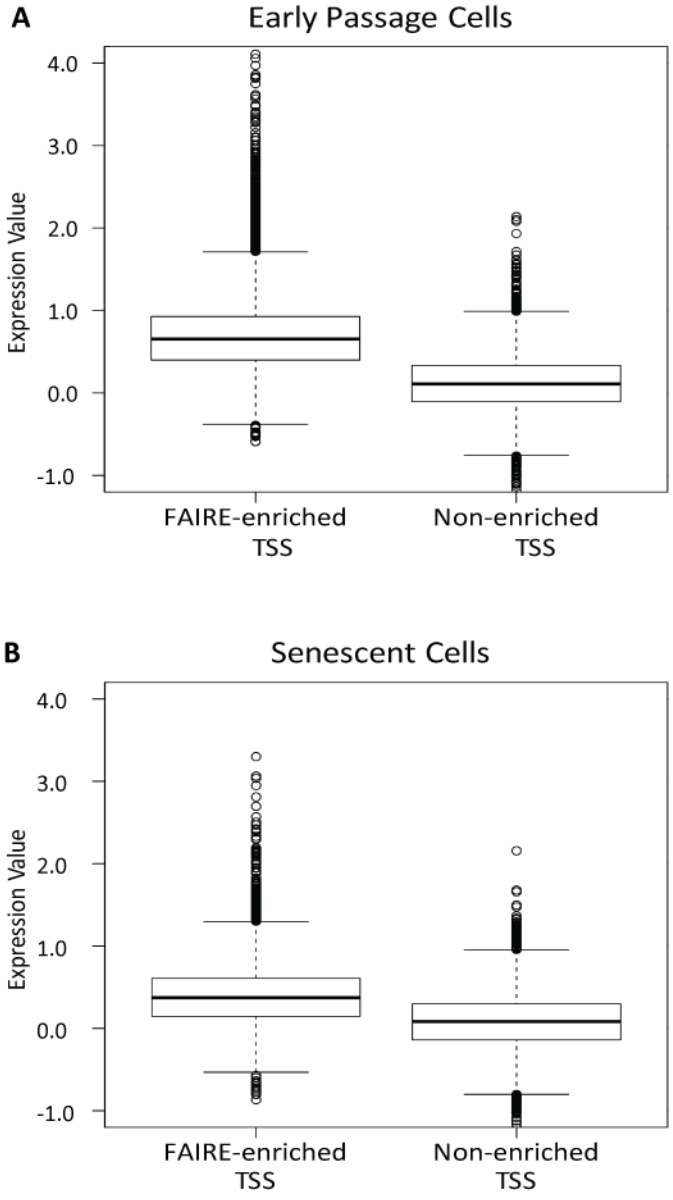
A
Early Passage Cells
Expression Value
4.0
3.0
2.0
1.0
0.0
-1.0
FAIRE-enriched TSS
Non-enriched TSS
B
Senescent Cells
Expression Value
4.0
3.0
2.0
1.0
0.0
-1.0
FAIRE-enriched TSS
Non-enriched TSS

Figure 3-10 Open cluster genes are more highly expressed than closed cluster genes

The 18,264 genes that were found in both the FAIRE TSS clustering and gene expression data sets were separated into cluster 1 (open) and cluster 2 (closed; see Figure 3-9), and the expression values were plotted for each cluster. The solid black line represents the median expression score, the central box delineates the 25^{th} and 75^{th} percentiles, and the thin lines represent the 5^{th} and 95^{th} percentile. (A) Expression scores of open and closed TSS in early passage cells. (B) Expression scores of open and closed TSS clusters in senescent cells.

Y-axis: log2 gcRMA expression value. X-axis: cluster 1 (left) and cluster 2 (right). Figure adapted from an image generated by Sara Hellenmyer.

Figure 3-11

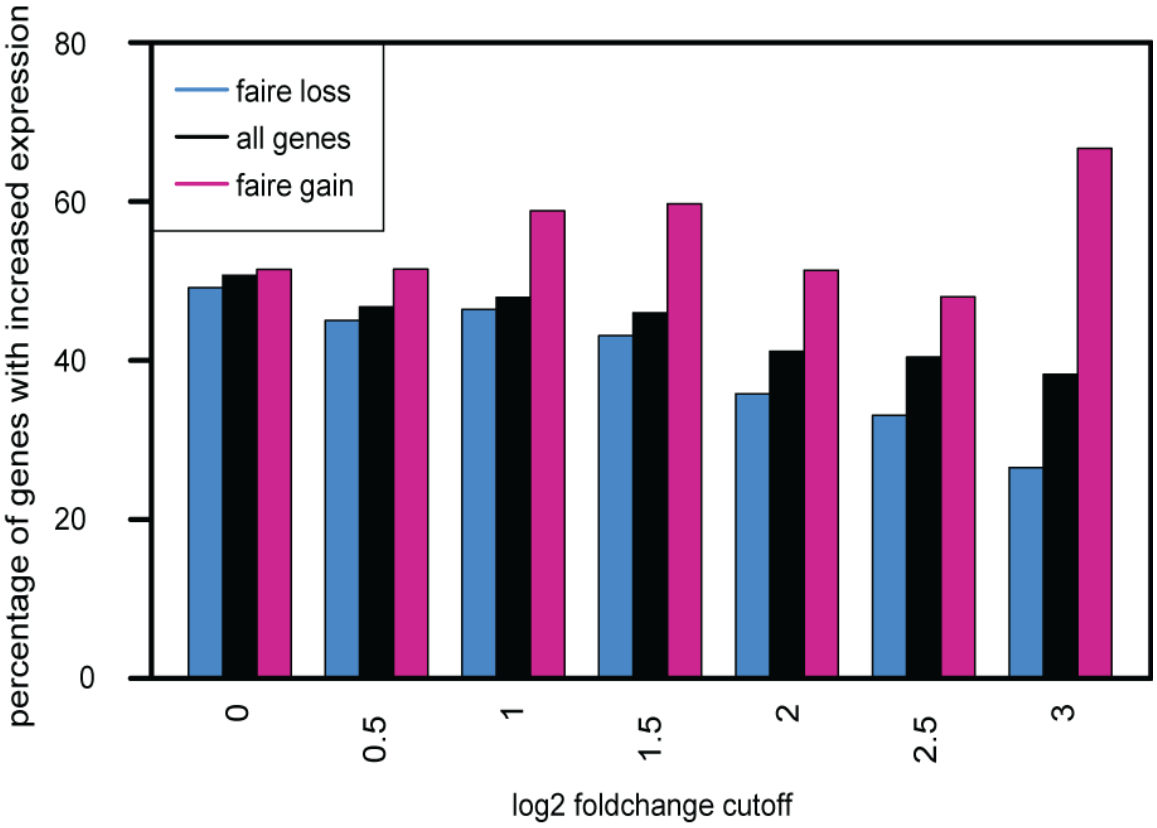
percentage of genes with increased expression
80
60
40
20
0
faire loss
all genes
faire gain
0
0.5
1
1.5
2
2.5
3
log2 foldchange cutoff

Figure 3-11 Change in FAIRE signal correlates with a change in expression in senescent cells

The percentage of genes with increased expression values in senescent cells is plotted against increasing log2 fold-change cutoffs for three sets of genes; all genes are represented in black, genes that loose FAIRE enrichment in senescent cells represented in blue, and genes that gain FAIRE enrichment in senescent cells represented in red. Each cutoff threshold represents the genes in each category that display a change in expression value between early passage and senescent cells equal to or greater than the cutoff. Y-axis: % of genes with increased expression. X-axis: log2 fold-change cutoff. Figure adapted from an image generated by Sara Hellenmyer.

Figure 3-12

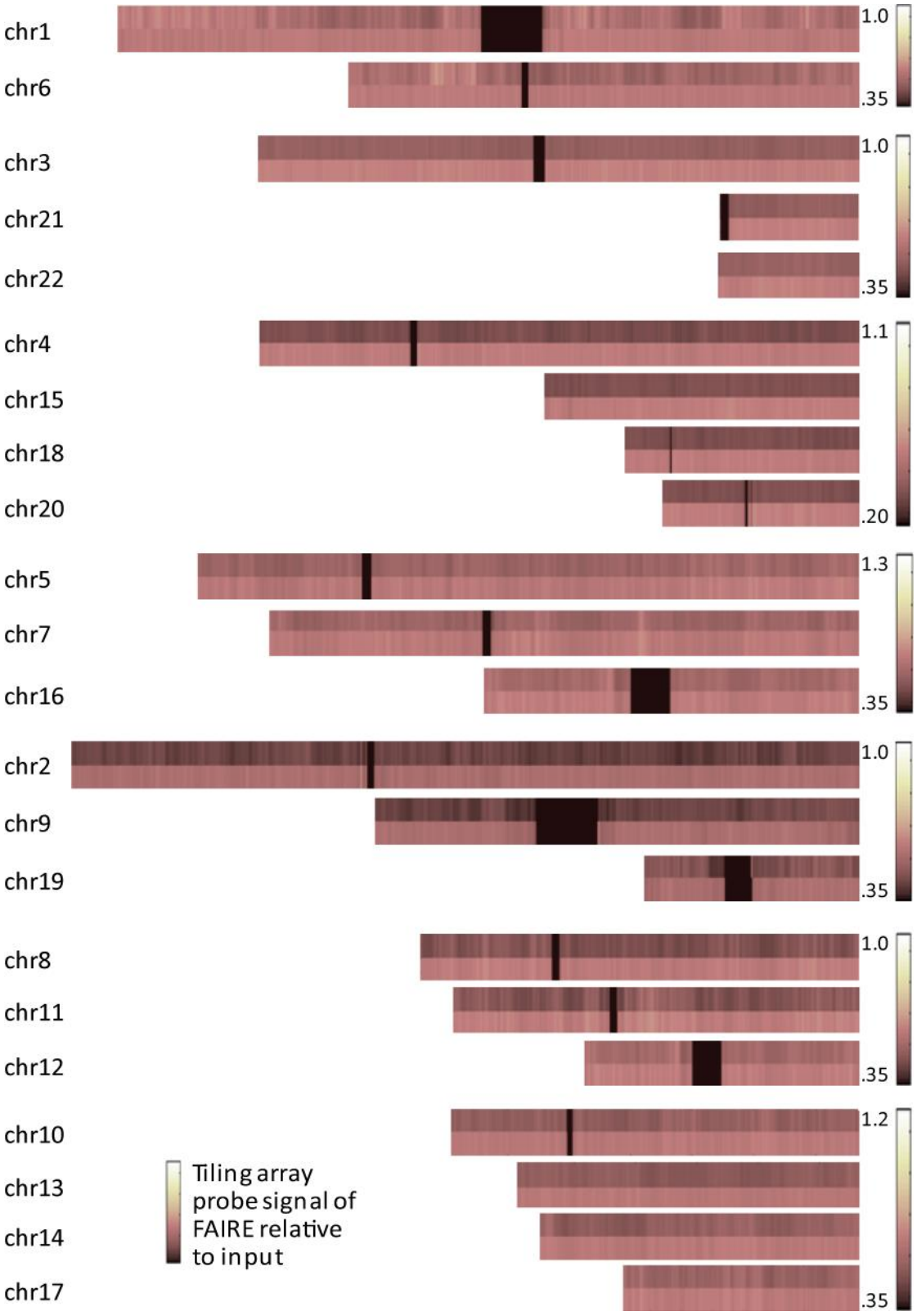
chr1
chr6
chr3
chr21
chr22
chr4
chr15
chr18
chr20
chr5
chr7
chr16
chr2
chr9
chr19
chr8
chr11
chr12
chr10
chr13
chr14
chr17
1.0
.35
1.0
.35
1.1
.20
1.3
.35
1.0
.35
1.0
.35
1.2
.35
Tiling array probe signal of FAIRE relative to input

Figure 3-12 Global FAIRE enrichment becomes homogeneous in senescent cells

FAIRE enrichment data is shown expressed as a heat map across all human chromosomes. The higher the enrichment signal, the brighter the image. Signal was calculated across 1 Mbp sliding windows at 100,000 bp intervals. Centromeres are shown as black regions and telomeres are omitted. Each chromosome shows data for both early passage (top) and senescent cells (bottom). The relative FAIRE enrichment range is displayed for each set of chromosomes whose probes were contained on a single array. The entire human genome was represented on 7 arrays. Figure adapted from an image generated by Sara Hellenmyer.

Figure 3-13

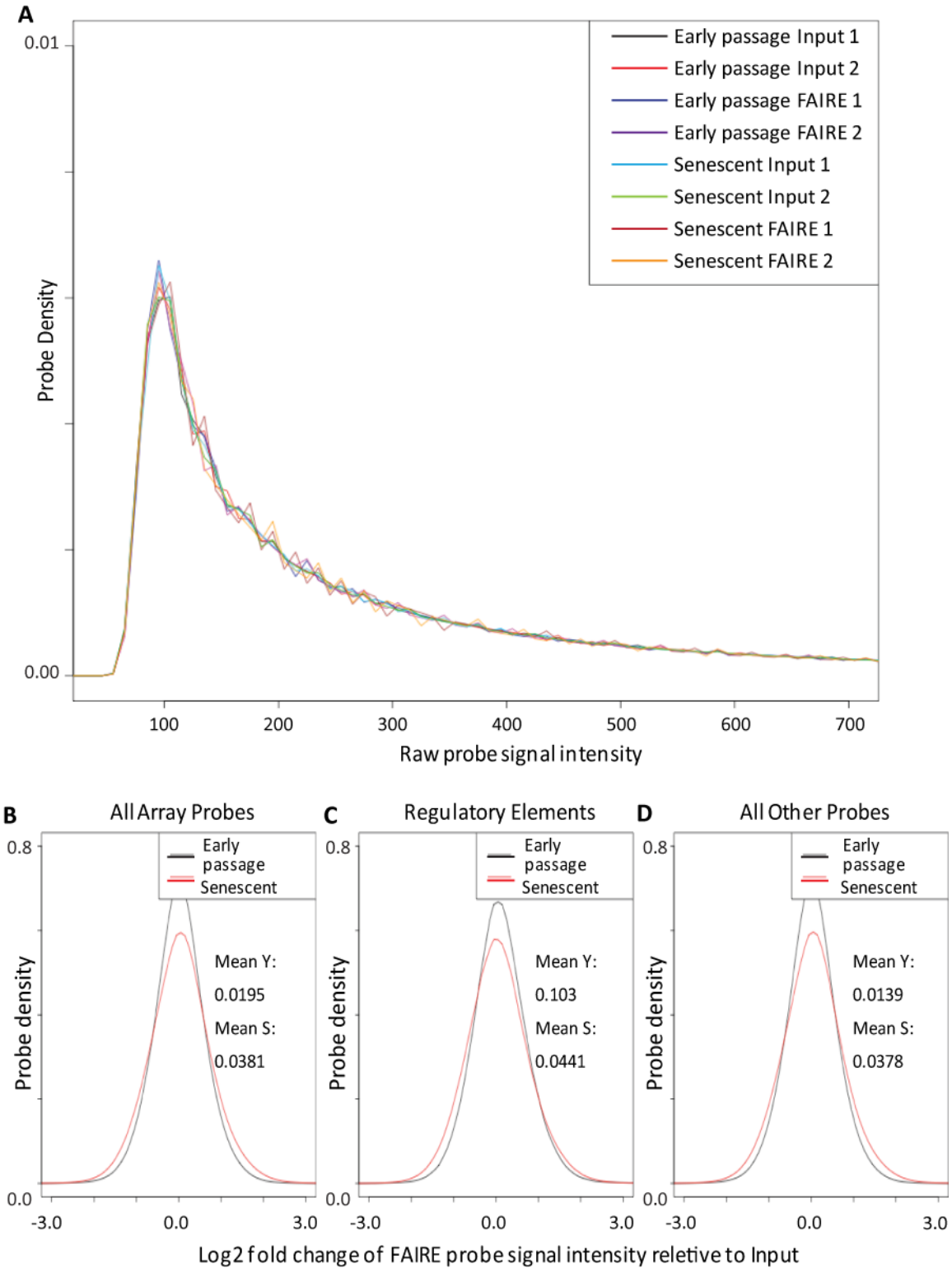
A
0.01
0.00
Probe Density
100
200
300
400
500
600
700
Raw probe signal intensity
Early passage Input 1
Early passage Input 2
Early passage FAIRE 1
Early passage FAIRE 2
Senescent Input 1
Senescent Input 2
Senescent FAIRE 1
Senescent FAIRE 2
B
All Array Probes
C
Regulatory Elements
D
All Other Probes
0.8
0.0
-3.0
0.0
3.0
Probe density
Early passage
Senescent
Mean Y:
0.0195
Mean S:
0.0381
Mean Y:
0.103
Mean S:
0.0441
Mean Y:
0.0139
Mean S:
0.0378
Log2 fold change of FAIRE probe signal intensity reletive to Input

Figure 3-13 Normalization and distribution of genomic FAIRE signal

The raw signal intensities were extracted for all of the arrays (1-7) for each condition. A standard quantile normalization was used on all of the intensities (7 arrays put together) from each condition, equalizing their histograms. (A) The distribution of genomic FAIRE signals represented as histograms. Y-axis: probe density plotted such that the total area of the graph = 1. X-axis: normalized probe intensity scores. (B-D) Histograms plotting the averaged normalized FAIRE enrichment signal based on the quantile normalized arrays. The panels represent the distribution of signals in three sets of probes: (B) All probes in the array; (C) probes within a 3,000 bp window centered on regulatory elements (TSS, enhancers and origins of replication; (D) Probes in non-regulatory regions (B - C). Y-axis: probe density plotted such that total area of the graph = 1. X-axis: FAIRE enrichment shown as the log2 ratio relative to input signal. Figure adapted from an image generated by Sara Hellenmyer.

Figure 3-14

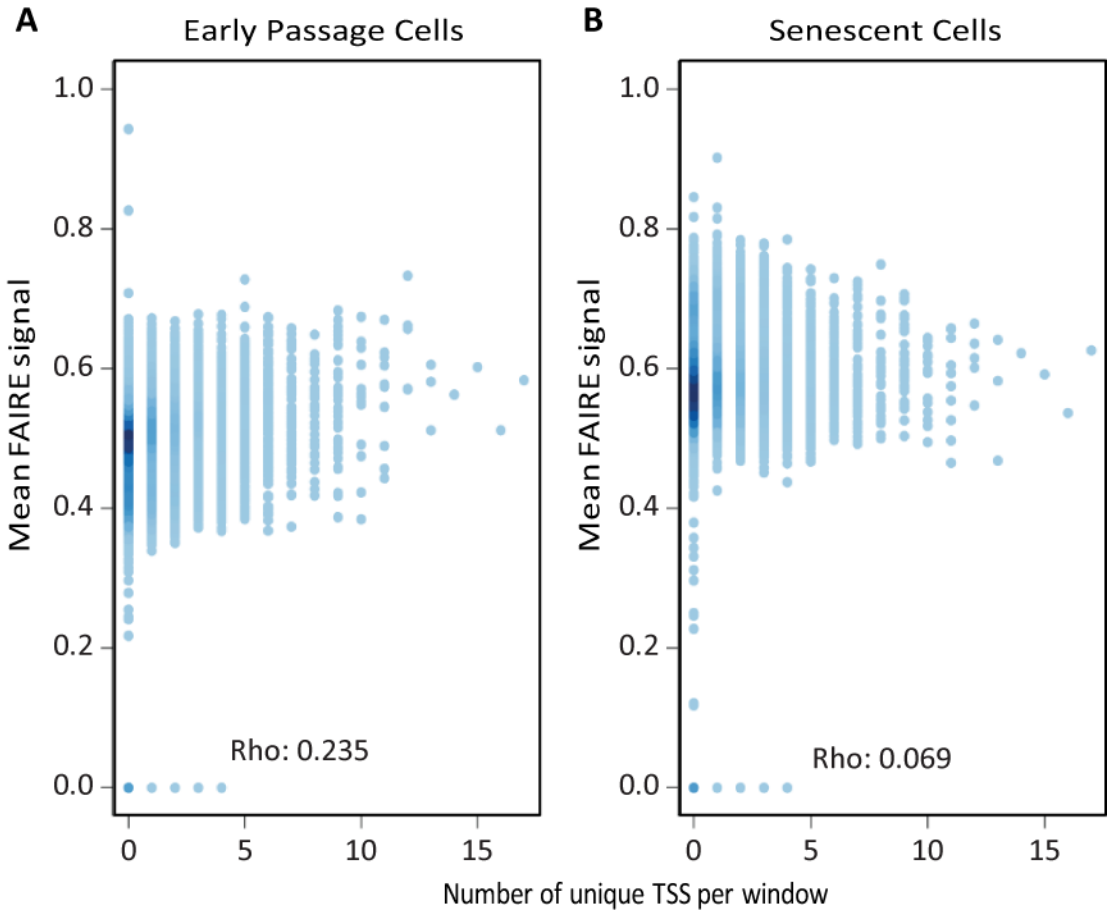
A
Early Passage Cells
B
Senescent Cells
Mean FAIRE signal
1.0
0.8
0.6
0.4
0.2
0.0
Rho: 0.235
Rho: 0.069
0
5
10
15
Number of unique TSS per window

Figure 3-14 Correlation of TSS clustering to positive FAIRE signal in early passage cells

Mean positive FAIRE signal and number of TSS were calculated in non-overlapping windows 100 kbp tiled across the genome. Mean FAIRE signal versus number of unique TSS is plotted for each window for both early passage and senescent cells. Spearman's coefficient (rho) was calculated for each panel. (A) Early passage cells had a rho of 0.235. (B) Senescent cells had a rho of 0.069. Y-axis: FAIRE enrichment shown as the log2 ratio relative to input signal. X-axis: number of TSS in each window. Figure adapted from an image generated by Sara Hellenmyer.

Chapter 4: Changes in Chromatin Accessibility of the Repetitive Human Genome During Cellular Senescence

4-1) Goals of the Study

The objective of this set of experiments was to begin to investigate chromatin changes during cellular senescence that take place in the repetitive portion of the human genome. Repetitive DNA comprises approximately half of the human genome, but the Affymetrix tiling arrays contain probes only to the unique sequences of the genome. Thus, our analysis described in Chapter 3 was in effect blind to any changes that may have been occurring in the repetitive genome. In addition to being of intrinsic interest, our own FAIRE data pointed out an interesting paradox in the chromatin changes observed during senescence. While a number of studies, including our own (Adams, 2007a; Greer et al., 2011; Kreiling et al., 2011) have indicated an overall increase of heterochromatin as cells become senescent, our FAIRE data indicated a global increase in openness. While the changes observed by FAIRE were small in magnitude, they are not consistent with the 2-3-fold increases in heterochromatic proteins, such as mH2A and HP1β (Kreiling et al., 2011), that have been documented in senescent cells. We therefore thought it could be possible that heterochromatin increased specifically in the repetitive portion of the genome, which our FAIRE analysis could not detect. We thought this was especially reasonable, as it is known that the repetitive portion of the genome is heavily heterochomatinized, and accounts for a large fraction of the total heterochromatin that is observed in cells.

4-2) Overview of Experimental Design

To determine the relative enrichment of repetitive DNA in senescent FAIRE cells we use a dot blot assay to determine the relative abundance of L1 and Alu sequences in early

passage and senescent cell FAIRE samples compared to total genomic DNA. For the dot-blot experiments DNA was isolated using the FAIRE procedure from early passage and senescent cells in biological triplicates as described in the previously. The blots were hybridized with α-32P labeled Alu and L1 probes. The probe signal intensities were calculated and the ratio of FAIRE to Input samples were compared to determine the relative enrichment for each element between early passage and senescent conditions.

Additionally we examine the change in expression of L1 and Alu using RT-qPCR and evidence of L1 transposition using a multiplex qPCR assay. The expression activity of LINE-1 and Alu elements was determined using quantitative PCR methods. Total RNA was prepared from biological triplicates of early passage and senescent cells. Reactions for L1 expression used the L1 ORF2 primers described in Chapter 2. Alu transcription primers were based on the expressed Alu repeat (EAR) also described in Chapter 2. In each experiment GAPDH was used as the normalization control, and relative expression was further normalized to the lowest early passage sample.

The L1 transposition assay was adapted from the quantitative PCR experiments described in Coufal et al., (2009). Total genomic DNA was isolated from 3 biological replicates of senescent and early passage cells. Mutiplex qPCR experiments were performed comparing L1 ORF2 copy number to L1 5' UTR and 5S rDNA control probes.

4-3) Dot Blot Analysis of LINE and SINE Sequences in FAIRE Fractions

In order to examine the relative representation of sequences corresponding to L1 (LINE) and Alu (SINE) retrotransposable elements in input and FAIRE DNA preparations, we devised a dot blot strategy. Probes for Alu and L1 sequences were made by amplifying

representative fragments from genomic DNA and subsequently labeling the amplified fragments with ^{32}P. Alu primers were designed using the Alu consensus sequence (Batzer et al., 1996) and placed in regions that demonstrate minimal sequence divergence between Alu families (Figure 4-1A). The L1 probe was designed from a region near the 3' end of L1 ORF2 (Figure 4-1B). The L1 sequence was obtained from L1 Base (Zemojtel and Penzkofer), an online database of annotated active and full-length L1 elements. The 3' end of ORF2 was chosen as the probe because the majority of L1 elements present in the genome have truncated 5' ends. Thus, placing the probe towards the 3' end should pick up the majority of L1 elements in the genome. The 383 bp probe sequence we chose mapped to all 11,901 annotated L1 elements in the L1 database using the NCBI36/hg18 2006 annotated human genome data set.

FAIRE DNA samples from three replicates of early passage and senescent cells were prepared using our standard procedure (Chapters 2 and 3). The same HDF cell strain (LF1) was used as in Chapter 3, and cells were propagated from the same frozen stocks, but the cells were expanded for harvest on a separate occasion (after the experiments in Chapter 3 were concluded). The three replicates for the dot blots were expanded from the same frozen stock, but the dishes were harvested at different times and all the subsequent processing was done separately. The input DNA samples were prepared by separating an aliquot equal to 10% of the total sample after the sonication step. This aliquot was then de-crosslinked, proteinase-k treated, and phenol extracted. The FAIRE and input DNA samples were thus treated in parallel, with the exception that for FAIRE the phenol extraction was performed on cross-linked chromatin, whereas for input the extraction was performed on de-crosslinked material. This procedure resulted in 4 categories of samples,

early passage input, early passage FAIRE, senescent input, and senescent FAIRE. Each in turn was made in triplicate, for a total of 12 samples.

The amount of DNA present in each sample was first quantified using the Nanodrop instrument (Thermo Scientific). Each sample was then spotted in two-fold dilution series from 40 ng to 2.5 ng DNA per spot.The blots were made by spotting the DNA samples onto positively charged nylon membranes under alkaline conditions using a 96 well vacuum manifold. It subsequently became apparent that the Nanodrop measurements were not sufficiently accurate, and we thus used two additional methods to quantify the amount of DNA present in our samples: Quant-it PicoGreen dsDNA Assay Kit (Invitrogen) and qPCR. The qPCR was performed with 5 distinct primer pairs to genomic regions that were found not to be FAIRE enriched in either early passage or senescent cells (Chapter 3). The results of the Pico green and qPCR measurements were in close agreement. We then used the qPCR quantification (average of the 5 distinct primer pairs) which we felt was the most accurate method to calculate the effective concentration of the DNA samples that were deposited on the dot blot membranes. The details of these calculations are presented in Chapter 2.

Radiolabled Alu and L1 probes were hybridized to the membranes, exposed to storage phosphor screens, and imaged on a Typhoon 9410 (GE Healthcare) scanner. The raw scans are shown in Figure 4-2 for the Alu probe, and in Figure 4-3 for the L1 probe. In order to account for inherent variability on each membrane, and to increase the data sets for each probe, once image files were acquired for each blot, the blots were stripped and rehybridized with the alternative probe. The resulting image files were quantified using

ImageJ software, signal intensity values were calculated based on the pixel intensity for each spot, and normalized to the amount of DNA present in each spot.

Based on a regression analysis of the dilution series, an overall DNA normalized hybridization signal was derived for each sample (condition and replicate). The calculations are discussed in detail in Chapter 2, and the derived data are presented in Figure 4-4A. The three replicates for each condition were then averaged (Figure 4-4B), and the ratio of FAIRE to input signal was calculated (Figure 4-4C). These data were obtained for the Alu and L1 probes, and for the two blots that were done for each probe. From this treatment it was apparent that the relative abundance of both Alu and L1 signal was lower in the FAIRE fraction than the input DNA, and this was true for both early passage and senescent cells. Given that repetitive elements are known to be largely heterochromatinized in cells, this was an expected result, given that the FAIRE procedure enriches for sequences in a relatively open conformation. We can thus infer that both Alu and L1 sequences are under-represented in FAIRE extracted DNA because of their relatively closed conformation.

We next compared the relative representation of Alu and L1 in FAIRE extracted DNA for early passage and senescent cells, by normalizing the FAIRE value in senescent cells to the value in early passage cells (Figure 4-8B). Interestingly, it became evident that both Alu and L1 sequences were enriched in the senescent FAIRE samples relative to the early passage samples. The Alu elements showed an average enrichment of two-fold in senescent FAIRE samples relative to early passage samples, and the L1 elements showed an average enrichment of four-fold. Taken together these data show that repetitive elements become more abundant in FAIRE samples prepared from senescent cells, which

in turn suggests that repetitive sequences may adopt a more open chromatin conformation in senescent cells.

4-4) Analysis of L1 Retrotransposition Events

One possible explanation for the increased abundance of Alu and L1 sequences in senescent cells would be an increased copy number of these elements. Mobilization of retrotransposons has been documented in somatic cells, for example, experiments reported by Gage's group showed that engineered L1 elements could retrotranspose in human embryonic stem-cell derived brain tissue, and further, developed a quantitative multiplex PCR assay that detected increased copy number of endogenous L1 elements in adult brain tissue samples relative to other somatic tissues (Coufal et al., 2009). Whether retrotransposition can occur in senescent cells has however not been examined. To investigate whether the enrichment of L1 elements in senescent cells we observed in our dot blot experiments reflected an increased activity of this retroelement, we adapted the multiplex quantitative PCR method of Coufal *et al.* (2009) to examine relative L1 copy number in early passage and senescent LF1 cell genomes. Total genomic DNA was extracted from three biological replicates of early passage and senescent LF1 cells, and the copy number of the L1 ORF2 was determined relative to two different control sequences: the L1 UTR, which does not retrotranspose, and the 5S RNA gene, a high copy number gene encoding a RNA component of the large ribosomal subunit. Relative L1 ORF2 copy number was calculated as the inverse ratio of the L1 ORF2 Ct value over the control Ct value. Relative L1 ORF2 values were averaged between early passage and senescent replicates, and standardized so that the value of the early passage replicate

relative L1 ORF2 was normalized to 1 (Figure 4-6). These experiments did not detect any significant increase of L1 retroelement copy number in the senescent cell populations.

4-5) Analysis of Alu and L1 Transcription

We next investigated whether the increased openness of Alu and L1 elements, indicated by the relative enrichment of these DNA sequences in senescent cell FAIRE preparations, was functionally correlated with changes in RNA expression. If increased FAIRE signal is associated with decreased heterochromatinization, then in turn this would be expected to possibly lead to increased transcription. We therefore performed RT qPCR analysis to assess the relative transcript levels of these repetitive elements. Total RNA was isolated from three replicates of early passage and senescent LF1 cells, and reverse transcribed using using the Taqman poly-T reverse transcription reaction kit. The resulting cDNA was then subjected to quantitative PCR to determine the transcript levels of Alu and L1 ORF2 in early passage and senescent cells (Figure 4-7). The Alu transcript was detected in senescent cells at three times higher levels than in early passage cells, and L1 transcripts were detected at ten times higher levels. These data are in agreement with the increased enrichment of Alu and L1 DNA elements in senescent cell FAIRE samples we observed in the dot blot assays. We thus hypothesize that the heterochromatinization and silencing of some retrotransposons families in the repetitive portion of the human genome may become relaxed during cellular senescence.

4-6) Summary

In these experiments we found a distinct under-representation of both Alu and L1 elements in FAIRE DNA, prepared from both early passage and senescent cells (this under-representation was most evident for the Alu element in early passage cells and least evident for the L1 element in senescent cells). These findings are consistent with the fact that SINE and LINE repetitive elements are typically heavily heterochromatinized in the genome, and would thus be expected to be negatively enriched by the FAIRE procedure. When the relative negative enrichment of the Alu and L1 elements between early passage and senescent cells were compared, we found clear evidence for a relative increase of representation for both the Alu and L1 elements in senescent FAIRE samples. Alu elements were present at 2.4-fold higher levels in senescent FAIRE samples, and L1 elements were found at 4.6-fold higher levels. Quantitative PCR analysis of early passage and senescent cell RNA indeed revealed an increase in the transcriptional activity of both Alu and L1 elements. Alu transcripts were detected in senescent cells at levels three times above early passage cells, and L1 transcription levels in senescent cells were elevated by more than 10-fold. These data thus establish a positive correlation between the FAIRE enrichment of retrotransposable elements seen in senescent cells and transcriptional activity of the elements.

Figure 4-1

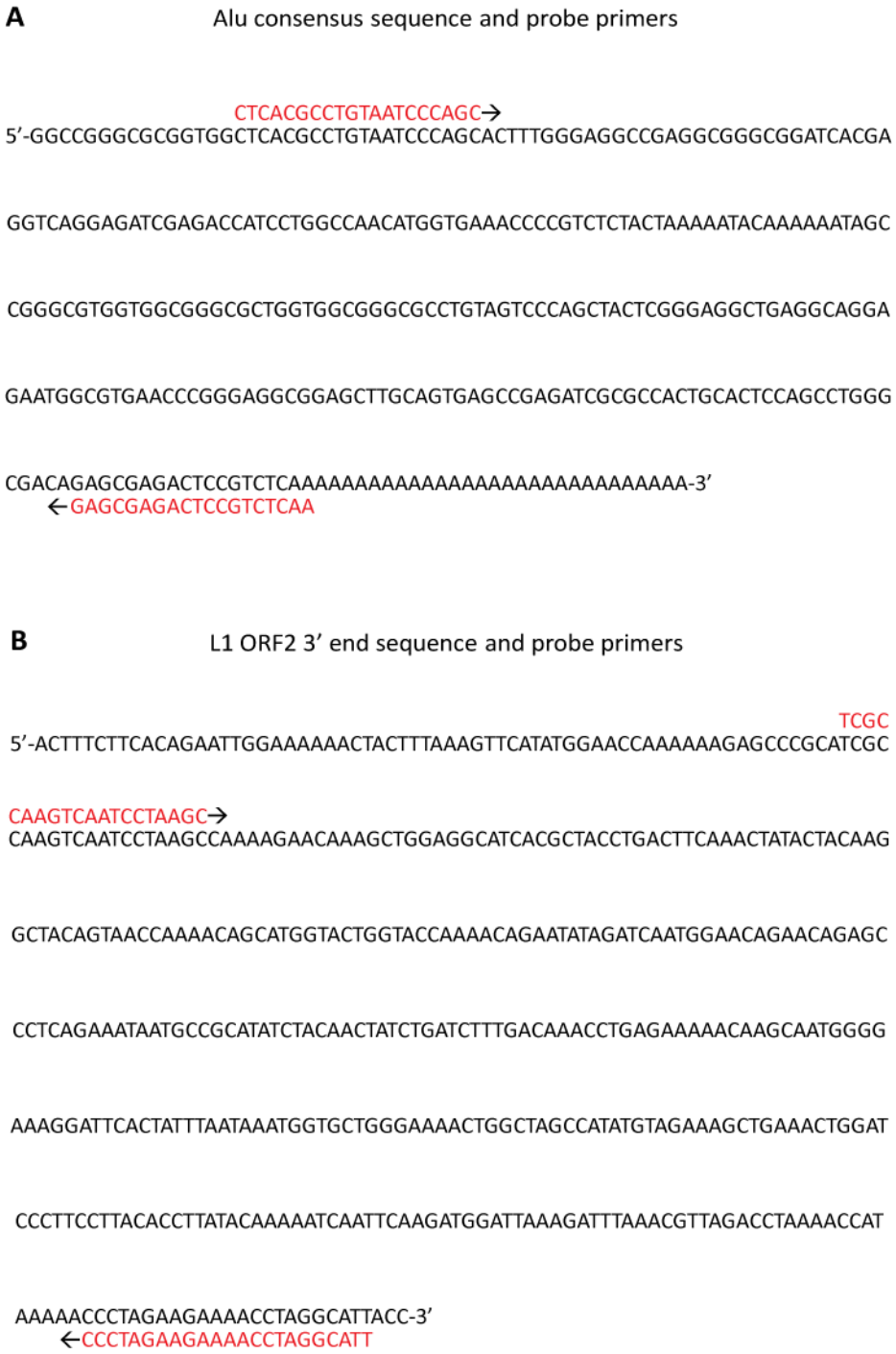
A
Alu consensus sequence and probe primers
CTCACGCCTGTAATCCCAGC→
5'-GGCCGGGCGCGGTGGCTCACGCCTGTAATCCCAGCACTTTGGGAGGCCGAGGCGGGCGGATCACGA
GGTCAGGAGATCGAGACCATCCTGGCCAACATGGTGAAACCCCGTCTCTACTAAAAATACAAAAAATAGC
CGGGCGTGGTGGCGGGCGCTGGTGGCGGGCGCCTGTAGTCCCAGCTACTCGGGAGGCTGAGGCAGGA
GAATGGCGTGAACCCGGGAGGCGGAGCTTGCAGTGAGCCGAGATCGCGCCACTGCACTCCAGCCTGGG
CGACAGAGCGAGACTCCGTCTCAAAAAAAAAAAAAAAAAAAAAAAAAAAAA-3'
←GAGCGAGACTCCGTCTCAA
B
L1 ORF2 3' end sequence and probe primers
TCGC
5'-ACTTTCTTCACAGAATTGGAAAAAACTACTTTAAAGTTCATATGGAACCAAAAAAGAGCCCGCATCGC
CAAGTCAATCCTAAGC→
CAAGTCAATCCTAAGCCAAAAGAACAAAGCTGGAGGCATCACGCTACCTGACTTCAAACTATACTACAAG
GCTACAGTAACCAAAACAGCATGGTACTGGTACCAAAACAGAATATAGATCAATGGAACAGAACAGAGC
CCTCAGAAATAATGCCGCATATCTACAACTATCTGATCTTTGACAAACCTGAGAAAAACAAGCAATGGGG
AAAGGATTCACTATTTAATAAATGGTGCTGGGAAAACTGGCTAGCCATATGTAGAAAGCTGAAACTGGAT
CCCTTCCTTACACCTTATACAAAAATCAATTCAAGATGGATTAAAGATTTAAACGTTAGACCTAAAACCAT
AAAAACCCTAGAAGAAAACCTAGGCATTACC-3'
←CCCTAGAAGAAAACCTAGGCATT

Figure 4-1 Alu and L1 dot blot probe templates

A) The Alu consensus sequence is shown in black. The sequences and positions of the forward and reverse primers that were used to amplify a fragment that was subsequently labeled as a probe are shown in red. B) A region of the L1 consensus sequence corresponding to the 3' end of ORF2 is shown in balck. The sequences and positions of the forward and reverse primers that were used to amplify a L1 probe fragment are shown in red.

Figure 4-2

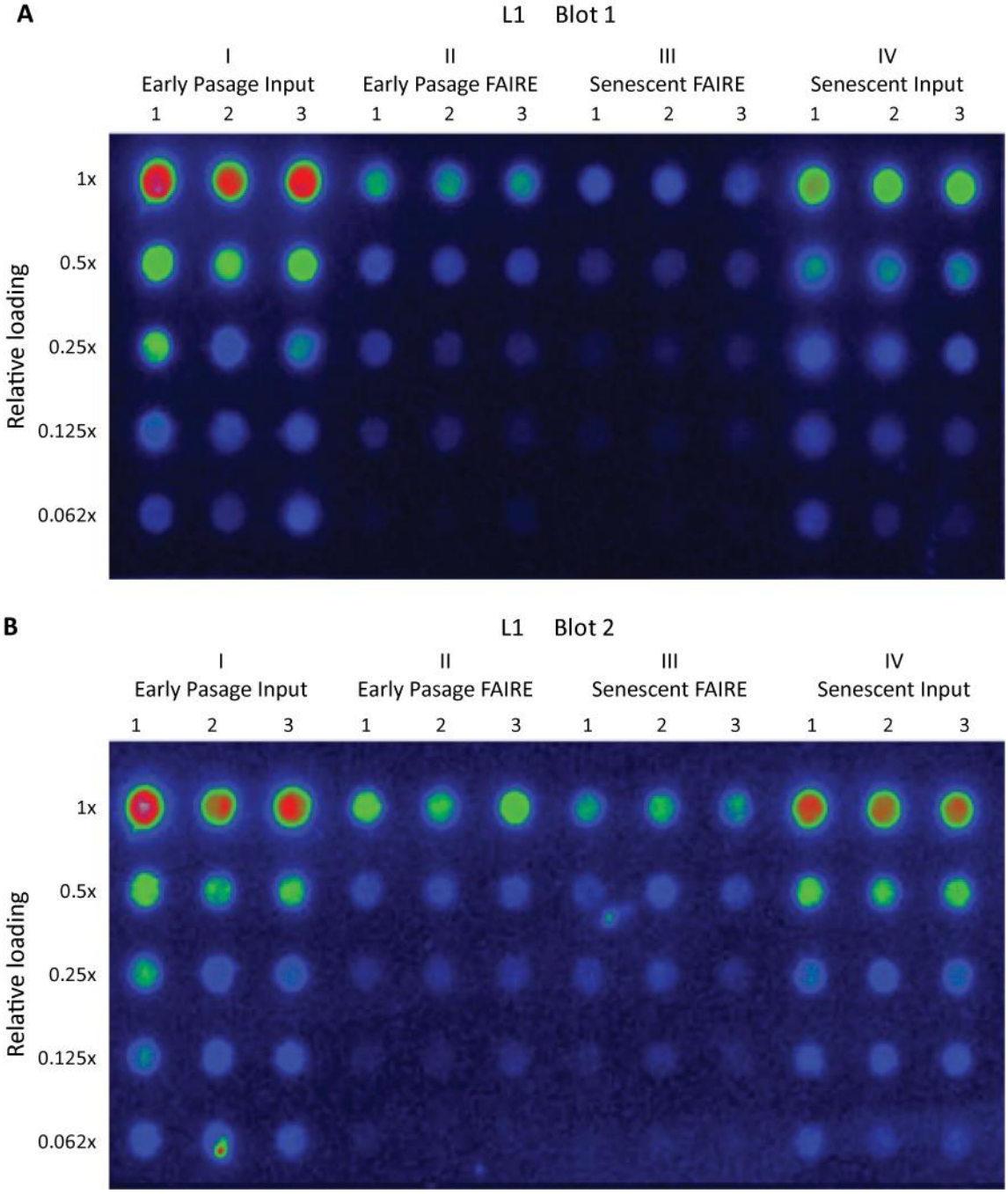
A
L1 Blot 1
I
Early Pasage Input
II
Early Pasage FAIRE
III
Senescent FAIRE
IV
Senescent Input
1 2 3 1 2 3 1 2 3 1 2 3
Relative loading
1x
0.5x
0.25x
0.125x
0.062x
B
L1 Blot 2
I
Early Pasage Input
II
Early Pasage FAIRE
III
Senescent FAIRE
IV
Senescent Input
1 2 3 1 2 3 1 2 3 1 2 3
Relative loading
1x
0.5x
0.25x
0.125x
0.062x

Figure 4-2 Dot blots hybridized with L1 probe.

Each sample was spotted as a series of dilutions arranged vertically, and the amount of DNA relative to the topmost spot is shown in the Y-axis. The identity of the samples is indicated across the top: I-Early Passage Input; II-Early Passage FAIRE; III-Senescent FAIRE; IV-Senescent Input. The replicates for each group of samples are labeled 1-3. L1 Blot 1 (A) was initially hybridized with L1 probe. L1 Blot 2 (B) was initially hybridized with Alu probe, stripped and rehybridized with L1 probe.

Figure 4-3

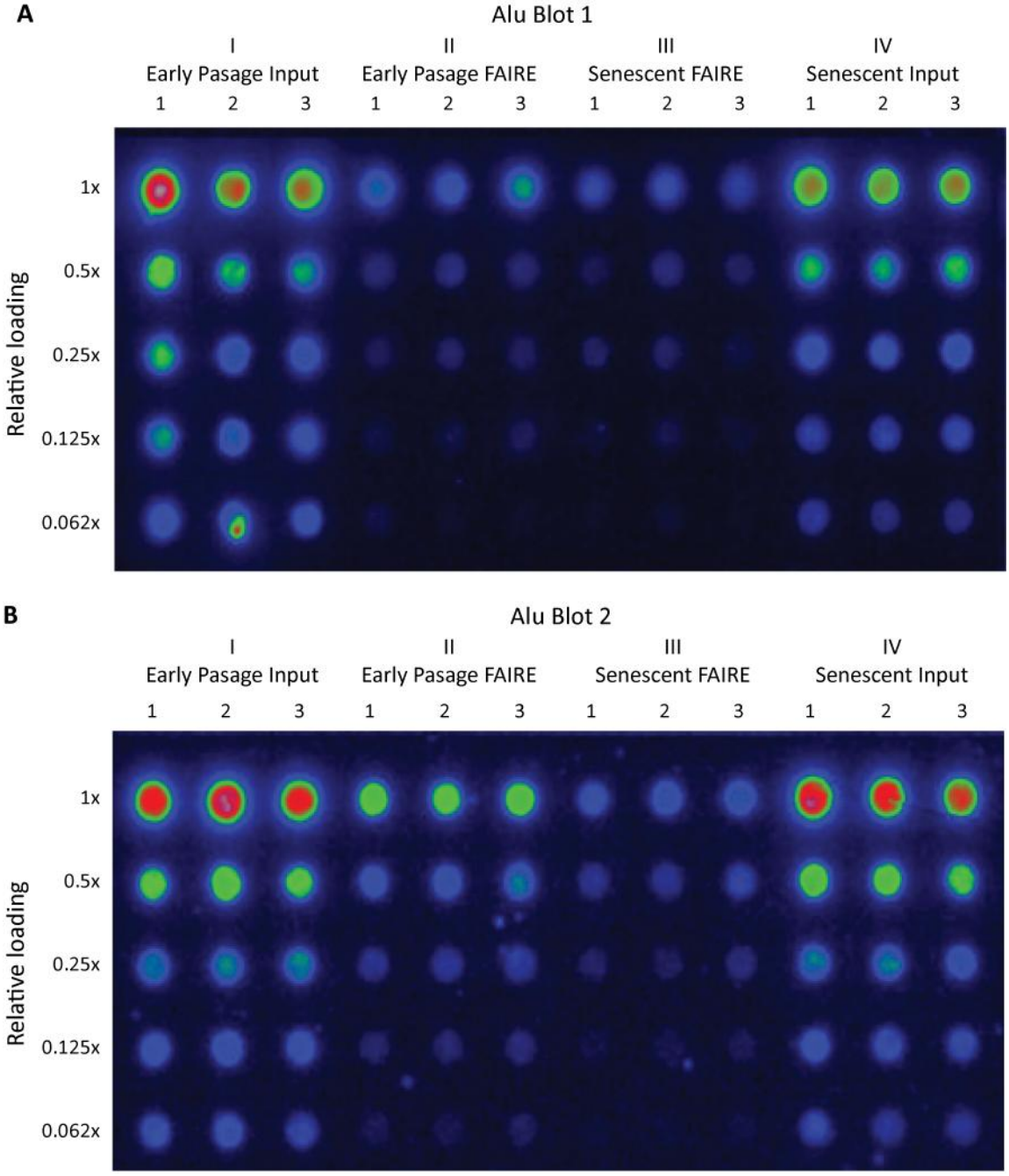
A
Alu Blot 1
I
Early Pasage Input
II
Early Pasage FAIRE
III
Senescent FAIRE
IV
Senescent Input
1 2 3 1 2 3 1 2 3 1 2 3
Relative loading
1x
0.5x
0.25x
0.125x
0.062x
B
Alu Blot 2
I
Early Pasage Input
II
Early Pasage FAIRE
III
Senescent FAIRE
IV
Senescent Input
1 2 3 1 2 3 1 2 3 1 2 3
Relative loading
1x
0.5x
0.25x
0.125x
0.062x

Figure 4-3 Dot blots hybridized with Alu probe.

Each sample was spotted as a series of dilutions arranged vertically, and the amount of DNA relative to the topmost spot is shown in the Y-axis. The identity of the samples is indicated across the top: I-Early Passage Input; II-Early Passage FAIRE; III-Senescent FAIRE; IV-Senescent Input. The replicates for each group of samples are labeled 1-3. Alu Blot 1 (A) was initially hybridized with Alu probe. Alu Blot 2 (B) was initially hybridized with L1 probe, stripped and rehybridized with Alu probe.

Figure 4-4

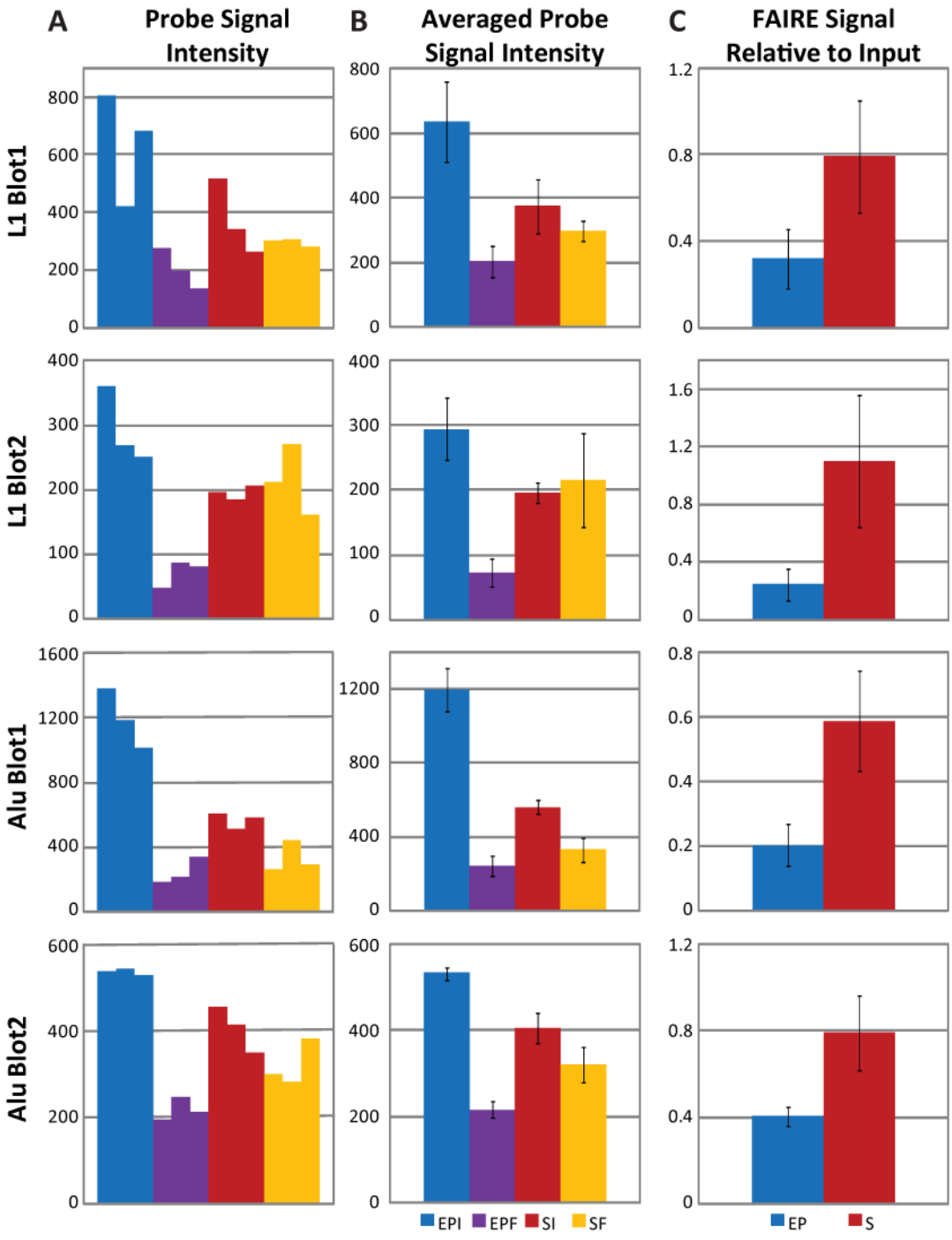
A
Probe Signal Intensity
B
Averaged Probe Signal Intensity
C
FAIRE Signal Relative to Input
L1 Blot1
L1 Blot2
Alu Blot1
Alu Blot2
EPI
EPF
SI
SF
EP
S

Figure 4-4 Normalized blot signal for 5 ng of DNA show increased TE enrichment in senescent cells

(A) the calculated probe intensity value for 5 ng from each sample on the 4 blots. Y-axis: probe intensity value. X-axis: DNA content (5 ng). (B) The probe intensity values from A averaged across the three biological replicates. Y-axis: probe intensity value. X-axis: DNA content (5 ng). (C) The enrichment of the FAIRE samples relative to Input signal. Early passage is depicted as blue and senescent as red. Y-axis: FAIRE enrichment as the ratio of FAIRE probe intensity signal to input probe intensity signal.

Abbreviations (B): EPI, early passage input; EPF, early passage FAIRE; SI, senescent input; SF, senescent FAIRE; (C): EP, early passage; S, senescent

Figure 4-5

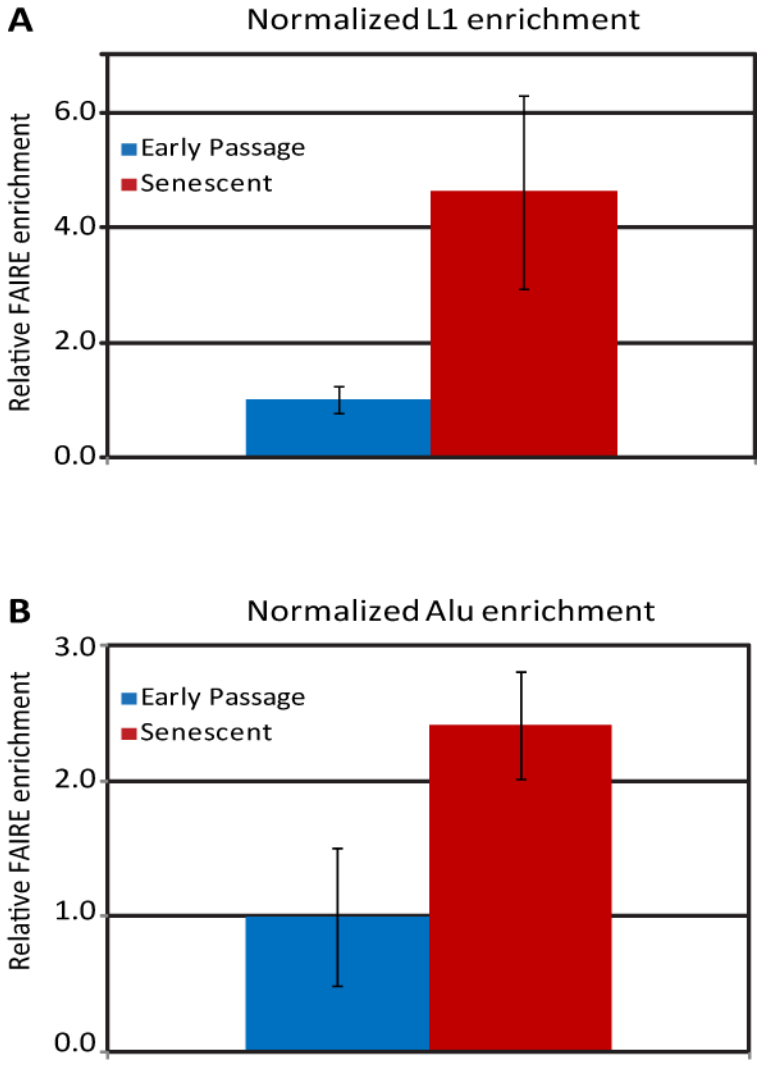
A
Normalized L1 enrichment
Relative FAIRE enrichment
6.0
4.0
2.0
0.0
Early Passage
Senescent
B
Normalized Alu enrichment
Relative FAIRE enrichment
3.0
2.0
1.0
0.0
Early Passage
Senescent

Figure 4-5 Normalized FAIRE enrichment values show increased TE enrichment in senescent cells

The calculations shown in Figures 2-1, 2-2 and Table 2-1 were used to determine FAIRE enrichment for L1 blot 2, Alu blo1 and Alu blot 2. (A) The values from Figure 4-4C for the L1 blots averaged and normalized to early passage cell values. (B) The values from Figure 4-4C for the Alu blots averaged and normalized to early passage cell values. Y-axis: FAIRE enrichment as the ratio of FAIRE probe intensity signal to input probe intensity signal and then normalized to the early passage values.

The % errors were carried through and combined at each successive calculation, and the final error bars reflect this combined error calculation.

Figure 4-6

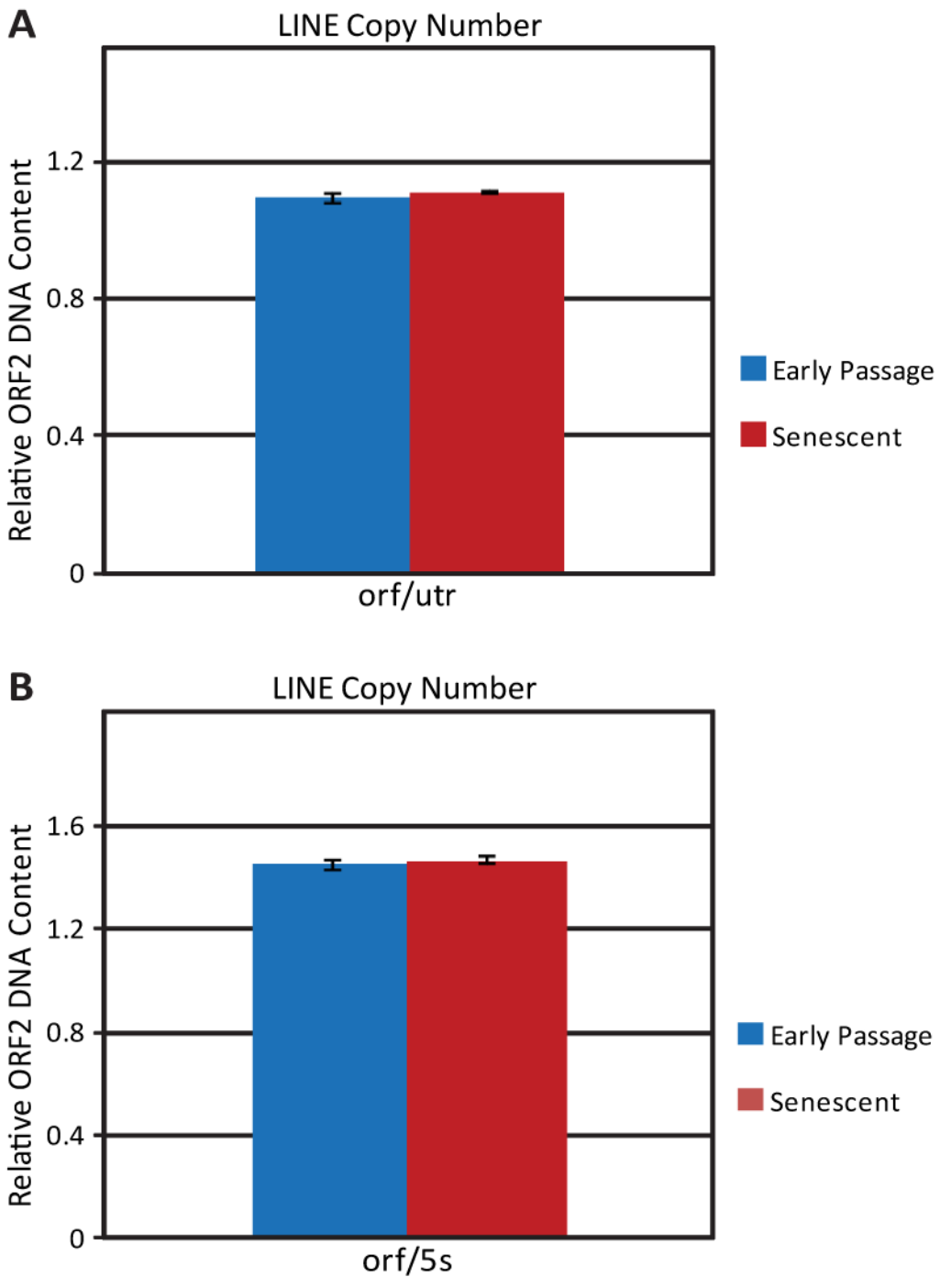
A
LINE Copy Number
Relative ORF2 DNA Content
1.2
0.8
0.4
0
orf/utr
Early Passage
Senescent
B
LINE Copy Number
Relative ORF2 DNA Content
1.6
1.2
0.8
0.4
0
orf/5s
Early Passage
Senescent

Figure 4-6 No increase of L1 copy number in the genome of senescent cells.

L1 ORF2 copy number in total genomic DNA of early passage and senescent cells was determined using multiplex qPCR. Blue bars represent early passage cells, red bars represent senescent cells. (A) The L1 ORF2 content relative to the L1 UTR. Y-axis: the inverse ratio of L1 ORF2 Ct over L1 UTR Ct. (B) The L1 ORF2 content relative to the ribosomal 5S DNA. Y-axis: the inverse ratio of L1 ORF2 Ct over 5S DNA Ct.

Figure 4-7

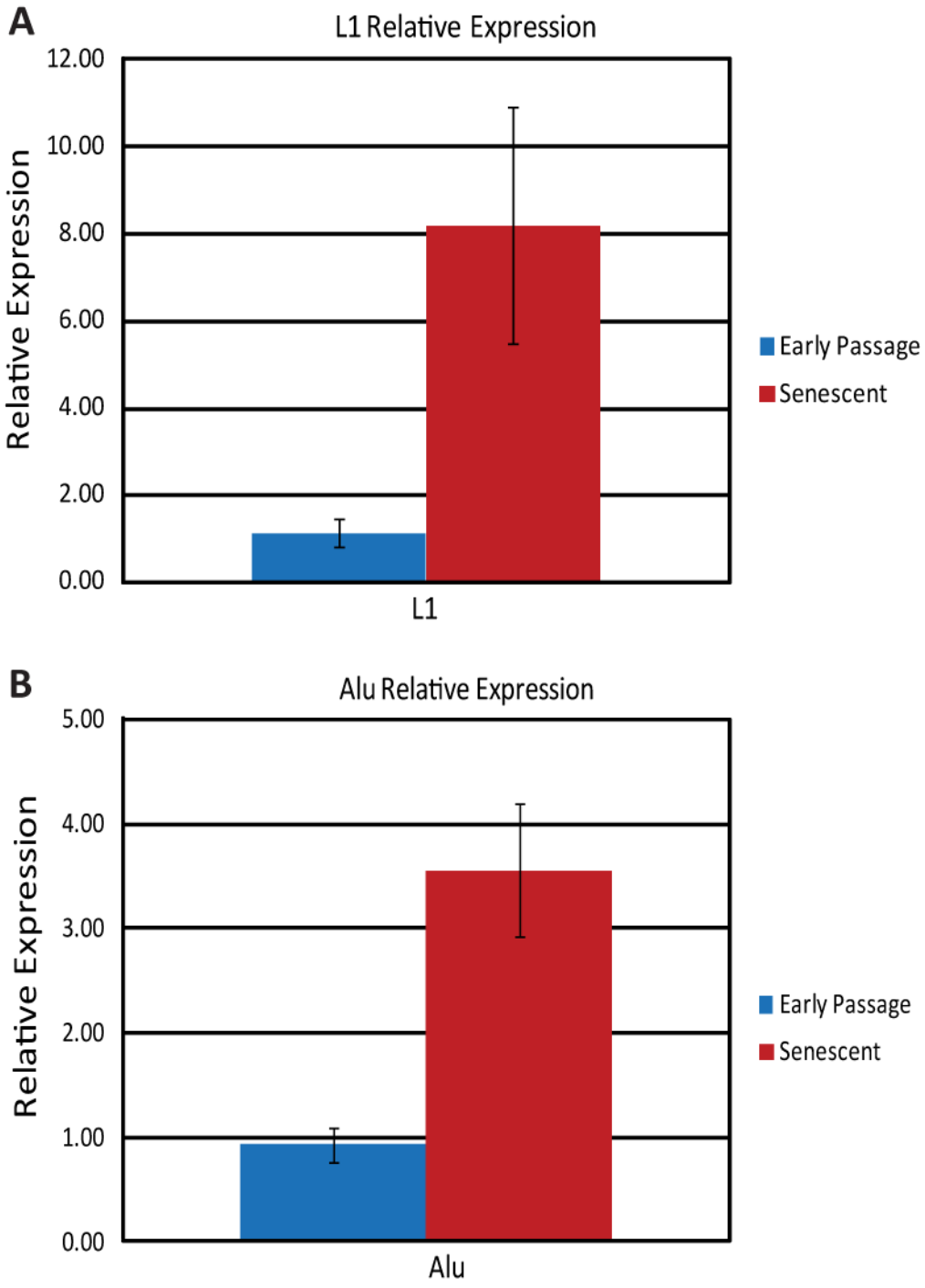
A
L1 Relative Expression
12.00
10.00
8.00
6.00
4.00
2.00
0.00
Relative Expression
L1
Early Passage
Senescent
B
Alu Relative Expression
5.00
4.00
3.00
2.00
1.00
0.00
Relative Expression
Alu
Early Passage
Senescent

Figure 4-7 RNA expression of L1 and Alu elements increases in senescent cells

The relative levels of L1 and Alu transcripts in early passage and senescent cells were measured by quantitative PCR. The reactions were normalized to GAP-DH and relative expression was further normalized to the lowest early passage sample (A) L1 transcripts. (B) Alu transcripts. Y-axis: qPCR enrichment was calculated using the comparative Ct method and is shown as the ratio relative to the lowest input sample.

Chapter 5: Discussion

5-1) FAIRE is a Promising Method to Study Genome Wide Chromatin Changes

Cellular senescence has been associated with changes in the frequency and distribution of molecular markers of chromatin organization; however it is still unclear as to how these changes affect chromatin structure on a genomic scale. Changes in DNA methylation have been described, showing an overall loss of methylation with age, yet an increase in CpG island (CGI) methylation (Bjornsson et al., 2008; Fraga and Esteller, 2007; Fuke et al., 2004; Tra et al., 2002; Wilson and Jones, 1983). Histone modifications, the other major epigenetic regulator of chromatin states, can also be mapped using ChIP-chip and ChIP-seq approaches to generate global distribution patterns, however over 60 histone modifications have been identified, and at least a dozen (H4ac, H3k9me, H3K9me2, H3k9me3, H3K9ac, H3S10ph, H3K27me3, H4K8ac, H4K12ac, H3K56ac, H4K16ac, H4K20me, H4K20me2, H4K20me3 (Feser and Tyler, 2011)) have been shown to change with age, making a complete assessment of the human genome using histone marks a complex endeavor (Feser and Tyler, 2011; Kouzarides, 2007; Mikkelsen et al., 2007). An alternative technique, formaldehyde assisted isolation of regulatory elements (FAIRE), has been shown to identify regulatory elements associated with multiple features of open chromatin, including multiple histone marks, DNase sensitivity and RNA polymerase occupancy (Giresi et al., 2007; Giresi and Lieb, 2009; Nagy et al., 2003). The goal of this project was to identify redistributions in the global pattern of open chromatin in senescent cells using the FAIRE technique.

5-2) FAIRE Enrichment of Regulatory Elements

Transcription start sites (TSS) are an important regulatory element for gene transcription, and the position of nucleosomes within these regions has a major impact on the activity of associated genes (Mellor, 2005; Ozsolak et al., 2007). Previously it has been shown that FAIRE preferentially enriches DNA sequences associated with regions of nucleosome vacancy, a feature shared by active TSS in both human and *S. cerevisiae* cells (Bernstein et al., 2004; Giresi et al., 2007; Yuan et al., 2005). Using whole genome tiling array analysis of FAIRE DNA, we were able to demonstrate a significant difference in the magnitude of the TSS signal between early passage and senescent cells. Senescent cells showed a decrease in the FAIRE enrichment at TSS, suggesting a loss of open chromatin at these loci. This analysis encompassed the TSS of 19,538 of the 26,083 annotated genes in the human genome. Our results are consistent with previous findings that documented an average enrichment across all TSS (Giresi et al., 2007; Nagy et al., 2003; Yuan et al., 2005). We found that this enrichment occured in both early passage and senescent cells, but when the averaged signals were compared between the two we saw a distinct decrease in the magnitude of the TSS enrichment in senescent cells. This finding suggests that relative to early passage cells, TSS in senescent cells have a higher density of nucleosome occupancy, which could point to a senescence-associated increase in chromatin compaction in the genic regions. Since compact chromatin is less accessible to the transcriptional machinery, this evidence points to senescence-associated chromatin organizational changes in many TSS, which could contribute at least partially to the changes in gene expression that have been documented in senescent cells (Bayreuther et al., 1988; Coppe et al., 2006; Dimri et al., 1995; Narita et al., 2003; Zhang et al., 2003).

To further examine the potential loss of open chromatin in important regulatory regions of senescent cells, we compared the enrichment of enhancers between early passage and senescent cells. Enhancers are cis-acting regulators of transcriptional activity, and can greatly enhance transcription rates for multiple target promoters at various times under distinct conditions, and over substantial genomic distance (Maston et al., 2006). As with the TSS regions, we were able to identify FAIRE enrichment peaks in both early passage and senescent cells that corresponded with a list of 36,589 previously identified and annotated enhancer regions (Heintzman et al., 2009). Enhancers were identified by a computational prediction algorithm that identifies enhancers by comparing chromatin signatures to a training set comprised of sequences determined to be enhancers through a combination of criteria; p300 binding, a distance greater than 2.5 kb from known 5' ends of genes, DNase1 hypersensitivity, cross species conservation, presence of predicted regulatory modules (PReMods)(Blanchette et al., 2006), enrichment for H3K4me, and depletion of H3K4me3(Heintzman et al., 2007). The 36,589 enhancers were identified from H3K4me ChIP-chip in HeLa cells, while an additional set of 24,566 enhancers were identified in K562 cells. The majority of the enhancers identified were cell line specific, with few shared between HeLa and K562 (Heintzman et al., 2009). This indicates that the list is unlikely to be a comprehensive list, and probably includes a lot of enhancers that are not active in HDF, and also misses a lot of enhancers that are. As with the TSS, we found a decrease in the enrichment of the enhancer regions in senescent cells relative to early passage cells. This finding is further evidence for an increase in chromatin condensation in the regulatory regions of the genome, and suggests a reduction in enhancer-mediated gene activity in senescent cell populations.

In addition to TSS and enhancers we evaluated the FAIRE enrichment patterns associated with replication domains. These are not canonical regulatory elements in the sense that TSS or enhancers are, as they do not directly alter the rate of gene expression. However, replication domains have been suggested to be regions of substantial genomic organization (Gilbert et al., 2004; Huvet et al., 2007; Necsulea et al., 2009; Sproul et al., 2005). Replication domains are considered to be the regions of the genome that fall between two origins of replication. A high levels of gene density and activity has been associated with origin-proximal regions, and the transcription of genes in these regions is oriented with replication progression, with a higher proportion of + genes in the 5' halves of replication domains and a higher proportion of – genes in the 3' halves (Huvet et al., 2007; Necsulea et al., 2009). We examined 679 of these domains identified by Huvet *et al.*, 2007, and found a pattern of enrichment across regions proximal to origins in early passage cells that was not seen in the replication domain centers. Enrichment was not detectable in senescent cells either in the transitional (origin) or central regions. Since senescent cells do not replicate their DNA, it is understandable that chromatin near origin regions would become more compact, and the surrounding genes could also be affected by this chromatin reorganization, partially contributing to the observed reduction of TSS enrichment.

Since our initial exploration of TSS evaluated the average TSS enrichment across all genes in the genome, we did not know if the reduction of FAIRE enrichment in senescent cells was due to a reduced number of FAIRE enriched genes, a reduction of FAIRE enrichment in all genes, or a combination of both. In order to examine in greater detail the populations of genes that undergo a change in FAIRE enrichment during senescence,

a clustering analysis was performed to generate 4 groups based on TSS enrichment: early passage FAIRE enriched, senescent FAIRE enriched, early passage non-enriched and senescent non-enriched. From this analysis it emerged that senescent cells had a reduced number of genes enriched by FAIRE, and those that were enriched had lower average enrichment signals. Of the 19,524 genes clustered in the analysis, 11,561 were FAIRE-enriched in early passage cells, compared to 9,187 in senescent cells. In addition to the reduced number of TSS that were enriched in senescent cells, we also noted an overall reduction in the magnitude of the FAIRE enrichment peak. This observation stood in contrast to the pattern seen in the non-enriched clusters, where the average enrichment values for early passage and senescent cells were not noticeably different. When we examined all the genes that clustered into the enriched group for both early passage and senescent cells, we found that 6,698 genes were common to both populations, 4,863 genes were uniquely enriched in early passage cells, and 2,489 were uniquely enriched in senescent cells. These observations further indicate an overall loss of open chromatin at the TSS of senescent cells. However, the presence of TSS that lack enrichment in early passage cells but gain enrichment in senescent cells is indicative of gene regulation patterns occurring in both directions during senescence, which has been amply demonstrated by gene expression studies. Nevertheless, while changes in TSS FAIRE signals between early passage and senescent cells did occur in both directions, loss of signal in senescent cells was the predominant effect (by some 2-fold).

5-3) Genome-wide Patterns of FAIRE Enrichment

In order to determine the distribution of open chromatin on a more global scale we examined the total FAIRE signal across the genome in both early passage and senescent cells. We made graphs where the log2 fold changes between corresponding input and FAIRE probes were plotted as histograms to visualize the number of probes that fell in any given fold change category. In order to verify what we had previously seen in TSS and regulatory regions, we examined the distribution of combined probe signals in 3,000 bp regions centered on TSS, enhancers and replication domain origins. We found that the mean signal in early passage FAIRE samples was 2.3-fold higher in these regions as compared to senescent cells, demonstrating that this method of analysis agrees with the interpolated background subtracted data used in our initial analysis of FAIRE enrichment. The loss of FAIRE signal in senescent cells becomes even more pronounced (4.6-fold) when the regulatory region mean signals are normalized to the means of the corresponding total array probes.

We also used this method to examine the signal distribution across the entire genome, and found that the total mean FAIRE enrichment signal was slightly higher in senescent cells when compared to early passage cells. This was also the case for probes in non-regulatory regions (which were defined as the total probes minus the probes in the regulatory regions), where senescent cells had a slightly higher mean signal compared to early passage cells. It should be pointed out that the mean signal in total (as well as non-regulatory) probes was very close to zero (0.0195 and 0.0139 for early passage total and non-regulatory, respectively), and that the changes in senescent cells were very small (0.0381 and 0.0378 for senescent total and non-regulatory, respectively). Given the nature of the quantile normalization process, one would expect the means of all the

values (probes) of two data sets that were quantile normalized together to be very similar (if not identical), and hence the difference between the two should be zero (or very close to it). Hence, it is unlikely that the very small differences in the mean signals (FAIRE-input log2 fold change) between early passage versus senescent cells have a significant meaning.

We also devised a qualitative visualization of the distribution of open chromatin across the genome, which we called chromatin painting. This treatment calculates the average FAIRE enrichment signal in a 1 Mb window sliding at 100,000 bp intervals across the genome, and presents it as a heat map aligned with the chromosome coordinates. This analysis also showed the overall increase in FAIRE signal across the genome of senescent cells, since the colors of the heat map were set so as to pick up the small differences in mean values discussed above. More interestingly, we also observed noticeable variations in the patterns of FAIRE signal distribution between early passage and senescent cells. Whereas in senescent cells the signal was more evenly distributed, in early passage cells the distribution showed more distinct regions of high and low FAIRE enrichment.

As TSS were found to be enriched in FAIRE signal in early passage cells, we asked whether the uneven distribution in FAIRE enrichment along chromosomes seen by chromatin painting may correspond to regions of high gene density. To evaluate this, the mean FAIRE signal and number of TSS present were calculated in a series of non-overlapping tilled windows of 100 kb across all the regions represented on the arrays. When the mean FAIRE signal was plotted against the number of unique TSS within each window, a positive correlation trend appeared in early passage cells (Spearman's

coefficient of 0.235). Thus, as the number of unique TSS within a window increases, the mean FAIRE signal also tends to increase. When this analysis was applied to senescent cells this trend was not observed (Spearman's coefficient of 0.069). This may at least in part explain the more homogeneous signal seen by chromatin painting in senescent cells, although other factors may also be at play.

5-4) FAIRE Enrichment of LINE and SINE Repetitive Elements

A major limitation of the microarray platform is that the repetitive portion of the human genome is essentially ignored in the analysis. As we were interested in making a truly global and genome-wide assessment of chromatin changes during cellular senescence, these limitations became very significant. The importance of this issue is underscored by the fact that about half of the human genome is composed of repetitive elements which comprise most of the heterochromatin in the cell. Since we were unable to evaluate this part of the genome using FAIRE-chip, we devised an alternative method based on dot blotting hybridization to quantify the representation of repetitive elements in FAIRE preparations of DNA.

The repetitive fraction of the human genome consists primarily of retrotransposable elements (Lander et al., 2001; Richard et al., 2008). We investigated two common classes of retrotransposons to obtain an indication of what was occurring in the repetitive regions of the genome. These elements were the Long Interspersed Element (LINE) family 1 (L1), and the Short Interspersed Element (SINE) Alu. Together, these two families make up about 70% of the repetitive DNA found in the human genome, and 30% of the total DNA content (Richard et al., 2008). This level of coverage should provide a

representative view of how the repetitive regions of the genome associated with facultative heterochromatin change in senescent cells.

The experimental design was to prepare FAIRE DNA using standard procedures, and use it to prepare, along with input control DNA, dot blot membranes. These were then hybridized with radioactive probes, and the signal was normalized to the total DNA content of each dot. Using this methodology we found a distinct under-representation of both Alu and L1 elements in FAIRE DNA, prepared from both early passage and senescent cells (this under-representation was most evident for the Alu element in early passage cells and least evident for the L1 element in senescent cells). These findings are consistent with the fact that SINE and LINE repetitive elements are typically heavily heterochromatinized in the genome, and would thus be expected to be negatively enriched by the FAIRE procedure.

We next compared the relative negative enrichment of the Alu and L1 elements between early passage and senescent cells. To do this, in addition to normalizing the FAIRE signals to their corresponding inputs, we additionally compared these normalized values between early passage and senescent cell populations. After this standardization we found clear evidence for a relative increase of representation for both the Alu and L1 elements in senescent FAIRE samples. Alu elements were present at 2.4-fold higher levels in senescent FAIRE samples, and L1 elements were found at 4.6-fold higher levels

If we consider L1 and Alu elements as representative of facultative heterochromatin present in much of the repetitive genome, our experiments indicate that these regions partition more frequently into FAIRE fractionated DNA prepared from senescent cells. Since FAIRE preferentially isolates genomic regions that have low nucleosome content

(Giresi et al., 2007; Nagy et al., 2003), the increased enrichment of transposable elements in senescent FAIRE DNA points to a relaxation of the chromatin structure in these normally heterochromatic sequences. This result is concordant with a number of reports that have shown global DNA hypomethylation in senescent cells and aging tissues (Fairweather et al., 1987; Shmookler Reis and Goldstein, 1982; Wilson et al., 1987), and that much of this hypomethylation occurs in transposable element sequences (Baccarelli et al., 2010; Barbot et al., 2002; Jintaridth and Mutirangura, 2010; Zhu et al., 2011).

5-5) Relationship Between FAIRE Enrichment and Transcription

If the changes in FAIRE enrichment we detected using the tilling arrays and dot blots were indicative of altered chromatin states, we would in turn expect changes in transcriptional activity in these regions, as chromatin structure has been shown to have a profound effect on the regulation of transcriptional activity (Gilbert et al., 2004; Guenther et al., 2007; Li et al., 2007; Sproul et al., 2005). To explore this possibility we first compared the FAIRE TSS data obtained from the genome tiling arrays to gene expression data obtained from mRNA expression arrays. We focused on genes that showed changes in TSS FAIRE enrichment between early passage and senescent cells, and compared the direction of the TSS enrichment with the mRNA expression level. We indeed observed a positive relationship between the change in TSS FAIRE enrichment and transcriptional activity. If a TSS showed an increased enrichment in senescent cells, the associated gene tended to be more active in senescent cells, and the same was also observed in the other direction. First, mean expression scores were calculated for all the genes whose TSS were analyzed in the FAIRE data. When the mean expression scores were compared between

the FAIRE enriched and non-enriched clusters, for both early passage and senescent cells, 80% of genes in early passage cells with enriched TSS had a higher expression value than the median of genes with non-enriched TSS. This value dropped to 75% of genes with enriched TSS in senescent cells. In addition to showing a positive correlation between TSS enrichment and gene expression, these data also show a small trend towards reduced transcriptional activity of TSS enriched genes in senescent cells.

Although retrotransposable elements are in general heavily repressed, some transcriptional activity can be detected in many types of somatic cells (Belancio et al., 2010; Faulkner et al., 2009; Rangwala et al., 2009). Changes in activity have also been documented under certain conditions: L1 transcripts are up-regulated in some cancer cells (Skowronski et al., 1988; Skowronski and Singer, 1985), and both Alu and L1 transcription is induced by genotoxic stresses (Hagan et al., 2003; Li and Schmid, 2001; Liu et al., 1995; Rudin and Thompson, 2001). There is some evidence that an increase in expression of Alu elements is associated with senescence in adipose derived mesenchymal stem cells, and that stable depletion of the Alu transcripts increased replicative capacity (Wang et al., 2011). To our knowledge, beyond this example transcriptional activity of transposable elements during cellular senescence has not been examined. Given the increased abundance of Alu and L1 element DNA in FAIRE DNA prepared from senescent cells, we examined the transcription of these elements into RNA. We also investigated whether L1 elements can be mobilized in senescent cells, leading to increased copy number. Quantitative PCR analysis of early passage and senescent cell RNA indeed revealed an increase in the transcriptional activity of both Alu and L1 elements. Alu transcripts were detected in senescent cells at levels three times

above early passage cells, and L1 transcription levels in senescent cells were elevated by more than 10-fold. These data thus establish a positive correlation between the FAIRE enrichment of retrotransposable elements seen in senescent cells and transcriptional activity of the elements. Furthermore, this correlation is quantitative, as L1 FAIRE enrichment and transcription were both higher than those measured for Alu. Our results interestingly provide a possible link between stress and cellular senescence, given that Alu and L1 transcription has been reported to be induced by genotoxic stress, and that replicative senescence is known to be mediated by a DNA damage response. The relationship between retrotransposable element activation and genotoxic stress is likely to be complex; since transposition (and especially abortive transposition) can lead to DNA double strand breaks (Belancio et al., 2010; Lunyak and Atallah, 2011). A potential for deleterious feed-forward mechanisms can thus be envisioned, for example, DNA damage could lead to transposable element expression and mobilization, which in turn could lead to more DNA damage.

It was therefore of considerable interest to investigate possible retrotransposition of L1 elements in senescent cells. For this we used a quantitative multiplex PCR method to compare the relative copy number of the L1 ORF2 sequence to that of the L1 5'UTR and the 5S ribosomal RNA gene. This analysis failed to detect any significant change in ORF2 copy number relative to these controls in senescent cells compared to early passage cells. This indicates that the L1 FAIRE enrichment we detected in the dot blot experiments was due to an opening of the L1 TSS, making it partition more readily in the FAIRE fraction, rather than to an increase in L1 element genomic representation. Although the multiplex PCR method we used to assess L1 copy number is sensitive and

has previously been used to show L1 mobilization in human brain (Coufal et al., 2009), it must be kept in mind that due to the high copy number of L1 elements, a small increase in copy number is beyond the resolution of any quantitative PCR method. Given that the mobilization of even a few transposable elements could have deleterious effects, more direct assays to score discrete transposition events will have to be devised.

5-6)Conclusions

The new insights provided by this work fall into several categories. First, it is clear that the FAIRE method can reveal very interesting and relevant changes in genome-wide chromatin organization. Second, it is evident that very extensive chromatin changes take place as cells undergo replicative senescence. The latter provides a potential mechanism to account for the widespread changes in gene expression that have already been documented, as our study is one of the first to investigate these changes at the chromatin level.

More specifically, the analysis of the unique fraction of the genome on whole genome tiling arrays revealed a general loss of FAIRE signal in senescent cells. Loss of FAIRE signal has previously been shown to correlate with higher nucleosome occupancy. This loss of signal can thus be inferred to correspond to a more closed chromatin structure. The loss of signal affected both TSS and enhancers, two of the most important cis-regulatory elements for the regulation of transcription. Senescent cells had fewer open TSS, and those that were open had a quantitatively lower signal. This conclusion was reached using independent methods of data analysis, and it is also supported by recent unpublished FAIRE-seq data from the Sedivy lab. Finally, loss of FAIRE openness was

correlated with reduced gene expression. A subset of TSS were shown to gain FAIRE signal in senescent cells (and also increase their transcription), but this was a small effect relative to the overall trend.

The effects described above were made possible by comparing FAIRE signal in regulatory regions to either randomly chosen regions or non-regulatory regions of the genome within a single condition (e.g., early passage cells, or senescent cells). It is unfortunately not possible to obtain, because of the manner in which the array data are normalized, comparisons of whole array mean signals between different arrays or conditions. We do however know, from other experiments (Kreiling et al., 2011) that senescent cells contain 2-3-fold elevated levels of heterochromatin-associated proteins, such as mH2A or HP1. Thus, although the FAIRE experiments cannot measure the total heterochromatin content of a cell, the data indicate that senescent cells contain more heterochromatin, which results in a general trend of decreasing the openness of TSS and decreasing gene expression. It should also be noted that in contrast to some other reports (Feser and Tyler, 2011; Li et al., 2008b; O'Sullivan et al., 2010) we do not see changes in overall histone content of senescent cells (Kreiling et al., 2011). We thus believe that the predominant change that happens in senescent cells is compaction of existing chromatin into higher order heterochromatic structures.

In contrast to what was observed in the unique fraction of the genome on the tiling arrays, FAIRE accessibility in the repetitive fraction of the genome increased, as determined by dot blot analysis. Although we have not comprehensively examined all regions of the repetitive genome, the same trend was observed for Alu and L1 elements, which between them comprise a very significant fraction of the repetitive genome. Increased FAIRE

signal was accompanied by increased Alu and L1 RNA transcription, further reinforcing the overall positive correlation between FAIRE accessibility and permissiveness for transcription. The overall effect on genome organization in senescent cells is thus one of remarkable homogenization: the repetitive fraction of the genome, which is typically more heterochromatic becomes more accessible, and the unique fraction of the genome, which is typically more euchromatic becomes more closed.

5-7) Future Directions

High throughput sequencing technology has become more affordable since the inception of this project and is now an equitable alternative to FAIRE-Chip assays. High throughput sequencing also provides a number of advantages over microarray analysis. The lack of a need for pre-existing array bound probes allows for an unbiased analysis of a DNA sample without the high levels of background signal typical of microarray technology. Additionally a single genomic sample can be run on a single lane of a sequencing flowcell, eliminating the difficult task of normalization between multiple arrays necessary for analyzing total genomic human DNA on tiled arrays. Also, since the sequencing utilizes libraries derived directly from the DNA experimental and control samples, the sequence of repetitive elements are present on the flow cells. While by default these regions tend to be ignored by analysis software, programs may be developed especially when using paired end reads, that could differentiate certain repetitive elements from others based on flanking non-repetitive sequence, or by the random variations that have arisen due to random mutation. Current experiments in our lab have provided data from the FAIRE samples described in this study as well as new samples

that have shown similar results as to those produced by our FAIRE-Chip data, providing an independent confirmation of the results discernible in this project (Unpublished Data).

We would further like to use high throughput sequencing to evaluate a number of histone markers associated with gene activation and silencing in order to independently corroborate what we have observed with data found in the literature. Additionally this project specifically examined senescence induced by replicative exhaustion; there are multiple other methods by which to induce the senescent state with genotoxic stresses including ROS and radiation, as well as activation of oncogenes, some of which give rise to the unique development of SAHF. It would be very interesting to determine if these additional senescence stimuli presented discernible patterns of FAIRE enrichment distinct from replicative senescence, and also if SAHF would be detectable from the more open chromatin conformation we observed in our studies.

Ultimately it is our desire to develop this assay to be used on mammalian tissues to examine senescence *in vivo*. Previous work by the Lieb group has shown that FAIRE can successfully be used on tissue samples; however, whether it can be used to detect changes in the number of senescent cells in a tissue sample is still untested (Gaulton et al., 2010; Giresi and Lieb, 2009). There are additional obstacles when working with a non-homogeneous collection of cells as presented in tissue, and differentiating senescence in one subset of cells may provide difficult. There is a currently active project attempting to elucidate this issue in our lab.

Supplemental Tables

Table S-1

Chromosome 21 primers from Jason Lieb's group			
ch21-1	ttcagagccccaaagaagaa	aatctcagcaggacccttca	chr21:32813792+32813858
ch21-2	tgctgactttccatccatga	ctcagacaagcccggtgtat	chr21:32814145+32814214
ch21-3	tgctgagaggagtggttgtg	ccgaggaaacacctgtagga	chr21:32814395+32814482
ch21-4	ctctcgtgcacaaatctcca	acactccctggtccacagac	chr21:32814503+32814578
ch21-5	ggaaagaagtgcccacaaga	tccagggactcatggagaag	chr21:32814730+32814793
ch21-6	cccagcttctgctctgactt	tgaggaaactgaggcacaga	chr21:32815066+32815133
ch21-7	accacactaagggcatttcg	tgaaggaggctggcttgtta	chr21:32815298+32815378
ch21-8	taagcctgagcaccagtgtg	tccaaggctaccatccagtc	chr21:32815580+32815642
ch21-9	ggaaagagccacgataacca	agtcccggatccttagttgg	chr21:32815717+32815783
ch21-10	agtcacatttcaagcgctca	gctcagcactgtccaacaga	chr21:32815998+32816082
ch21-11	aggcacagaaatgtgggaac	gacaagagacatgcaggggta	chr21:32816190+32816271
ch21-12	ctgtcacctctctgggcact	agccctttaggctctccaag	chr21:32816464+32816554
ch21-13	acccaggaaggaactgcac	gggctcagcaaagagaagaa	chr21:32816676+32816749
ch21-14	ggctgaggcttgagagtctg	gctggagtacagtggcacaa	chr21:32817003+32817078
ch21-15	cctggacgacaagagcaaa	ggtttggccatttactgtca	chr21:32817386+32817484

Table S-1 Primers from Jason Lieb's group

This set of primers spans a region of chromosome 21 and were used to validate our FAIRE protocol. The results of our qPCR and FAIRE-chip analysis were in agreement with the results seen by Lieb's group (Giresi et al., 2007).

Table S-2

A

PPM1B housekeeping gene primers			
PPM1B1	atcggcctgttaaaccccta	ccaagaaaggcttcacaaaga	chr2:44248029+44248094
PPM1B3	cggcgatgatttcattgtta	agagtgggaaactgggaagg	chr2:44248505+44248593
PPM1B9	aggtgggcgttatttgattg	taggtcctacctcccgaacg	chr2:44249111+44249194
PPM1B13	ttggaagatgctccagagaga	gccttctctccaccctagc	chr2:44249650+44249734
PPM1B14	ctcttccctccgcttcagtc	catgcaccaggaagagaagc	chr2:44250207+44250296

B

Additional peak verification primers			
Primer	Forward	Reverse	Genomic Coordinates
CH13-1	ttccattcaactttattgttgtgg	tcctaagttggtggctcttca	chr13:32511557+32511622
CH13-2	gctgcaagcgcagaaaata	cgctcggtttccgtctaata	chr13:102296108+102296186
CH13-3	cactccacacattctacccaga	cggcaggagacttggatct	chr13:44936761+44936827
CH14-1	aggtttgggggaaaaagga	cctccaaataacggcatctt	chr14:99219955+99220016
CH15-1	gtgccgtgttcatgatggta	caaccatttgtcaccctcct	chr15:67741087+67741157
CH15-2	gagggagggaggagttatgg	ttggacctgttacttccatcc	chr15:97234822+97234890
CH15-3	gcaagcatcaggtgactgaa	ggttgagtcacttcccctctc	chr15:83757812+83757878
CH15-4	accctccacagtgtctggat	ctttggaatgaggtgggaga	chr15:23627385+23627447
CH15-5	aaatctgagccctgcagttg	ctcagaaacccaatacacaagat	chr15:57255127+57255200
CH15-6	cctagagcgggtagtgtgga	ctgcactgactcccactcaa	chr15:65225855+65225925
CH16-1	cttctgatccctgggctaaa	gtgcttgtctgggatcaaca	chr16:71469085+71469145
CH16-2	gtagccggaactgctgctg	cagatactgccgccactcac	chr16:1602381+1602444
CH17-1	tcctaaagagcaggcgaaag	cggtgtcaggctgagaacta	chr17:1566576+1566652
CH17-2	gggttggaactggggtaaaa	ccagcggtcttgcttaaatg	chr17:60263326+60263385
CH17-3	ggaacattaagaatcatccaggtt	ggtcccggtatagcagttga	chr17:72633204+72633288
CH17-4	cgggcctaggtactcattgg	tggctgagtgtacctcctca	chr17:43480504+43480583
CH17-5	accaagtgaaaccgaaagca	cagcgccgtagtttttgag	chr17:38793793+38793860
CH17-6	agcaactaagcgctcgaaag	cctttacgtcggatcactgg	chr17:38793809+38793887
CH17-7	gcttccaccctcccagtg	acccgagcctaccacctct	chr17:4683289+4683350
CH17-8	caaaaagcgcggagtcac	ctttccaactgcccgctaat	chr17:72245177+72245236
CH17-9	ccactggattggtagcaaaaa	cctcgattctgattggctgt	chr17:35697547+35697622
CH17-10	accccgaactcctctcctta	gcgattggctgggatagtag	chr17:43081874+43081943
CH18-1	tggcatagtgcctagagggta	ctaatgtccccctgcatgac	chr18:1363600+1363693
CH18-2	ttggtacagacattcaatcaaaca	gctcatgttttaggatgattttg	chr18:18858254+18858348

Table S-2 Peak Validation Primers

A: Primers used for the PPM1B housekeeping gene which showed a prominent enrichment peak in both replicating and senescent cells. B: Primers used to validate additional peaks on chromosomes 13, 14, 15, 16, 17 and 18.

Table S-3

Non-peak primers used to set standard curve for dot blot calculations				
Gene	Primer	Forward	Reverse	Genomic Coordinates
TNFAIP6	TNF 1	cttacgggcattggaacatt	gctgaaaacccagcaagact	chr2:151919656+151919735
ETFB	ETF 3	tccagaacgagggaaaagag	gggcaaaaatccaagagtga	chr19:51869308+51869386
ZNF285A	Z28 1	cctagtctcagaagaagcagaagg	cagtactcctgcaattccccta	chr19:44906214+44906287
CCDC75	CCD 1	ttcccatcacaactcgatcc	gaccataaaaacccccaggt	chr2:37159612+37159694
C19orf2	C192 1	atgatgtggaacgaacacga	gtgaaagtggccttgcctta	chr19:35123931+35124000

Table S-3 Primers used for generating a standard curve for dot blot sample calculations

These primers were in non peak regions, and showed little to no FAIRE enrichment in either replicating or senescent cells. They were used in qPCR to generate a standard curve (shown in Figure 2-1) from genomic DNA to calculate the concentration of the replicating and senescent cell DNA samples used in the dot blot experiments.

Literature Cited

Acosta, J. C., O'Loghlen, A., Banito, A., Guijarro, M. V., Augert, A., Raguz, S., Fumagalli, M., Da Costa, M., Brown, C., Popov, N.*, et al.* (2008). Chemokine signaling via the CXCR2 receptor reinforces senescence. Cell *133*, 1006-1018.

Adams, P. D. (2007a). Remodeling chromatin for senescence. Aging Cell *6*, 425-427.

Adams, P. D. (2007b). Remodeling of chromatin structure in senescent cells and its potential impact on tumor suppression and aging. Gene *397*, 84-93.

Adams, P. D. (2009). Healing and hurting: molecular mechanisms, functions, and pathologies of cellular senescence. Mol Cell *36*, 2-14.

Agherbi, H., Gaussmann-Wenger, A., Verthuy, C., Chasson, L., Serrano, M., and Djabali, M. (2009). Polycomb mediated epigenetic silencing and replication timing at the INK4a/ARF locus during senescence. PLoS One *4*, e5622.

Ahuja, N., Li, Q., Mohan, A. L., Baylin, S. B., and Issa, J. P. (1998). Aging and DNA methylation in colorectal mucosa and cancer. Cancer Res *58*, 5489-5494.

Antosh, M., Fox, D., Helfand, S. L., Cooper, L. N., and Neretti, N. (2011). New comparative genomics approach reveals a conserved health span signature across species. Aging (Albany NY) *3*, 576-583.

Atadja, P., Wong, H., Garkavtsev, I., Veillette, C., and Riabowol, K. (1995). Increased activity of p53 in senescing fibroblasts. Proc Natl Acad Sci U S A *92*, 8348-8352.

Baccarelli, A., Tarantini, L., Wright, R. O., Bollati, V., Litonjua, A. A., Zanobetti, A., Sparrow, D., Vokonas, P., and Schwartz, J. (2010). Repetitive element DNA methylation and circulating endothelial and inflammation markers in the VA normative aging study. Epigenetics *5*.

Baerlocher, G. M., Vulto, I., de Jong, G., and Lansdorp, P. M. (2006). Flow cytometry and FISH to measure the average length of telomeres (flow FISH). Nat Protoc *1*, 2365-2376.

Baker, D. J., Wijshake, T., Tchkonia, T., LeBrasseur, N. K., Childs, B. G., van de Sluis, B., Kirkland, J. L., and van Deursen, J. M. (2011). Clearance of p16Ink4a-positive senescent cells delays ageing-associated disorders. Nature *479*, 232-236.

Ball, S. E., Gibson, F. M., Rizzo, S., Tooze, J. A., Marsh, J. C., and Gordon-Smith, E. C. (1998). Progressive telomere shortening in aplastic anemia. Blood *91*, 3582-3592.

Ballestar, E., and Esteller, M. (2005). Methyl-CpG-binding proteins in cancer: blaming the DNA methylation messenger. Biochem Cell Biol *83*, 374-384.

Barbot, W., Dupressoir, A., Lazar, V., and Heidmann, T. (2002). Epigenetic regulation of an IAP retrotransposon in the aging mouse: progressive demethylation and de-silencing of the element by its repetitive induction. Nucleic Acids Res *30*, 2365-2373.

Barja, G., and Herrero, A. (2000). Oxidative damage to mitochondrial DNA is inversely related to maximum life span in the heart and brain of mammals. FASEB J *14*, 312-318.

Batzer, M. A., Deininger, P. L., Hellmann-Blumberg, U., Jurka, J., Labuda, D., Rubin, C. M., Schmid, C. W., Zietkiewicz, E., and Zuckerkandl, E. (1996). Standardized nomenclature for Alu repeats. J Mol Evol *42*, 3-6.

Bayreuther, K., Rodemann, H. P., Francz, P. I., and Maier, K. (1988). Differentiation of fibroblast stem cells. J Cell Sci Suppl *10*, 115-130.

Beausejour, C. M., Krtolica, A., Galimi, F., Narita, M., Lowe, S. W., Yaswen, P., and Campisi, J. (2003). Reversal of human cellular senescence: roles of the p53 and p16 pathways. EMBO J *22*, 4212-4222.

Belancio, V. P., Roy-Engel, A. M., Pochampally, R. R., and Deininger, P. (2010). Somatic expression of LINE-1 elements in human tissues. Nucleic Acids Res *38*, 3909-3922.

Beltrami, A. P., Barlucchi, L., Torella, D., Baker, M., Limana, F., Chimenti, S., Kasahara, H., Rota, M., Musso, E., Urbanek, K.*, et al.* (2003). Adult cardiac stem cells are multipotent and support myocardial regeneration. Cell *114*, 763-776.
Ben-Porath, I., and Weinberg, R. A. (2005). The signals and pathways activating cellular senescence. Int J Biochem Cell Biol *37*, 961-976.
Berger, S. L. (2007). The complex language of chromatin regulation during transcription. Nature *447*, 407-412.
Berger, S. L., Kouzarides, T., Shiekhattar, R., and Shilatifard, A. (2009). An operational definition of epigenetics. Genes Dev *23*, 781-783.
Bermudez, V. P., Farina, A., Raghavan, V., Tappin, I., and Hurwitz, J. (2011). Studies on human DNA polymerase epsilon and GINS complex and their role in DNA replication. J Biol Chem *286*, 28963-28977.
Bernstein, B. E., Liu, C. L., Humphrey, E. L., Perlstein, E. O., and Schreiber, S. L. (2004). Global nucleosome occupancy in yeast. Genome Biol *5*, R62.
Bernstein, B. E., Meissner, A., and Lander, E. S. (2007). The mammalian epigenome. Cell *128*, 669-681.
Bierman, E. L. (1978). The effect of donor age on the in vitro life span of cultured human arterial smooth-muscle cells. In Vitro *14*, 951-955.
Bird, A. (2002). DNA methylation patterns and epigenetic memory. Genes Dev *16*, 6-21.
Bjornsson, H. T., Sigurdsson, M. I., Fallin, M. D., Irizarry, R. A., Aspelund, T., Cui, H., Yu, W., Rongione, M. A., Ekstrom, T. J., Harris, T. B.*, et al.* (2008). Intra-individual change over time in DNA methylation with familial clustering. JAMA *299*, 2877-2883.
Blanchette, M., Bataille, A. R., Chen, X., Poitras, C., Laganiere, J., Lefebvre, C., Deblois, G., Giguere, V., Ferretti, V., Bergeron, D.*, et al.* (2006). Genome-wide computational prediction of transcriptional regulatory modules reveals new insights into human gene expression. Genome Res *16*, 656-668.
Blasco, M. A. (2005). Telomeres and human disease: ageing, cancer and beyond. Nat Rev Genet *6*, 611-622.
Blasco, M. A., Lee, H. W., Hande, M. P., Samper, E., Lansdorp, P. M., DePinho, R. A., and Greider, C. W. (1997). Telomere shortening and tumor formation by mouse cells lacking telomerase RNA. Cell *91*, 25-34.
Bodnar, A. G., Ouellette, M., Frolkis, M., Holt, S. E., Chiu, C. P., Morin, G. B., Harley, C. B., Shay, J. W., Lichtsteiner, S., and Wright, W. E. (1998). Extension of life-span by introduction of telomerase into normal human cells. Science *279*, 349-352.
Bohr, V. A. (2002). Repair of oxidative DNA damage in nuclear and mitochondrial DNA, and some changes with aging in mammalian cells. Free Radic Biol Med *32*, 804-812.
Breiling, A., and Orlando, V. (2001). Binding Sights in Chromatin by X-ChIP.
Brown, J. P., Wei, W., and Sedivy, J. M. (1997). Bypass of senescence after disruption of p21CIP1/WAF1 gene in normal diploid human fibroblasts. Science *277*, 831-834.
Bruce, S. A., Deamond, S. F., and Ts'o, P. O. (1986). In vitro senescence of Syrian hamster mesenchymal cells of fetal to aged adult origin. Inverse relationship between in vivo donor age and in vitro proliferative capacity. Mech Ageing Dev *34*, 151-173.
Bryan, T. M., Englezou, A., Gupta, J., Bacchetti, S., and Reddel, R. R. (1995). Telomere elongation in immortal human cells without detectable telomerase activity. EMBO J *14*, 4240-4248.
Bulyk, M. L. (2004). Integrative functional genomics. Genome Biol *5*, 331.
Bunz, F., Dutriaux, A., Lengauer, C., Waldman, T., Zhou, S., Brown, J. P., Sedivy, J. M., Kinzler, K. W., and Vogelstein, B. (1998). Requirement for p53 and p21 to sustain G2 arrest after DNA damage. Science *282*, 1497-1501.

Burhans, W. C., and Weinberger, M. (2007). DNA replication stress, genome instability and aging. Nucleic Acids Res *35*, 7545-7556.
Campisi, J. (2005). Senescent cells, tumor suppression, and organismal aging: good citizens, bad neighbors. Cell *120*, 513-522.
Campisi, J., and d'Adda di Fagagna, F. (2007). Cellular senescence: when bad things happen to good cells. Nat Rev Mol Cell Biol *8*, 729-740.
Canto, C., Gerhart-Hines, Z., Feige, J. N., Lagouge, M., Noriega, L., Milne, J. C., Elliott, P. J., Puigserver, P., and Auwerx, J. (2009). AMPK regulates energy expenditure by modulating NAD+ metabolism and SIRT1 activity. Nature *458*, 1056-1060.
Cao, R., and Zhang, Y. (2004). The functions of E(Z)/EZH2-mediated methylation of lysine 27 in histone H3. Curr Opin Genet Dev *14*, 155-164.
Casillas, M. A., Jr., Lopatina, N., Andrews, L. G., and Tollefsbol, T. O. (2003). Transcriptional control of the DNA methyltransferases is altered in aging and neoplastically-transformed human fibroblasts. Mol Cell Biochem *252*, 33-43.
Castro, P., Giri, D., Lamb, D., and Ittmann, M. (2003). Cellular senescence in the pathogenesis of benign prostatic hyperplasia. Prostate *55*, 30-38.
Cawthon, R. M., Smith, K. R., O'Brien, E., Sivatchenko, A., and Kerber, R. A. (2003). Association between telomere length in blood and mortality in people aged 60 years or older. Lancet *361*, 393-395.
Chambers, S. M., Shaw, C. A., Gatza, C., Fisk, C. J., Donehower, L. A., and Goodell, M. A. (2007). Aging hematopoietic stem cells decline in function and exhibit epigenetic dysregulation. PLoS Biol *5*, e201.
Chan, H. M., Narita, M., Lowe, S. W., and Livingston, D. M. (2005). The p400 E1A-associated protein is a novel component of the p53 --> p21 senescence pathway. Genes Dev *19*, 196-201.
Chan, S. W., Chang, J., Prescott, J., and Blackburn, E. H. (2001). Altering telomere structure allows telomerase to act in yeast lacking ATM kinases. Curr Biol *11*, 1240-1250.
Chang, S., Multani, A. S., Cabrera, N. G., Naylor, M. L., Laud, P., Lombard, D., Pathak, S., Guarente, L., and DePinho, R. A. (2004). Essential role of limiting telomeres in the pathogenesis of Werner syndrome. Nat Genet *36*, 877-882.
Chen, Q. M., Prowse, K. R., Tu, V. C., Purdom, S., and Linskens, M. H. (2001). Uncoupling the senescent phenotype from telomere shortening in hydrogen peroxide-treated fibroblasts. Exp Cell Res *265*, 294-303.
Chen, T., Tsujimoto, N., and Li, E. (2004). The PWWP domain of Dnmt3a and Dnmt3b is required for directing DNA methylation to the major satellite repeats at pericentric heterochromatin. Mol Cell Biol *24*, 9048-9058.
Chen, Z., Trotman, L. C., Shaffer, D., Lin, H. K., Dotan, Z. A., Niki, M., Koutcher, J. A., Scher, H. I., Ludwig, T., Gerald, W.*, et al.* (2005). Crucial role of p53-dependent cellular senescence in suppression of Pten-deficient tumorigenesis. Nature *436*, 725-730.
Choi, H. R., Cho, K. A., Kang, H. T., Lee, J. B., Kaeberlein, M., Suh, Y., Chung, I. K., and Park, S. C. (2011). Restoration of senescent human diploid fibroblasts by modulation of the extracellular matrix. Aging Cell *10*, 148-157.
Clark, P. A., Llanos, S., and Peters, G. (2002). Multiple interacting domains contribute to p14ARF mediated inhibition of MDM2. Oncogene *21*, 4498-4507.
Collado, M., Blasco, M. A., and Serrano, M. (2007). Cellular senescence in cancer and aging. Cell *130*, 223-233.
Conley, A. B., Miller, W. J., and Jordan, I. K. (2008). Human cis natural antisense transcripts initiated by transposable elements. Trends Genet *24*, 53-56.

Coppe, J. P., Kauser, K., Campisi, J., and Beausejour, C. M. (2006). Secretion of vascular endothelial growth factor by primary human fibroblasts at senescence. J Biol Chem *281*, 29568-29574.
Coppe, J. P., Patil, C. K., Rodier, F., Sun, Y., Munoz, D. P., Goldstein, J., Nelson, P. S., Desprez, P. Y., and Campisi, J. (2008). Senescence-associated secretory phenotypes reveal cell-nonautonomous functions of oncogenic RAS and the p53 tumor suppressor. PLoS Biol *6*, 2853-2868.
Core, N., Joly, F., Boned, A., and Djabali, M. (2004). Disruption of E2F signaling suppresses the INK4a-induced proliferative defect in M33-deficient mice. Oncogene *23*, 7660-7668.
Coufal, N. G., Garcia-Perez, J. L., Peng, G. E., Yeo, G. W., Mu, Y., Lovci, M. T., Morell, M., O'Shea, K. S., Moran, J. V., and Gage, F. H. (2009). L1 retrotransposition in human neural progenitor cells. Nature *460*, 1127-1131.
Courtois-Cox, S., Genther Williams, S. M., Reczek, E. E., Johnson, B. W., McGillicuddy, L. T., Johannessen, C. M., Hollstein, P. E., MacCollin, M., and Cichowski, K. (2006). A negative feedback signaling network underlies oncogene-induced senescence. Cancer Cell *10*, 459-472.
Crabbe, L., Jauch, A., Naeger, C. M., Holtgreve-Grez, H., and Karlseder, J. (2007). Telomere dysfunction as a cause of genomic instability in Werner syndrome. Proc Natl Acad Sci U S A *104*, 2205-2210.
Crawford, G. E., Davis, S., Scacheri, P. C., Renaud, G., Halawi, M. J., Erdos, M. R., Green, R., Meltzer, P. S., Wolfsberg, T. G., and Collins, F. S. (2006). DNase-chip: a high-resolution method to identify DNase I hypersensitive sites using tiled microarrays. Nat Methods *3*, 503-509.
Cristofalo, V. J., Allen, R. G., Pignolo, R. J., Martin, B. G., and Beck, J. C. (1998). Relationship between donor age and the replicative lifespan of human cells in culture: a reevaluation. Proc Natl Acad Sci U S A *95*, 10614-10619.
d'Adda di Fagagna, F., Reaper, P. M., Clay-Farrace, L., Fiegler, H., Carr, P., Von Zglinicki, T., Saretzki, G., Carter, N. P., and Jackson, S. P. (2003). A DNA damage checkpoint response in telomere-initiated senescence. Nature *426*, 194-198.
d'Adda di Fagagna, F., Teo, S. H., and Jackson, S. P. (2004). Functional links between telomeres and proteins of the DNA-damage response. Genes Dev *18*, 1781-1799.
Dang, W., Steffen, K. K., Perry, R., Dorsey, J. A., Johnson, F. B., Shilatifard, A., Kaeberlein, M., Kennedy, B. K., and Berger, S. L. (2009). Histone H4 lysine 16 acetylation regulates cellular lifespan. Nature *459*, 802-807.
De Bont, R., and van Larebeke, N. (2004). Endogenous DNA damage in humans: a review of quantitative data. Mutagenesis *19*, 169-185.
de Lange, T. (2005). Shelterin: the protein complex that shapes and safeguards human telomeres. Genes Dev *19*, 2100-2110.
Debacq-Chainiaux, F., Erusalimsky, J. D., Campisi, J., and Toussaint, O. (2009). Protocols to detect senescence-associated beta-galactosidase (SA-betagal) activity, a biomarker of senescent cells in culture and in vivo. Nat Protoc *4*, 1798-1806.
Denoyelle, C., Abou-Rjaily, G., Bezrookove, V., Verhaegen, M., Johnson, T. M., Fullen, D. R., Pointer, J. N., Gruber, S. B., Su, L. D., Nikiforov, M. A.*, et al.* (2006). Anti-oncogenic role of the endoplasmic reticulum differentially activated by mutations in the MAPK pathway. Nat Cell Biol *8*, 1053-1063.
DeRan, M., Pulvino, M., Greene, E., Su, C., and Zhao, J. (2008). Transcriptional activation of histone genes requires NPAT-dependent recruitment of TRRAP-Tip60 complex to histone promoters during the G1/S phase transition. Mol Cell Biol *28*, 435-447.
Dhalluin, C., Carlson, J. E., Zeng, L., He, C., Aggarwal, A. K., and Zhou, M. M. (1999). Structure and ligand of a histone acetyltransferase bromodomain. Nature *399*, 491-496.

Di Micco, R., Fumagalli, M., Cicalese, A., Piccinin, S., Gasparini, P., Luise, C., Schurra, C., Garre, M., Nuciforo, P. G., Bensimon, A.*, et al.* (2006). Oncogene-induced senescence is a DNA damage response triggered by DNA hyper-replication. Nature *444*, 638-642.
Dilley, T. K., Bowden, G. T., and Chen, Q. M. (2003). Novel mechanisms of sublethal oxidant toxicity: induction of premature senescence in human fibroblasts confers tumor promoter activity. Exp Cell Res *290*, 38-48.
Dimri, G. P., Lee, X., Basile, G., Acosta, M., Scott, G., Roskelley, C., Medrano, E. E., Linskens, M., Rubelj, I., Pereira-Smith, O., and et al. (1995). A biomarker that identifies senescent human cells in culture and in aging skin in vivo. Proc Natl Acad Sci U S A *92*, 9363-9367.
Ding, S. L., and Shen, C. Y. (2008). Model of human aging: recent findings on Werner's and Hutchinson-Gilford progeria syndromes. Clin Interv Aging *3*, 431-444.
Dirac, A. M., and Bernards, R. (2003). Reversal of senescence in mouse fibroblasts through lentiviral suppression of p53. J Biol Chem *278*, 11731-11734.
Dostie, J., Richmond, T. A., Arnaout, R. A., Selzer, R. R., Lee, W. L., Honan, T. A., Rubio, E. D., Krumm, A., Lamb, J., Nusbaum, C.*, et al.* (2006). Chromosome Conformation Capture Carbon Copy (5C): a massively parallel solution for mapping interactions between genomic elements. Genome Res *16*, 1299-1309.
Dryden, S. C., Nahhas, F. A., Nowak, J. E., Goustin, A. S., and Tainsky, M. A. (2003). Role for human SIRT2 NAD-dependent deacetylase activity in control of mitotic exit in the cell cycle. Mol Cell Biol *23*, 3173-3185.
Eads, C. A., Danenberg, K. D., Kawakami, K., Saltz, L. B., Blake, C., Shibata, D., Danenberg, P. V., and Laird, P. W. (2000). MethyLight: a high-throughput assay to measure DNA methylation. Nucleic Acids Res *28*, E32.
Eden, S., Hashimshony, T., Keshet, I., Cedar, H., and Thorne, A. W. (1998). DNA methylation models histone acetylation. Nature *394*, 842.
Eitoku, M., Sato, L., Senda, T., and Horikoshi, M. (2008). Histone chaperones: 30 years from isolation to elucidation of the mechanisms of nucleosome assembly and disassembly. Cell Mol Life Sci *65*, 414-444.
Fahraeus, R., Paramio, J. M., Ball, K. L., Lain, S., and Lane, D. P. (1996). Inhibition of pRb phosphorylation and cell-cycle progression by a 20-residue peptide derived from p16CDKN2/INK4A. Curr Biol *6*, 84-91.
Fairweather, D. S., Fox, M., and Margison, G. P. (1987). The in vitro lifespan of MRC-5 cells is shortened by 5-azacytidine-induced demethylation. Exp Cell Res *168*, 153-159.
Faulkner, G. J., Kimura, Y., Daub, C. O., Wani, S., Plessy, C., Irvine, K. M., Schroder, K., Cloonan, N., Steptoe, A. L., Lassmann, T.*, et al.* (2009). The regulated retrotransposon transcriptome of mammalian cells. Nat Genet *41*, 563-571.
Feser, J., Truong, D., Das, C., Carson, J. J., Kieft, J., Harkness, T., and Tyler, J. K. (2010). Elevated histone expression promotes life span extension. Mol Cell *39*, 724-735.
Feser, J., and Tyler, J. (2011). Chromatin structure as a mediator of aging. FEBS Lett *585*, 2041-2048.
Finkel, T., Deng, C. X., and Mostoslavsky, R. (2009). Recent progress in the biology and physiology of sirtuins. Nature *460*, 587-591.
Flanary, B. E., Sammons, N. W., Nguyen, C., Walker, D., and Streit, W. J. (2007). Evidence that aging and amyloid promote microglial cell senescence. Rejuvenation Res *10*, 61-74.
Flatt, T., and Schmidt, P. S. (2009). Integrating evolutionary and molecular genetics of aging. Biochim Biophys Acta *1790*, 951-962.
Ford, E., Voit, R., Liszt, G., Magin, C., Grummt, I., and Guarente, L. (2006). Mammalian Sir2 homolog SIRT7 is an activator of RNA polymerase I transcription. Genes Dev *20*, 1075-1080.

Fraga, M. F., Ballestar, E., Villar-Garea, A., Boix-Chornet, M., Espada, J., Schotta, G., Bonaldi, T., Haydon, C., Ropero, S., Petrie, K.*, et al.* (2005). Loss of acetylation at Lys16 and trimethylation at Lys20 of histone H4 is a common hallmark of human cancer. Nat Genet *37*, 391-400.
Fraga, M. F., and Esteller, M. (2007). Epigenetics and aging: the targets and the marks. Trends Genet *23*, 413-418.
Frommer, M., McDonald, L. E., Millar, D. S., Collis, C. M., Watt, F., Grigg, G. W., Molloy, P. L., and Paul, C. L. (1992). A genomic sequencing protocol that yields a positive display of 5-methylcytosine residues in individual DNA strands. Proc Natl Acad Sci U S A *89*, 1827-1831.
Fuke, C., Shimabukuro, M., Petronis, A., Sugimoto, J., Oda, T., Miura, K., Miyazaki, T., Ogura, C., Okazaki, Y., and Jinno, Y. (2004). Age related changes in 5-methylcytosine content in human peripheral leukocytes and placentas: an HPLC-based study. Ann Hum Genet *68*, 196-204.
Funayama, R., Saito, M., Tanobe, H., and Ishikawa, F. (2006). Loss of linker histone H1 in cellular senescence. J Cell Biol *175*, 869-880.
Garcia-Cao, I., Garcia-Cao, M., Tomas-Loba, A., Martin-Caballero, J., Flores, J. M., Klatt, P., Blasco, M. A., and Serrano, M. (2006). Increased p53 activity does not accelerate telomere-driven ageing. EMBO Rep *7*, 546-552.
Garinis, G. A., van der Horst, G. T., Vijg, J., and Hoeijmakers, J. H. (2008). DNA damage and ageing: new-age ideas for an age-old problem. Nat Cell Biol *10*, 1241-1247.
Gaulton, K. J., Nammo, T., Pasquali, L., Simon, J. M., Giresi, P. G., Fogarty, M. P., Panhuis, T. M., Mieczkowski, P., Secchi, A., Bosco, D.*, et al.* (2010). A map of open chromatin in human pancreatic islets. Nat Genet *42*, 255-259.
Gil, J., and Peters, G. (2006). Regulation of the INK4b-ARF-INK4a tumour suppressor locus: all for one or one for all. Nat Rev Mol Cell Biol *7*, 667-677.
Gilbert, N., Boyle, S., Fiegler, H., Woodfine, K., Carter, N. P., and Bickmore, W. A. (2004). Chromatin architecture of the human genome: gene-rich domains are enriched in open chromatin fibers. Cell *118*, 555-566.
Giresi, P. G., Kim, J., McDaniell, R. M., Iyer, V. R., and Lieb, J. D. (2007). FAIRE (Formaldehyde-Assisted Isolation of Regulatory Elements) isolates active regulatory elements from human chromatin. Genome Res *17*, 877-885.
Giresi, P. G., and Lieb, J. D. (2009). Isolation of active regulatory elements from eukaryotic chromatin using FAIRE (Formaldehyde Assisted Isolation of Regulatory Elements). Methods *48*, 233-239.
Goldberg, A. D., Allis, C. D., and Bernstein, E. (2007). Epigenetics: a landscape takes shape. Cell *128*, 635-638.
Goldstein, S., Murano, S., Benes, H., Moerman, E. J., Jones, R. A., Thweatt, R., Shmookler Reis, R. J., and Howard, B. H. (1989). Studies on the molecular-genetic basis of replicative senescence in Werner syndrome and normal fibroblasts. Exp Gerontol *24*, 461-468.
Goll, M. G., and Bestor, T. H. (2005). Eukaryotic cytosine methyltransferases. Annu Rev Biochem *74*, 481-514.
Gonzalo, S. (2010). Epigenetic alterations in aging. J Appl Physiol *109*, 586-597.
Greer, E. L., Maures, T. J., Ucar, D., Hauswirth, A. G., Mancini, E., Lim, J. P., Benayoun, B. A., Shi, Y., and Brunet, A. (2011). Transgenerational epigenetic inheritance of longevity in Caenorhabditis elegans. Nature *479*, 365-371.
Greider, C. W., and Blackburn, E. H. (1985). Identification of a specific telomere terminal transferase activity in Tetrahymena extracts. Cell *43*, 405-413.
Grewal, S. I., and Jia, S. (2007). Heterochromatin revisited. Nat Rev Genet *8*, 35-46.
Grinnell, F. (2003). Fibroblast biology in three-dimensional collagen matrices. Trends Cell Biol *13*, 264-269.

Groth, A., Rocha, W., Verreault, A., and Almouzni, G. (2007). Chromatin challenges during DNA replication and repair. Cell *128*, 721-733.
Gruber, H. E., Hoelscher, G. L., Ingram, J. A., Zinchenko, N., and Hanley, E. N., Jr. (2010). Senescent vs. non-senescent cells in the human annulus in vivo: cell harvest with laser capture microdissection and gene expression studies with microarray analysis. BMC Biotechnol *10*, 5.
Grunstein, M. (1997). Histone acetylation in chromatin structure and transcription. Nature *389*, 349-352.
Guarente, L. (2011). Franklin H. Epstein Lecture: Sirtuins, aging, and medicine. N Engl J Med *364*, 2235-2244.
Guenther, M. G., Levine, S. S., Boyer, L. A., Jaenisch, R., and Young, R. A. (2007). A chromatin landmark and transcription initiation at most promoters in human cells. Cell *130*, 77-88.
Hagan, C. R., Sheffield, R. F., and Rudin, C. M. (2003). Human Alu element retrotransposition induced by genotoxic stress. Nat Genet *35*, 219-220.
Hagege, H., Klous, P., Braem, C., Splinter, E., Dekker, J., Cathala, G., de Laat, W., and Forne, T. (2007). Quantitative analysis of chromosome conformation capture assays (3C-qPCR). Nat Protoc *2*, 1722-1733.
Haigis, M. C., and Guarente, L. P. (2006). Mammalian sirtuins--emerging roles in physiology, aging, and calorie restriction. Genes Dev *20*, 2913-2921.
Haigis, M. C., Mostoslavsky, R., Haigis, K. M., Fahie, K., Christodoulou, D. C., Murphy, A. J., Valenzuela, D. M., Yancopoulos, G. D., Karow, M., Blander, G.*, et al.* (2006). SIRT4 inhibits glutamate dehydrogenase and opposes the effects of calorie restriction in pancreatic beta cells. Cell *126*, 941-954.
Haigis, M. C., and Sinclair, D. A. (2010). Mammalian sirtuins: biological insights and disease relevance. Annu Rev Pathol *5*, 253-295.
Hampel, B., Wagner, M., Teis, D., Zwerschke, W., Huber, L. A., and Jansen-Durr, P. (2005). Apoptosis resistance of senescent human fibroblasts is correlated with the absence of nuclear IGFBP-3. Aging Cell *4*, 325-330.
Hanahan, D., and Weinberg, R. A. (2000). The hallmarks of cancer. Cell *100*, 57-70.
Hara, E., Tsurui, H., Shinozaki, A., Nakada, S., and Oda, K. (1991). Cooperative effect of antisense-Rb and antisense-p53 oligomers on the extension of life span in human diploid fibroblasts, TIG-1. Biochem Biophys Res Commun *179*, 528-534.
Hardy, K., Mansfield, L., Mackay, A., Benvenuti, S., Ismail, S., Arora, P., O'Hare, M. J., and Jat, P. S. (2005). Transcriptional networks and cellular senescence in human mammary fibroblasts. Mol Biol Cell *16*, 943-953.
Harley, C. B., Futcher, A. B., and Greider, C. W. (1990). Telomeres shorten during ageing of human fibroblasts. Nature *345*, 458-460.
Hassan, A. H., Prochasson, P., Neely, K. E., Galasinski, S. C., Chandy, M., Carrozza, M. J., and Workman, J. L. (2002). Function and selectivity of bromodomains in anchoring chromatin-modifying complexes to promoter nucleosomes. Cell *111*, 369-379.
Hayflick, L. (1965). The Limited in Vitro Lifetime of Human Diploid Cell Strains. Exp Cell Res *37*, 614-636.
Hayflick, L. (1976). The cell biology of human aging. N Engl J Med *295*, 1302-1308.
Hayflick, L., and Moorhead, P. S. (1961). The serial cultivation of human diploid cell strains. Exp Cell Res *25*, 585-621.
Heard, E. (2005). Delving into the diversity of facultative heterochromatin: the epigenetics of the inactive X chromosome. Curr Opin Genet Dev *15*, 482-489.

Heintzman, N. D., Hon, G. C., Hawkins, R. D., Kheradpour, P., Stark, A., Harp, L. F., Ye, Z., Lee, L. K., Stuart, R. K., Ching, C. W*., et al.* (2009). Histone modifications at human enhancers reflect global cell-type-specific gene expression. Nature *459*, 108-112.
Heintzman, N. D., Stuart, R. K., Hon, G., Fu, Y., Ching, C. W., Hawkins, R. D., Barrera, L. O., Van Calcar, S., Qu, C., Ching, K. A*., et al.* (2007). Distinct and predictive chromatin signatures of transcriptional promoters and enhancers in the human genome. Nat Genet *39*, 311-318.
Heiss, N. S., Knight, S. W., Vulliamy, T. J., Klauck, S. M., Wiemann, S., Mason, P. J., Poustka, A., and Dokal, I. (1998). X-linked dyskeratosis congenita is caused by mutations in a highly conserved gene with putative nucleolar functions. Nat Genet *19*, 32-38.
Henikoff, J. G., Belsky, J. A., Krassovsky, K., MacAlpine, D. M., and Henikoff, S. (2011). Epigenome characterization at single base-pair resolution. Proc Natl Acad Sci U S A *108*, 18318-18323.
Herbig, U., Ferreira, M., Condel, L., Carey, D., and Sedivy, J. M. (2006). Cellular senescence in aging primates. Science *311*, 1257.
Herbig, U., Jobling, W. A., Chen, B. P., Chen, D. J., and Sedivy, J. M. (2004). Telomere shortening triggers senescence of human cells through a pathway involving ATM, p53, and p21(CIP1), but not p16(INK4a). Mol Cell *14*, 501-513.
Herbig, U., and Sedivy, J. M. (2006). Regulation of growth arrest in senescence: telomere damage is not the end of the story. Mech Ageing Dev *127*, 16-24.
Hinkal, G., and Donehower, L. A. (2008). How does suppression of IGF-1 signaling by DNA damage affect aging and longevity? Mech Ageing Dev *129*, 243-253.
Hiyama, K., Hirai, Y., Kyoizumi, S., Akiyama, M., Hiyama, E., Piatyszek, M. A., Shay, J. W., Ishioka, S., and Yamakido, M. (1995). Activation of telomerase in human lymphocytes and hematopoietic progenitor cells. J Immunol *155*, 3711-3715.
Hogan, G. J., Lee, C. K., and Lieb, J. D. (2006). Cell cycle-specified fluctuation of nucleosome occupancy at gene promoters. PLoS Genet *2*, e158.
Huang, S., Risques, R. A., Martin, G. M., Rabinovitch, P. S., and Oshima, J. (2008). Accelerated telomere shortening and replicative senescence in human fibroblasts overexpressing mutant and wild-type lamin A. Exp Cell Res *314*, 82-91.
Hughes, K. A., and Reynolds, R. M. (2005). Evolutionary and mechanistic theories of aging. Annu Rev Entomol *50*, 421-445.
Huvet, M., Nicolay, S., Touchon, M., Audit, B., d'Aubenton-Carafa, Y., Arneodo, A., and Thermes, C. (2007). Human gene organization driven by the coordination of replication and transcription. Genome Res *17*, 1278-1285.
Ishimi, Y., Kojima, M., Takeuchi, F., Miyamoto, T., Yamada, M., and Hanaoka, F. (1987). Changes in chromatin structure during aging of human skin fibroblasts. Exp Cell Res *169*, 458-467.
Issa, J. P., Ottaviano, Y. L., Celano, P., Hamilton, S. R., Davidson, N. E., and Baylin, S. B. (1994). Methylation of the oestrogen receptor CpG island links ageing and neoplasia in human colon. Nat Genet *7*, 536-540.
Issa, J. P., Vertino, P. M., Boehm, C. D., Newsham, I. F., and Baylin, S. B. (1996). Switch from monoallelic to biallelic human IGF2 promoter methylation during aging and carcinogenesis. Proc Natl Acad Sci U S A *93*, 11757-11762.
Itahana, K., Campisi, J., and Dimri, G. P. (2007). Methods to detect biomarkers of cellular senescence: the senescence-associated beta-galactosidase assay. Methods Mol Biol *371*, 21-31.
Jacobson, R. H., Ladurner, A. G., King, D. S., and Tjian, R. (2000). Structure and function of a human TAFII250 double bromodomain module. Science *288*, 1422-1425.
Jenuwein, T., and Allis, C. D. (2001). Translating the histone code. Science *293*, 1074-1080.
Jeyapalan, J. C., Ferreira, M., Sedivy, J. M., and Herbig, U. (2007). Accumulation of senescent cells in mitotic tissue of aging primates. Mech Ageing Dev *128*, 36-44.

Jeyapalan, J. C., and Sedivy, J. M. (2008). Cellular senescence and organismal aging. Mech Ageing Dev *129*, 467-474.
Jin, C., Zang, C., Wei, G., Cui, K., Peng, W., Zhao, K., and Felsenfeld, G. (2009). H3.3/H2A.Z double variant-containing nucleosomes mark 'nucleosome-free regions' of active promoters and other regulatory regions. Nat Genet *41*, 941-945.
Jintaridth, P., and Mutirangura, A. (2010). Distinctive patterns of age-dependent hypomethylation in interspersed repetitive sequences. Physiol Genomics.
Kaeberlein, M., McVey, M., and Guarente, L. (1999). The SIR2/3/4 complex and SIR2 alone promote longevity in Saccharomyces cerevisiae by two different mechanisms. Genes Dev *13*, 2570-2580.
Khorasanizadeh, S. (2004). The nucleosome: from genomic organization to genomic regulation. Cell *116*, 259-272.
Kim, J. H., Ebersole, T., Kouprina, N., Noskov, V. N., Ohzeki, J., Masumoto, H., Mravinac, B., Sullivan, B. A., Pavlicek, A., Dovat, S.*, et al.* (2009). Human gamma-satellite DNA maintains open chromatin structure and protects a transgene from epigenetic silencing. Genome Res *19*, 533-544.
Kim, J. Y., Tavare, S., and Shibata, D. (2005). Counting human somatic cell replications: methylation mirrors endometrial stem cell divisions. Proc Natl Acad Sci U S A *102*, 17739-17744.
Kim, N. W., Piatyszek, M. A., Prowse, K. R., Harley, C. B., West, M. D., Ho, P. L., Coviello, G. M., Wright, W. E., Weinrich, S. L., and Shay, J. W. (1994). Specific association of human telomerase activity with immortal cells and cancer. Science *266*, 2011-2015.
Kim, W. Y., and Sharpless, N. E. (2006). The regulation of INK4/ARF in cancer and aging. Cell *127*, 265-275.
Kimura, M., Barbieri, M., Gardner, J. P., Skurnick, J., Cao, X., van Riel, N., Rizzo, M. R., Paoliso, G., and Aviv, A. (2007). Leukocytes of exceptionally old persons display ultra-short telomeres. Am J Physiol Regul Integr Comp Physiol *293*, R2210-2217.
Kipling, D., and Cooke, H. J. (1990). Hypervariable ultra-long telomeres in mice. Nature *347*, 400-402.
Kircher, M., and Kelso, J. (2010). High-throughput DNA sequencing--concepts and limitations. Bioessays *32*, 524-536.
Kirkwood, T. B. (2005). Understanding the odd science of aging. Cell *120*, 437-447.
Kirkwood, T. L., Kapahi, P., and Shanley, D. P. (2000). Evolution, stress, and longevity. J Anat *197 Pt 4*, 587-590.
Klose, R. J., and Bird, A. P. (2006). Genomic DNA methylation: the mark and its mediators. Trends Biochem Sci *31*, 89-97.
Koff, A., Giordano, A., Desai, D., Yamashita, K., Harper, J. W., Elledge, S., Nishimoto, T., Morgan, D. O., Franza, B. R., and Roberts, J. M. (1992). Formation and activation of a cyclin E-cdk2 complex during the G1 phase of the human cell cycle. Science *257*, 1689-1694.
Kong, Y., Cui, H., Ramkumar, C., and Zhang, H. (2011). Regulation of senescence in cancer and aging. J Aging Res *2011*, 963172.
Kosar, M., Bartkova, J., Hubackova, S., Hodny, Z., Lukas, J., and Bartek, J. (2011). Senescence-associated heterochromatin foci are dispensable for cellular senescence, occur in a cell type- and insult-dependent manner and follow expression of p16(ink4a). Cell Cycle *10*, 457-468.
Kouzarides, T. (2002). Histone methylation in transcriptional control. Curr Opin Genet Dev *12*, 198-209.
Kouzarides, T. (2007). Chromatin modifications and their function. Cell *128*, 693-705.
Kreiling, J. A., Tamamori-Adachi, M., Sexton, A. N., Jeyapalan, J. C., Munoz-Najar, U., Peterson, A. L., Manivannan, J., Rogers, E. S., Pchelintsev, N. A., Adams, P. D., and Sedivy, J. M. (2011). Age-

associated increase in heterochromatic marks in murine and primate tissues. Aging Cell *10*, 292-304.
Krishnamurthy, J., and Sharpless, N. E. (2007). Stem cells and the rate of living. Cell Stem Cell *1*, 9-11.
Krtolica, A., Parrinello, S., Lockett, S., Desprez, P. Y., and Campisi, J. (2001). Senescent fibroblasts promote epithelial cell growth and tumorigenesis: a link between cancer and aging. Proc Natl Acad Sci U S A *98*, 12072-12077.
Ku, H. H., Brunk, U. T., and Sohal, R. S. (1993). Relationship between mitochondrial superoxide and hydrogen peroxide production and longevity of mammalian species. Free Radic Biol Med *15*, 621-627.
Kuilman, T., Michaloglou, C., Mooi, W. J., and Peeper, D. S. (2010). The essence of senescence. Genes Dev *24*, 2463-2479.
Kuilman, T., Michaloglou, C., Vredeveld, L. C., Douma, S., van Doorn, R., Desmet, C. J., Aarden, L. A., Mooi, W. J., and Peeper, D. S. (2008). Oncogene-induced senescence relayed by an interleukin-dependent inflammatory network. Cell *133*, 1019-1031.
Kuo, M. H., and Allis, C. D. (1998). Roles of histone acetyltransferases and deacetylases in gene regulation. Bioessays *20*, 615-626.
Kurz, D. J., Decary, S., Hong, Y., and Erusalimsky, J. D. (2000). Senescence-associated (beta)-galactosidase reflects an increase in lysosomal mass during replicative ageing of human endothelial cells. J Cell Sci *113 (Pt 20)*, 3613-3622.
Kuzmichev, A., Jenuwein, T., Tempst, P., and Reinberg, D. (2004). Different EZH2-containing complexes target methylation of histone H1 or nucleosomal histone H3. Mol Cell *14*, 183-193.
Lachner, M., O'Sullivan, R. J., and Jenuwein, T. (2003). An epigenetic road map for histone lysine methylation. J Cell Sci *116*, 2117-2124.
Lander, E. S., Linton, L. M., Birren, B., Nusbaum, C., Zody, M. C., Baldwin, J., Devon, K., Dewar, K., Doyle, M., FitzHugh, W*., et al.* (2001). Initial sequencing and analysis of the human genome. Nature *409*, 860-921.
Lebel, M., and Leder, P. (1998). A deletion within the murine Werner syndrome helicase induces sensitivity to inhibitors of topoisomerase and loss of cellular proliferative capacity. Proc Natl Acad Sci U S A *95*, 13097-13102.
Lee, B. Y., Han, J. A., Im, J. S., Morrone, A., Johung, K., Goodwin, E. C., Kleijer, W. J., DiMaio, D., and Hwang, E. S. (2006). Senescence-associated beta-galactosidase is lysosomal beta-galactosidase. Aging Cell *5*, 187-195.
Lee, H. W., Blasco, M. A., Gottlieb, G. J., Horner, J. W., 2nd, Greider, C. W., and DePinho, R. A. (1998). Essential role of mouse telomerase in highly proliferative organs. Nature *392*, 569-574.
Li, B., Carey, M., and Workman, J. L. (2007). The role of chromatin during transcription. Cell *128*, 707-719.
Li, H., Mitchell, J. R., and Hasty, P. (2008a). DNA double-strand breaks: a potential causative factor for mammalian aging? Mech Ageing Dev *129*, 416-424.
Li, J., Ebata, A., Dong, Y., Rizki, G., Iwata, T., and Lee, S. S. (2008b). Caenorhabditis elegans HCF-1 functions in longevity maintenance as a DAF-16 regulator. PLoS Biol *6*, e233.
Li, T. H., and Schmid, C. W. (2001). Differential stress induction of individual Alu loci: implications for transcription and retrotransposition. Gene *276*, 135-141.
Lin, A. W., Barradas, M., Stone, J. C., van Aelst, L., Serrano, M., and Lowe, S. W. (1998). Premature senescence involving p53 and p16 is activated in response to constitutive MEK/MAPK mitogenic signaling. Genes Dev *12*, 3008-3019.
Lin, S. J., Defossez, P. A., and Guarente, L. (2000). Requirement of NAD and SIR2 for life-span extension by calorie restriction in Saccharomyces cerevisiae. Science *289*, 2126-2128.

Lindahl, T. (1993). Instability and decay of the primary structure of DNA. Nature *362*, 709-715.
Liszt, G., Ford, E., Kurtev, M., and Guarente, L. (2005). Mouse Sir2 homolog SIRT6 is a nuclear ADP-ribosyltransferase. J Biol Chem *280*, 21313-21320.
Liu, W. M., Chu, W. M., Choudary, P. V., and Schmid, C. W. (1995). Cell stress and translational inhibitors transiently increase the abundance of mammalian SINE transcripts. Nucleic Acids Res *23*, 1758-1765.
Liu, W. M., Maraia, R. J., Rubin, C. M., and Schmid, C. W. (1994). Alu transcripts: cytoplasmic localisation and regulation by DNA methylation. Nucleic Acids Res *22*, 1087-1095.
Livak, K. J., and Schmittgen, T. D. (2001). Analysis of relative gene expression data using real-time quantitative PCR and the 2(-Delta Delta C(T)) Method. Methods *25*, 402-408.
Lohr, D., Tatchell, K., and Van Holde, K. E. (1977). On the occurrence of nucleosome phasing in chromatin. Cell *12*, 829-836.
Lois, C., and Alvarez-Buylla, A. (1993). Proliferating subventricular zone cells in the adult mammalian forebrain can differentiate into neurons and glia. Proc Natl Acad Sci U S A *90*, 2074-2077.
Lombard, D. B., Chua, K. F., Mostoslavsky, R., Franco, S., Gostissa, M., and Alt, F. W. (2005). DNA repair, genome stability, and aging. Cell *120*, 497-512.
Lorenzini, A., Johnson, F. B., Oliver, A., Tresini, M., Smith, J. S., Hdeib, M., Sell, C., Cristofalo, V. J., and Stamato, T. D. (2009). Significant correlation of species longevity with DNA double strand break recognition but not with telomere length. Mech Ageing Dev *130*, 784-792.
Lowe, S. W., Cepero, E., and Evan, G. (2004). Intrinsic tumour suppression. Nature *432*, 307-315.
Luger, K., Mader, A. W., Richmond, R. K., Sargent, D. F., and Richmond, T. J. (1997). Crystal structure of the nucleosome core particle at 2.8 A resolution. Nature *389*, 251-260.
Lunyak, V. V., and Atallah, M. (2011). Genomic relationship between SINE retrotransposons, Pol III-Pol II transcription, and chromatin organization: the journey from junk to jewel. Biochem Cell Biol *89*, 495-504.
Luo, J., Nikolaev, A. Y., Imai, S., Chen, D., Su, F., Shiloh, A., Guarente, L., and Gu, W. (2001). Negative control of p53 by Sir2alpha promotes cell survival under stress. Cell *107*, 137-148.
Macieira-Coelho, A., and Puvion-Dutilleul, F. (1989). Evaluation of the reorganization in the high-order structure of DNA occurring during cell senescence. Mutat Res *219*, 165-170.
Mallette, F. A., Gaumont-Leclerc, M. F., and Ferbeyre, G. (2007). The DNA damage signaling pathway is a critical mediator of oncogene-induced senescence. Genes Dev *21*, 43-48.
Mao, Z., Hine, C., Tian, X., Van Meter, M., Au, M., Vaidya, A., Seluanov, A., and Gorbunova, V. (2011). SIRT6 promotes DNA repair under stress by activating PARP1. Science *332*, 1443-1446.
Marciniak, R. A., Johnson, F. B., and Guarente, L. (2000). Dyskeratosis congenita, telomeres and human ageing. Trends Genet *16*, 193-195.
Marcotte, R., Lacelle, C., and Wang, E. (2004). Senescent fibroblasts resist apoptosis by downregulating caspase-3. Mech Ageing Dev *125*, 777-783.
Margueron, R., Trojer, P., and Reinberg, D. (2005). The key to development: interpreting the histone code? Curr Opin Genet Dev *15*, 163-176.
Martin, C., and Zhang, Y. (2005). The diverse functions of histone lysine methylation. Nat Rev Mol Cell Biol *6*, 838-849.
Martin, G. M., Sprague, C. A., and Epstein, C. J. (1970). Replicative life-span of cultivated human cells. Effects of donor's age, tissue, and genotype. Lab Invest *23*, 86-92.
Mason, P. J., and Bessler, M. (2004). Heterozygous telomerase deficiency in mouse and man: when less is definitely not more. Cell Cycle *3*, 1127-1129.
Maston, G. A., Evans, S. K., and Green, M. R. (2006). Transcriptional regulatory elements in the human genome. Annu Rev Genomics Hum Genet *7*, 29-59.

Matsumura, T., Pfendt, E. A., and Hayflick, L. (1979). DNA synthesis in the human diploid cell strain WI-38 during in vitro aging: an autoradiography study. J Gerontol *34*, 323-327.
Matthews, C., Gorenne, I., Scott, S., Figg, N., Kirkpatrick, P., Ritchie, A., Goddard, M., and Bennett, M. (2006). Vascular smooth muscle cells undergo telomere-based senescence in human atherosclerosis: effects of telomerase and oxidative stress. Circ Res *99*, 156-164.
Maxwell, M. M., Tomkinson, E. M., Nobles, J., Wizeman, J. W., Amore, A. M., Quinti, L., Chopra, V., Hersch, S. M., and Kazantsev, A. G. (2011). The Sirtuin 2 microtubule deacetylase is an abundant neuronal protein that accumulates in the aging CNS. Hum Mol Genet *20*, 3986-3996.
Maynard, S., Schurman, S. H., Harboe, C., de Souza-Pinto, N. C., and Bohr, V. A. (2009). Base excision repair of oxidative DNA damage and association with cancer and aging. Carcinogenesis *30*, 2-10.
Mellor, J. (2005). The dynamics of chromatin remodeling at promoters. Mol Cell *19*, 147-157.
Michaloglou, C., Vredeveld, L. C., Soengas, M. S., Denoyelle, C., Kuilman, T., van der Horst, C. M., Majoor, D. M., Shay, J. W., Mooi, W. J., and Peeper, D. S. (2005). BRAFE600-associated senescence-like cell cycle arrest of human naevi. Nature *436*, 720-724.
Mikkelsen, T. S., Ku, M., Jaffe, D. B., Issac, B., Lieberman, E., Giannoukos, G., Alvarez, P., Brockman, W., Kim, T. K., Koche, R. P*., et al.* (2007). Genome-wide maps of chromatin state in pluripotent and lineage-committed cells. Nature *448*, 553-560.
Minamino, T., and Komuro, I. (2007). Vascular cell senescence: contribution to atherosclerosis. Circ Res *100*, 15-26.
Mitchell, M. T., Smith, J. S., Mason, M., Harper, S., Speicher, D. W., Johnson, F. B., and Skordalakes, E. (2010). Cdc13 N-terminal dimerization, DNA binding, and telomere length regulation. Mol Cell Biol *30*, 5325-5334.
Morrison, S. J., Wandycz, A. M., Akashi, K., Globerson, A., and Weissman, I. L. (1996). The aging of hematopoietic stem cells. Nat Med *2*, 1011-1016.
Morrison, S. J., and Weissman, I. L. (1994). The long-term repopulating subset of hematopoietic stem cells is deterministic and isolatable by phenotype. Immunity *1*, 661-673.
Mostoslavsky, R., Chua, K. F., Lombard, D. B., Pang, W. W., Fischer, M. R., Gellon, L., Liu, P., Mostoslavsky, G., Franco, S., Murphy, M. M*., et al.* (2006). Genomic instability and aging-like phenotype in the absence of mammalian SIRT6. Cell *124*, 315-329.
Muller, K. C., Welker, L., Paasch, K., Feindt, B., Erpenbeck, V. J., Hohlfeld, J. M., Krug, N., Nakashima, M., Branscheid, D., Magnussen, H*., et al.* (2006). Lung fibroblasts from patients with emphysema show markers of senescence in vitro. Respir Res *7*, 32.
Multani, A. S., and Chang, S. (2007). WRN at telomeres: implications for aging and cancer. J Cell Sci *120*, 713-721.
Munoz-Najar, U., and Sedivy, J. M. (2011). Epigenetic control of aging. Antioxid Redox Signal *14*, 241-259.
Muntoni, A., and Reddel, R. R. (2005). The first molecular details of ALT in human tumor cells. Hum Mol Genet *14 Spec No. 2*, R191-196.
Nagy, P. L., Cleary, M. L., Brown, P. O., and Lieb, J. D. (2003). Genomewide demarcation of RNA polymerase II transcription units revealed by physical fractionation of chromatin. Proc Natl Acad Sci U S A *100*, 6364-6369.
Narita, M. (2007). Cellular senescence and chromatin organisation. Br J Cancer *96*, 686-691.
Narita, M., Krizhanovsky, V., Nunez, S., Chicas, A., Hearn, S. A., Myers, M. P., and Lowe, S. W. (2006). A novel role for high-mobility group a proteins in cellular senescence and heterochromatin formation. Cell *126*, 503-514.

Narita, M., Nunez, S., Heard, E., Lin, A. W., Hearn, S. A., Spector, D. L., Hannon, G. J., and Lowe, S. W. (2003). Rb-mediated heterochromatin formation and silencing of E2F target genes during cellular senescence. Cell *113*, 703-716.
Necsulea, A., Guillet, C., Cadoret, J. C., Prioleau, M. N., and Duret, L. (2009). The relationship between DNA replication and human genome organization. Mol Biol Evol *26*, 729-741.
Nemoto, S., Fergusson, M. M., and Finkel, T. (2005). SIRT1 functionally interacts with the metabolic regulator and transcriptional coactivator PGC-1{alpha}. J Biol Chem *280*, 16456-16460.
Nicol, J. W., Helt, G. A., Blanchard, S. G., Jr., Raja, A., and Loraine, A. E. (2009). The Integrated Genome Browser: free software for distribution and exploration of genome-scale datasets. Bioinformatics *25*, 2730-2731.
Nowak, S. J., and Corces, V. G. (2004). Phosphorylation of histone H3: a balancing act between chromosome condensation and transcriptional activation. Trends Genet *20*, 214-220.
O'Neill, L. P., and Turner, B. M. (2003). Immunoprecipitation of native chromatin: NChIP. Methods *31*, 76-82.
O'Sullivan, R. J., Kubicek, S., Schreiber, S. L., and Karlseder, J. (2010). Reduced histone biosynthesis and chromatin changes arising from a damage signal at telomeres. Nat Struct Mol Biol *17*, 1218-1225.
Ofir-Rosenfeld, Y., Boggs, K., Michael, D., Kastan, M. B., and Oren, M. (2008). Mdm2 regulates p53 mRNA translation through inhibitory interactions with ribosomal protein L26. Mol Cell *32*, 180-189.
Ohtani, N., Zebedee, Z., Huot, T. J., Stinson, J. A., Sugimoto, M., Ohashi, Y., Sharrocks, A. D., Peters, G., and Hara, E. (2001). Opposing effects of Ets and Id proteins on p16INK4a expression during cellular senescence. Nature *409*, 1067-1070.
Okano, M., Bell, D. W., Haber, D. A., and Li, E. (1999). DNA methyltransferases Dnmt3a and Dnmt3b are essential for de novo methylation and mammalian development. Cell *99*, 247-257.
Okano, M., Xie, S., and Li, E. (1998). Cloning and characterization of a family of novel mammalian DNA (cytosine-5) methyltransferases. Nat Genet *19*, 219-220.
Olovnikov, A. M. (1973). A theory of marginotomy. The incomplete copying of template margin in enzymic synthesis of polynucleotides and biological significance of the phenomenon. J Theor Biol *41*, 181-190.
Ozsolak, F., Song, J. S., Liu, X. S., and Fisher, D. E. (2007). High-throughput mapping of the chromatin structure of human promoters. Nat Biotechnol *25*, 244-248.
Paradis, V., Youssef, N., Dargere, D., Ba, N., Bonvoust, F., Deschatrette, J., and Bedossa, P. (2001). Replicative senescence in normal liver, chronic hepatitis C, and hepatocellular carcinomas. Hum Pathol *32*, 327-332.
Parrinello, S., Coppe, J. P., Krtolica, A., and Campisi, J. (2005). Stromal-epithelial interactions in aging and cancer: senescent fibroblasts alter epithelial cell differentiation. J Cell Sci *118*, 485-496.
Parrinello, S., Samper, E., Krtolica, A., Goldstein, J., Melov, S., and Campisi, J. (2003). Oxygen sensitivity severely limits the replicative lifespan of murine fibroblasts. Nat Cell Biol *5*, 741-747.
Pearson, K. J., Baur, J. A., Lewis, K. N., Peshkin, L., Price, N. L., Labinskyy, N., Swindell, W. R., Kamara, D., Minor, R. K., Perez, E.*, et al.* (2008). Resveratrol delays age-related deterioration and mimics transcriptional aspects of dietary restriction without extending life span. Cell Metab *8*, 157-168.
Pena, P. V., Davrazou, F., Shi, X., Walter, K. L., Verkhusha, V. V., Gozani, O., Zhao, R., and Kutateladze, T. G. (2006). Molecular mechanism of histone H3K4me3 recognition by plant homeodomain of ING2. Nature *442*, 100-103.

Pfister, J. A., Ma, C., Morrison, B. E., and D'Mello, S. R. (2008). Opposing effects of sirtuins on neuronal survival: SIRT1-mediated neuroprotection is independent of its deacetylase activity. PLoS One *3*, e4090.
Phokaew, C., Kowudtitham, S., Subbalekha, K., Shuangshoti, S., and Mutirangura, A. (2008). LINE-1 methylation patterns of different loci in normal and cancerous cells. Nucleic Acids Res *36*, 5704-5712.
Pignolo, R. J., Rotenberg, M. O., and Cristofalo, V. J. (1994). Alterations in contact and density-dependent arrest state in senescent WI-38 cells. In Vitro Cell Dev Biol Anim *30A*, 471-476.
Pina, B., and Suau, P. (1987). Changes in histones H2A and H3 variant composition in differentiating and mature rat brain cortical neurons. Dev Biol *123*, 51-58.
Pollina, E. A., and Brunet, A. (2011). Epigenetic regulation of aging stem cells. Oncogene *30*, 3105-3126.
Price, J. S., Waters, J. G., Darrah, C., Pennington, C., Edwards, D. R., Donell, S. T., and Clark, I. M. (2002). The role of chondrocyte senescence in osteoarthritis. Aging Cell *1*, 57-65.
Prowse, K. R., and Greider, C. W. (1995). Developmental and tissue-specific regulation of mouse telomerase and telomere length. Proc Natl Acad Sci U S A *92*, 4818-4822.
Pruitt, K., Zinn, R. L., Ohm, J. E., McGarvey, K. M., Kang, S. H., Watkins, D. N., Herman, J. G., and Baylin, S. B. (2006). Inhibition of SIRT1 reactivates silenced cancer genes without loss of promoter DNA hypermethylation. PLoS Genet *2*, e40.
Qiu, X., Brown, K., Hirschey, M. D., Verdin, E., and Chen, D. (2010). Calorie restriction reduces oxidative stress by SIRT3-mediated SOD2 activation. Cell Metab *12*, 662-667.
Ramirez, R. D., Morales, C. P., Herbert, B. S., Rohde, J. M., Passons, C., Shay, J. W., and Wright, W. E. (2001). Putative telomere-independent mechanisms of replicative aging reflect inadequate growth conditions. Genes Dev *15*, 398-403.
Rangwala, S. H., Zhang, L., and Kazazian, H. H., Jr. (2009). Many LINE1 elements contribute to the transcriptome of human somatic cells. Genome Biol *10*, R100.
Ressler, S., Bartkova, J., Niederegger, H., Bartek, J., Scharffetter-Kochanek, K., Jansen-Durr, P., and Wlaschek, M. (2006). p16INK4A is a robust in vivo biomarker of cellular aging in human skin. Aging Cell *5*, 379-389.
Richard, G. F., Kerrest, A., and Dujon, B. (2008). Comparative genomics and molecular dynamics of DNA repeats in eukaryotes. Microbiol Mol Biol Rev *72*, 686-727.
Rodgers, J. T., Lerin, C., Haas, W., Gygi, S. P., Spiegelman, B. M., and Puigserver, P. (2005). Nutrient control of glucose homeostasis through a complex of PGC-1alpha and SIRT1. Nature *434*, 113-118.
Rodier, F., Coppe, J. P., Patil, C. K., Hoeijmakers, W. A., Munoz, D. P., Raza, S. R., Freund, A., Campeau, E., Davalos, A. R., and Campisi, J. (2009). Persistent DNA damage signalling triggers senescence-associated inflammatory cytokine secretion. Nat Cell Biol *11*, 973-979.
Rogakou, E. P., Pilch, D. R., Orr, A. H., Ivanova, V. S., and Bonner, W. M. (1998). DNA double-stranded breaks induce histone H2AX phosphorylation on serine 139. J Biol Chem *273*, 5858-5868.
Rogakou, E. P., and Sekeri-Pataryas, K. E. (1999). Histone variants of H2A and H3 families are regulated during in vitro aging in the same manner as during differentiation. Exp Gerontol *34*, 741-754.
Rogina, B., and Helfand, S. L. (2004). Sir2 mediates longevity in the fly through a pathway related to calorie restriction. Proc Natl Acad Sci U S A *101*, 15998-16003.
Romanov, G. A., and Vanyushin, B. F. (1981). Methylation of reiterated sequences in mammalian DNAs. Effects of the tissue type, age, malignancy and hormonal induction. Biochim Biophys Acta *653*, 204-218.

Rudin, C. M., and Thompson, C. B. (2001). Transcriptional activation of short interspersed elements by DNA-damaging agents. Genes Chromosomes Cancer *30*, 64-71.
Rudolph, K. L., Chang, S., Lee, H. W., Blasco, M., Gottlieb, G. J., Greider, C., and DePinho, R. A. (1999). Longevity, stress response, and cancer in aging telomerase-deficient mice. Cell *96*, 701-712.
Sager, R. (1991). Senescence as a mode of tumor suppression. Environ Health Perspect *93*, 59-62.
Salmon, A. B., Richardson, A., and Perez, V. I. (2010). Update on the oxidative stress theory of aging: does oxidative stress play a role in aging or healthy aging? Free Radic Biol Med *48*, 642-655.
Sambrook, J., and Russell, D. W. (2001). Molecular Cloning a Laboratory Manual, Third Edition edn (New York: Cold Spring Harbor Laboratory Press).
Sarg, B., Koutzamani, E., Helliger, W., Rundquist, I., and Lindner, H. H. (2002). Postsynthetic trimethylation of histone H4 at lysine 20 in mammalian tissues is associated with aging. J Biol Chem *277*, 39195-39201.
Sasaki, T., Maier, B., Bartke, A., and Scrable, H. (2006). Progressive loss of SIRT1 with cell cycle withdrawal. Aging Cell *5*, 413-422.
Satyanarayana, A., Wiemann, S. U., Buer, J., Lauber, J., Dittmar, K. E., Wustefeld, T., Blasco, M. A., Manns, M. P., and Rudolph, K. L. (2003). Telomere shortening impairs organ regeneration by inhibiting cell cycle re-entry of a subpopulation of cells. EMBO J *22*, 4003-4013.
Scher, M. B., Vaquero, A., and Reinberg, D. (2007). SirT3 is a nuclear NAD+-dependent histone deacetylase that translocates to the mitochondria upon cellular stress. Genes Dev *21*, 920-928.
Schneider, E. L., and Mitsui, Y. (1976). The relationship between in vitro cellular aging and in vivo human age. Proc Natl Acad Sci U S A *73*, 3584-3588.
Sedelnikova, O. A., Horikawa, I., Zimonjic, D. B., Popescu, N. C., Bonner, W. M., and Barrett, J. C. (2004). Senescing human cells and ageing mice accumulate DNA lesions with unrepairable double-strand breaks. Nat Cell Biol *6*, 168-170.
Sedivy, J. M., Banumathy, G., and Adams, P. D. (2008). Aging by epigenetics--a consequence of chromatin damage? Exp Cell Res *314*, 1909-1917.
Serrano, M., Hannon, G. J., and Beach, D. (1993). A new regulatory motif in cell-cycle control causing specific inhibition of cyclin D/CDK4. Nature *366*, 704-707.
Serrano, M., Lin, A. W., McCurrach, M. E., Beach, D., and Lowe, S. W. (1997). Oncogenic ras provokes premature cell senescence associated with accumulation of p53 and p16INK4a. Cell *88*, 593-602.
Sfeir, A. J., Chai, W., Shay, J. W., and Wright, W. E. (2005). Telomere-end processing the terminal nucleotides of human chromosomes. Mol Cell *18*, 131-138.
Sharpless, N. E., and DePinho, R. A. (2004). Telomeres, stem cells, senescence, and cancer. J Clin Invest *113*, 160-168.
Sharpless, N. E., and DePinho, R. A. (2007). How stem cells age and why this makes us grow old. Nat Rev Mol Cell Biol *8*, 703-713.
Shay, J. W., and Bacchetti, S. (1997). A survey of telomerase activity in human cancer. Eur J Cancer *33*, 787-791.
Shay, J. W., Pereira-Smith, O. M., and Wright, W. E. (1991). A role for both RB and p53 in the regulation of human cellular senescence. Exp Cell Res *196*, 33-39.
Shelton, D. N., Chang, E., Whittier, P. S., Choi, D., and Funk, W. D. (1999). Microarray analysis of replicative senescence. Curr Biol *9*, 939-945.
Sherr, C. J., and DePinho, R. A. (2000). Cellular senescence: mitotic clock or culture shock? Cell *102*, 407-410.

Sherr, C. J., and Roberts, J. M. (1999). CDK inhibitors: positive and negative regulators of G1-phase progression. Genes Dev *13*, 1501-1512.
Shi, X., Hong, T., Walter, K. L., Ewalt, M., Michishita, E., Hung, T., Carney, D., Pena, P., Lan, F., Kaadige, M. R*., et al.* (2006). ING2 PHD domain links histone H3 lysine 4 methylation to active gene repression. Nature *442*, 96-99.
Shilatifard, A. (2006). Chromatin modifications by methylation and ubiquitination: implications in the regulation of gene expression. Annu Rev Biochem *75*, 243-269.
Shmookler Reis, R. J., and Goldstein, S. (1982). Variability of DNA methylation patterns during serial passage of human diploid fibroblasts. Proc Natl Acad Sci U S A *79*, 3949-3953.
Shumaker, D. K., Dechat, T., Kohlmaier, A., Adam, S. A., Bozovsky, M. R., Erdos, M. R., Eriksson, M., Goldman, A. E., Khuon, S., Collins, F. S*., et al.* (2006). Mutant nuclear lamin A leads to progressive alterations of epigenetic control in premature aging. Proc Natl Acad Sci U S A *103*, 8703-8708.
Siegert, J. L., Rushton, J. J., Sellers, W. R., Kaelin, W. G., Jr., and Robbins, P. D. (2000). Cyclin D1 suppresses retinoblastoma protein-mediated inhibition of TAFII250 kinase activity. Oncogene *19*, 5703-5711.
Simonis, M., Kooren, J., and de Laat, W. (2007). An evaluation of 3C-based methods to capture DNA interactions. Nat Methods *4*, 895-901.
Sinclair, D. A., and Guarente, L. (1997). Extrachromosomal rDNA circles--a cause of aging in yeast. Cell *91*, 1033-1042.
Sinclair, D. A., and Oberdoerffer, P. (2009). The ageing epigenome: damaged beyond repair? Ageing Res Rev *8*, 189-198.
Singer-Sam, J., LeBon, J. M., Tanguay, R. L., and Riggs, A. D. (1990). A quantitative HpaII-PCR assay to measure methylation of DNA from a small number of cells. Nucleic Acids Res *18*, 687.
Singhal, R. P., Mays-Hoopes, L. L., and Eichhorn, G. L. (1987). DNA methylation in aging of mice. Mech Ageing Dev *41*, 199-210.
Skowronski, J., Fanning, T. G., and Singer, M. F. (1988). Unit-length line-1 transcripts in human teratocarcinoma cells. Mol Cell Biol *8*, 1385-1397.
Skowronski, J., and Singer, M. F. (1985). Expression of a cytoplasmic LINE-1 transcript is regulated in a human teratocarcinoma cell line. Proc Natl Acad Sci U S A *82*, 6050-6054.
Smit, A. F. (1996). The origin of interspersed repeats in the human genome. Curr Opin Genet Dev *6*, 743-748.
Smyth, G. K. (2005). Limma: Linear Models for Microarray Data, (New York: Springer).
So, A. Y., Jung, J. W., Lee, S., Kim, H. S., and Kang, K. S. (2011). DNA Methyltransferase Controls Stem Cell Aging by Regulating BMI1 and EZH2 through MicroRNAs. PLoS One *6*, e19503.
So, K., Tamura, G., Honda, T., Homma, N., Waki, T., Togawa, N., Nishizuka, S., and Motoyama, T. (2006). Multiple tumor suppressor genes are increasingly methylated with age in non-neoplastic gastric epithelia. Cancer Sci *97*, 1155-1158.
Solomon, M. J., and Varshavsky, A. (1985). Formaldehyde-mediated DNA-protein crosslinking: a probe for in vivo chromatin structures. Proc Natl Acad Sci U S A *82*, 6470-6474.
Song, L., and Crawford, G. E. (2010). DNase-seq: a high-resolution technique for mapping active gene regulatory elements across the genome from mammalian cells. Cold Spring Harb Protoc *2010*, pdb prot5384.
Sproul, D., Gilbert, N., and Bickmore, W. A. (2005). The role of chromatin structure in regulating the expression of clustered genes. Nat Rev Genet *6*, 775-781.
Stein, G. H., Beeson, M., and Gordon, L. (1990). Failure to phosphorylate the retinoblastoma gene product in senescent human fibroblasts. Science *249*, 666-669.

Stein, G. H., Drullinger, L. F., Soulard, A., and Dulic, V. (1999). Differential roles for cyclin-dependent kinase inhibitors p21 and p16 in the mechanisms of senescence and differentiation in human fibroblasts. Mol Cell Biol *19*, 2109-2117.
Sterner, D. E., and Berger, S. L. (2000). Acetylation of histones and transcription-related factors. Microbiol Mol Biol Rev *64*, 435-459.
Stewart, S. A., Ben-Porath, I., Carey, V. J., O'Connor, B. F., Hahn, W. C., and Weinberg, R. A. (2003). Erosion of the telomeric single-strand overhang at replicative senescence. Nat Genet *33*, 492-496.
Sugimoto, M., Yamashita, R., and Ueda, M. (2006). Telomere length of the skin in association with chronological aging and photoaging. J Dermatol Sci *43*, 43-47.
Suzuki, K., and Koike, T. (2007). Mammalian Sir2-related protein (SIRT) 2-mediated modulation of resistance to axonal degeneration in slow Wallerian degeneration mice: a crucial role of tubulin deacetylation. Neuroscience *147*, 599-612.
Takai, H., Smogorzewska, A., and de Lange, T. (2003). DNA damage foci at dysfunctional telomeres. Curr Biol *13*, 1549-1556.
Tao, R., Coleman, M. C., Pennington, J. D., Ozden, O., Park, S. H., Jiang, H., Kim, H. S., Flynn, C. R., Hill, S., Hayes McDonald, W*., et al.* (2010). Sirt3-mediated deacetylation of evolutionarily conserved lysine 122 regulates MnSOD activity in response to stress. Mol Cell *40*, 893-904.
Thakur, M. K., and Kanungo, M. S. (1981). Methylation of chromosomal proteins and DNA of rat brain and its modulation by estradiol and calcium during aging. Exp Gerontol *16*, 331-336.
Thompson, R. F., Atzmon, G., Gheorghe, C., Liang, H. Q., Lowes, C., Greally, J. M., and Barzilai, N. (2010). Tissue-specific dysregulation of DNA methylation in aging. Aging Cell *9*, 506-518.
Tissenbaum, H. A., and Guarente, L. (2001). Increased dosage of a sir-2 gene extends lifespan in Caenorhabditis elegans. Nature *410*, 227-230.
Tomas-Loba, A., Flores, I., Fernandez-Marcos, P. J., Cayuela, M. L., Maraver, A., Tejera, A., Borras, C., Matheu, A., Klatt, P., Flores, J. M*., et al.* (2008). Telomerase reverse transcriptase delays aging in cancer-resistant mice. Cell *135*, 609-622.
Tra, J., Kondo, T., Lu, Q., Kuick, R., Hanash, S., and Richardson, B. (2002). Infrequent occurrence of age-dependent changes in CpG island methylation as detected by restriction landmark genome scanning. Mech Ageing Dev *123*, 1487-1503.
Trojer, P., and Reinberg, D. (2007). Facultative heterochromatin: is there a distinctive molecular signature? Mol Cell *28*, 1-13.
Tsai, Y. C., Greco, T. M., Boonmee, A., Miteva, Y., and Cristea, I. M. (2012). Functional proteomics establishes the interaction of SIRT7 with chromatin remodeling complexes and expands its role in regulation of RNA polymerase I transcription. Mol Cell Proteomics *11*, M111 015156.
Tsuji, T., Aoshiba, K., and Nagai, A. (2006). Alveolar cell senescence in patients with pulmonary emphysema. Am J Respir Crit Care Med *174*, 886-893.
Ulaner, G. A., Hu, J. F., Vu, T. H., Giudice, L. C., and Hoffman, A. R. (2001). Tissue-specific alternate splicing of human telomerase reverse transcriptase (hTERT) influences telomere lengths during human development. Int J Cancer *91*, 644-649.
Vaquero, A., Scher, M., Lee, D., Erdjument-Bromage, H., Tempst, P., and Reinberg, D. (2004). Human SirT1 interacts with histone H1 and promotes formation of facultative heterochromatin. Mol Cell *16*, 93-105.
Vasile, E., Tomita, Y., Brown, L. F., Kocher, O., and Dvorak, H. F. (2001). Differential expression of thymosin beta-10 by early passage and senescent vascular endothelium is modulated by VPF/VEGF: evidence for senescent endothelial cells in vivo at sites of atherosclerosis. FASEB J *15*, 458-466.

Vaziri, H., Dessain, S. K., Ng Eaton, E., Imai, S. I., Frye, R. A., Pandita, T. K., Guarente, L., and Weinberg, R. A. (2001). hSIR2(SIRT1) functions as an NAD-dependent p53 deacetylase. Cell *107*, 149-159.
Vaziri, H., West, M. D., Allsopp, R. C., Davison, T. S., Wu, Y. S., Arrowsmith, C. H., Poirier, G. G., and Benchimol, S. (1997). ATM-dependent telomere loss in aging human diploid fibroblasts and DNA damage lead to the post-translational activation of p53 protein involving poly(ADP-ribose) polymerase. EMBO J *16*, 6018-6033.
Verdin, E., Hirschey, M. D., Finley, L. W., and Haigis, M. C. (2010). Sirtuin regulation of mitochondria: energy production, apoptosis, and signaling. Trends Biochem Sci *35*, 669-675.
Vijg, J. (2004). Impact of genome instability on transcription regulation of aging and senescence. Mech Ageing Dev *125*, 747-753.
von Zglinicki, T., and Martin-Ruiz, C. M. (2005). Telomeres as biomarkers for ageing and age-related diseases. Curr Mol Med *5*, 197-203.
Vulliamy, T., Marrone, A., Goldman, F., Dearlove, A., Bessler, M., Mason, P. J., and Dokal, I. (2001). The RNA component of telomerase is mutated in autosomal dominant dyskeratosis congenita. Nature *413*, 432-435.
Vulliamy, T., Marrone, A., Szydlo, R., Walne, A., Mason, P. J., and Dokal, I. (2004). Disease anticipation is associated with progressive telomere shortening in families with dyskeratosis congenita due to mutations in TERC. Nat Genet *36*, 447-449.
Waki, T., Tamura, G., Sato, M., and Motoyama, T. (2003). Age-related methylation of tumor suppressor and tumor-related genes: an analysis of autopsy samples. Oncogene *22*, 4128-4133.
Wang, C. M., Tsai, S. N., Yew, T. W., Kwan, Y. W., and Ngai, S. M. (2010). Identification of histone methylation multiplicities patterns in the brain of senescence-accelerated prone mouse 8. Biogerontology *11*, 87-102.
Wang, E. (1995). Senescent human fibroblasts resist programmed cell death, and failure to suppress bcl2 is involved. Cancer Res *55*, 2284-2292.
Wang, J., Geesman, G. J., Hostikka, S. L., Atallah, M., Blackwell, B., Lee, E., Cook, P. J., Pasaniuc, B., Shariat, G., Halperin, E.*, et al.* (2011). Inhibition of activated pericentromeric SINE/Alu repeat transcription in senescent human adult stem cells reinstates self-renewal. Cell Cycle *10*, 3016-3030.
Wang, Y., and Tissenbaum, H. A. (2006). Overlapping and distinct functions for a Caenorhabditis elegans SIR2 and DAF-16/FOXO. Mech Ageing Dev *127*, 48-56.
Weaver, B. A., Silk, A. D., Montagna, C., Verdier-Pinard, P., and Cleveland, D. W. (2007). Aneuploidy acts both oncogenically and as a tumor suppressor. Cancer Cell *11*, 25-36.
Wei, W., Hemmer, R. M., and Sedivy, J. M. (2001). Role of p14(ARF) in replicative and induced senescence of human fibroblasts. Mol Cell Biol *21*, 6748-6757.
Wei, W., Herbig, U., Wei, S., Dutriaux, A., and Sedivy, J. M. (2003). Loss of retinoblastoma but not p16 function allows bypass of replicative senescence in human fibroblasts. EMBO Rep *4*, 1061-1066.
Weisenberger, D. J., Campan, M., Long, T. I., Kim, M., Woods, C., Fiala, E., Ehrlich, M., and Laird, P. W. (2005). Analysis of repetitive element DNA methylation by MethyLight. Nucleic Acids Res *33*, 6823-6836.
Wiemann, S. U., Satyanarayana, A., Tsahuridu, M., Tillmann, H. L., Zender, L., Klempnauer, J., Flemming, P., Franco, S., Blasco, M. A., Manns, M. P., and Rudolph, K. L. (2002). Hepatocyte telomere shortening and senescence are general markers of human liver cirrhosis. FASEB J *16*, 935-942.

Wilson, B. J., Tremblay, A. M., Deblois, G., Sylvain-Drolet, G., and Giguere, V. (2010). An acetylation switch modulates the transcriptional activity of estrogen-related receptor alpha. Mol Endocrinol *24*, 1349-1358.
Wilson, V. L., and Jones, P. A. (1983). DNA methylation decreases in aging but not in immortal cells. Science *220*, 1055-1057.
Wilson, V. L., Smith, R. A., Ma, S., and Cutler, R. G. (1987). Genomic 5-methyldeoxycytidine decreases with age. J Biol Chem *262*, 9948-9951.
Wright, W. E., Piatyszek, M. A., Rainey, W. E., Byrd, W., and Shay, J. W. (1996). Telomerase activity in human germline and embryonic tissues and cells. Dev Genet *18*, 173-179.
Wright, W. E., and Shay, J. W. (2001). Cellular senescence as a tumor-protection mechanism: the essential role of counting. Curr Opin Genet Dev *11*, 98-103.
Xue, W., Zender, L., Miething, C., Dickins, R. A., Hernando, E., Krizhanovsky, V., Cordon-Cardo, C., and Lowe, S. W. (2007). Senescence and tumour clearance is triggered by p53 restoration in murine liver carcinomas. Nature *445*, 656-660.
Yamaguchi, H., Calado, R. T., Ly, H., Kajigaya, S., Baerlocher, G. M., Chanock, S. J., Lansdorp, P. M., and Young, N. S. (2005). Mutations in TERT, the gene for telomerase reverse transcriptase, in aplastic anemia. N Engl J Med *352*, 1413-1424.
Yang, G., Rosen, D. G., Zhang, Z., Bast, R. C., Jr., Mills, G. B., Colacino, J. A., Mercado-Uribe, I., and Liu, J. (2006). The chemokine growth-regulated oncogene 1 (Gro-1) links RAS signaling to the senescence of stromal fibroblasts and ovarian tumorigenesis. Proc Natl Acad Sci U S A *103*, 16472-16477.
Yang, N., and Kazazian, H. H., Jr. (2006). L1 retrotransposition is suppressed by endogenously encoded small interfering RNAs in human cultured cells. Nat Struct Mol Biol *13*, 763-771.
Yang, N. C., and Hu, M. L. (2005). The limitations and validities of senescence associated-beta-galactosidase activity as an aging marker for human foreskin fibroblast Hs68 cells. Exp Gerontol *40*, 813-819.
Yatabe, Y., Tavare, S., and Shibata, D. (2001). Investigating stem cells in human colon by using methylation patterns. Proc Natl Acad Sci U S A *98*, 10839-10844.
Ye, X., Zerlanko, B., Zhang, R., Somaiah, N., Lipinski, M., Salomoni, P., and Adams, P. D. (2007). Definition of pRB- and p53-dependent and -independent steps in HIRA/ASF1a-mediated formation of senescence-associated heterochromatin foci. Mol Cell Biol *27*, 2452-2465.
Yeung, F., Hoberg, J. E., Ramsey, C. S., Keller, M. D., Jones, D. R., Frye, R. A., and Mayo, M. W. (2004). Modulation of NF-kappaB-dependent transcription and cell survival by the SIRT1 deacetylase. EMBO J *23*, 2369-2380.
Young, A. P., Schlisio, S., Minamishima, Y. A., Zhang, Q., Li, L., Grisanzio, C., Signoretti, S., and Kaelin, W. G., Jr. (2008). VHL loss actuates a HIF-independent senescence programme mediated by Rb and p400. Nat Cell Biol *10*, 361-369.
Yuan, G. C., Liu, Y. J., Dion, M. F., Slack, M. D., Wu, L. F., Altschuler, S. J., and Rando, O. J. (2005). Genome-scale identification of nucleosome positions in S. cerevisiae. Science *309*, 626-630.
Yunis, J. J., and Yasmineh, W. G. (1971). Heterochromatin, satellite DNA, and cell function. Structural DNA of eucaryotes may support and protect genes and aid in speciation. Science *174*, 1200-1209.
Zemojtel, T., and Penzkofer, T. L1Base http://line1.bioapps.biozentrum.uni-wuerzburg.de/. In.
Zhang, H., Pan, K. H., and Cohen, S. N. (2003). Senescence-specific gene expression fingerprints reveal cell-type-dependent physical clustering of up-regulated chromosomal loci. Proc Natl Acad Sci U S A *100*, 3251-3256.
Zhang, R., and Adams, P. D. (2007). Heterochromatin and its relationship to cell senescence and cancer therapy. Cell Cycle *6*, 784-789.

Zhang, R., Chen, W., and Adams, P. D. (2007). Molecular dissection of formation of senescence-associated heterochromatin foci. Mol Cell Biol *27*, 2343-2358.
Zhang, R., Poustovoitov, M. V., Ye, X., Santos, H. A., Chen, W., Daganzo, S. M., Erzberger, J. P., Serebriiskii, I. G., Canutescu, A. A., Dunbrack, R. L*., et al.* (2005). Formation of MacroH2A-containing senescence-associated heterochromatin foci and senescence driven by ASF1a and HIRA. Dev Cell *8*, 19-30.
Zhang, Y., and Reinberg, D. (2001). Transcription regulation by histone methylation: interplay between different covalent modifications of the core histone tails. Genes Dev *15*, 2343-2360.
Zhao, Z., Tavoosidana, G., Sjolinder, M., Gondor, A., Mariano, P., Wang, S., Kanduri, C., Lezcano, M., Sandhu, K. S., Singh, U*., et al.* (2006). Circular chromosome conformation capture (4C) uncovers extensive networks of epigenetically regulated intra- and interchromosomal interactions. Nat Genet *38*, 1341-1347.
Zhu, J., Woods, D., McMahon, M., and Bishop, J. M. (1998). Senescence of human fibroblasts induced by oncogenic Raf. Genes Dev *12*, 2997-3007.
Zhu, Z. Z., Sparrow, D., Hou, L., Tarantini, L., Bollati, V., Litonjua, A. A., Zanobetti, A., Vokonas, P., Wright, R. O., Baccarelli, A., and Schwartz, J. (2011). Repetitive element hypomethylation in blood leukocyte DNA and cancer incidence, prevalence, and mortality in elderly individuals: the Normative Aging Study. Cancer Causes Control *22*, 437-447.
Zindy, F., Quelle, D. E., Roussel, M. F., and Sherr, C. J. (1997). Expression of the p16INK4a tumor suppressor versus other INK4 family members during mouse development and aging. Oncogene *15*, 203-211.